NOAA Technical Memorandum OAR PSD-311

A GUIDE TO MAKING CLIMATE QUALITY METEOROLOGICAL AND FLUX MEASUREMENTS AT SEA

F. Bradley
C. Fairall

Earth System Research Laboratory
Physical Sciences Division
Boulder, Colorado
October 2006

noaa NATIONAL OCEANIC AND ATMOSPHERIC ADMINISTRATION / Office of Oceanic and Atmospheric Research

NOAA Technical Memorandum OAR PSD-311

A GUIDE TO MAKING CLIMATE QUALITY METEOROLOGICAL AND FLUX MEASUREMENTS AT SEA

Frank Bradley
CSIRO Land and Water, P.O. Box 1666, Canberra 2601 Australia

Christopher Fairall
NOAA Earth System Research Laboratory, Boulder, CO

Earth System Research Laboratory
Physical Sciences Division
Boulder, Colorado
October 2006

UNITED STATES DEPARTMENT OF COMMERCE

Carlos M. Gutierrez
Secretary

NATIONAL OCEANIC AND ATMOSPHERIC ADMINISTRATION

VADM Conrad C. Lautenbacher, Jr.
Under Secretary for Oceans and Atmosphere/Administrator

Office of Oceanic and Atmospheric Research

Dr. Richard Spinrad
Assistant Administrator

NOTICE

Mention of a commercial company or product does not constitute an endorsement by NOAA/Earth System Research Laboratory. Use of information from this publication concerning proprietary products or the test of such products for publicity or advertising purposes is not authorized.

For sale by the National Technical Information Service, 5285 Port Royal Road
Springfield, VA 22061

Contents

BACKGROUND

The importance of accurate fluxes of heat and momentum in the coupled ocean-atmosphere system has been acknowledged since the mid-1980s. Arbitrary adjustment to the air-sea fluxes when coupling ocean and atmospheric models was common practice as a means of keeping sea surface temperatures within realistic bounds. In response to this demonstrated sensitivity of coupled air-sea models to small changes in values of air-sea fluxes, the World Ocean Circulation Experiment (WOCE) observing program (WCRP 1989) and process studies such as the Tropical Ocean Global Atmosphere – Coupled Ocean-Atmosphere Response Experiment (TOGA-COARE) (Webster and Lukas 1992) set accuracy goals for the measurement of net heat exchange across the ocean-atmosphere interface of ±10 Wm^{-2} over short to medium time scales. However, the comparison of observations from several research ships during TOGA-COARE revealed that raw measurements fell short of this goal. In the subsequent analysis, the reasons for these disagreements were examined and identified, and in most cases corrections could be made.

Problems were traced to interference of the measurement by the ship including: poor location of sensors; inadequate knowledge of how an instrument designed for use over land performed on an unstable platform and in the marine environment; and inappropriate calibration procedures. Overall, it became apparent that, if the requirements of climate research were to be met, more care must be taken to ensure the accuracy of measurement of basic meteorological variables used for the calculation of turbulent and radiative air-sea fluxes (Weller et al. 2004). Such careful observations may be referred to as of "climate-quality".

Following the publication of its report on the status of air-sea flux datasets and observational methods (WCRP 2000), the WCRP/SCOR Air-Sea Fluxes Working Group convened an international workshop to discuss its findings, and to consider the implications for future air-sea flux measurement for climate research generally, and for validation of satellite observations and initialization of models (WCRP 2001). The Workshop noted that "the techniques to obtain high-quality data for flux estimation at sea are very demanding" and recommended "the assembly of a Technical Manual on air-sea flux measurement methods".

In March 2003, Florida State University hosted the First High-Resolution Marine Meteorology (HRMM) workshop, under the auspices of NOAA/OGP Ocean Observing Initiative. The quality of basic measurements needed to ensure accurate air-sea fluxes was discussed, as was the fact that valuable data could be obtained when research ships operate in rarely visited regions. Often these ships have the necessary sensors onboard, and technicians capable of maintaining them, but no mechanism or protocol exists to ensure that flux-relevant data are collected even when meteorological conditions are not important for the objectives of that particular cruise.

To improve this situation and ensure good data return from as many ships as possible, the first step is to make those who would be involved aware of the difficulties in collecting high-quality meteorological data at sea. Recommendation 5 from the report of that meeting (COAPS 2003) was to 'Produce a reference manual of best procedures and practices for the observation and documentation of meteorological parameters, including radiative and turbulent fluxes, in the marine environment. The manual will be maintained online and will be a resource for marine weather system standards.'

This manual is intended for a wide readership. Primarily, it is a guide for scientists and technicians who are responsible for installing and/or maintaining meteorological equipment onboard ships, whether research vessels specifically engaged in air-sea studies, ships able to provide relevant data of opportunity, or commercial vessels recruited as part of the Voluntary Observing Ship network (the same general principles apply to meteorological sensors installed on surface buoys). It is also intended to provide background for scientists on oceanographic research cruises who need air-sea flux information from the research vessel as auxiliary data for their study. A quick perusal of this document should allow the scientist to ask the right questions about the particular measurements for the cruise. Importantly, this manual should also serve as background material for students interested in ship-based meteorological and air-sea flux measurements.

The second workshop of the HRMM in April 2004 (COAPS 2004) decided that electronic meteorological sensors existing or subsequently installed on ships and maintained according to these principles be identified as part of the Shipboard Automated Meteorological and Oceanographic System (SAMOS) Initiative. SAMOS will collect and distribute climate-quality data via an assigned Data Assembly Centre (DAC) and ensure the data are archived at appropriate world data centers. This handbook will be a guide to SAMOS and similar projects. In prescribing costly equipment and calibration standards, and exacting installation procedures, we also presume that technical attention is available each day for the associated routine maintenance, monitoring and data archiving tasks. Reasonable time must also be committed to troubleshooting in event of instrument failure.

The organisation of the manual is as follows. We first provide a Summary of the most critical information and procedures, intended as a "stand-alone" practical reference. The main body of the handbook describes the nature of the environmental variables that need to be measured, and why this is so much more exacting at sea than over land. It deals with the practical issues of coping with these difficulties on board a ship or mooring, to ensure the data are as reliable as possible. We also refer to procedures such as calibration before and after the deployment, and comparison with other instruments, which help ensure the quality of the data. Emphasis is also given to the critical importance of documentation, particularly of the location and state of the measuring instruments (now easily captured with digital photos), and notes of any occurrence, e.g., roosting birds, which may impair data quality.

There are several specialized Appendices; physical formulae, constants and conversion factors used in the analysis of atmospheric data and the calculation of air-sea fluxes (which you can never find when you need them); a description of the TOGA-COARE bulk flux algorithm; an analysis of thermal radiative flux errors; examples of shipboard observations; the Beaufort wind scale; a list of links to relevant web sites; and details of the SAMOS DAC with specifications for standardization of data formats, and metadata requirements.

Acknowledgments

Many colleagues contributed to this handbook with careful reviews and writings. We are indebted to Liz Kent, Bob Weller, Roger Lukas, Ed Andreas, Peter Taylor, Shawn Smith, Ben Moat, Mark Bourassa, Mike Reynolds, Eric Schulz, Will Drennan, and Steven Hartz.

This work was supported by the NOAA Office of Climate Observation. Frank Bradley thanks the CSIRO Division of Land and Water for continuing support by way of a post-retirement fellowship.

QUICK REFERENCE

The body of this handbook describes in detail the factors to be considered in equipping a vessel to obtain climate-quality meteorological and flux data. It discusses the nature of the basic quantities to be measured, the relevant instruments, and special considerations because the measuring site is a ship at sea. This Summary is a practical reference for the benefit of the scientist or technician assigned the task of installing and maintaining a package of instruments on a ship, without needing too much detail or rationale. It follows roughly the order of the various procedures involved.

QR1. Instruments and Calibration

The meteorological measurements required for determination of air-sea fluxes comprise:

- Wind speed
- Wind direction
- Air temperature
- Air humidity
- Atmospheric pressure
- Downward shortwave radiation
- Downward longwave radiation
- Rainfall
- Sea surface temperature (not strictly meteorology, but a vital measurement)

Table 1 lists the required accuracy for each of these quantities; the suite of instruments provided should have been assembled to meet these specifications. Whether or not the accuracy is achieved will depend on installation and maintenance. In general, there will be more than one sensor of each type available. If possible, two sets of instruments should be deployed to ensure good exposure for any ship-relative wind or sun direction. At least one spare instrument of each type should be set aside as replacement should its operational counterpart fail. Spare instruments may be stored on the vessel if the operator feels that replacements at sea are feasible.

Each instrument comes with a calibration from a certified facility to which it should be returned for re-calibration as necessary, and at least once a year. It is important to record the **calibration** and **deployment** history of each sensor, so that the correct calibration can be applied should instruments be exchanged or replaced. These metadata (see section 9) are critical when the raw data are re-analysed during post-processing.

The data record will also include input from the ship's navigation system:

a) Latitude and longitude from GPS.
b) The ship's true heading, and the ship's course and speed over the ground, and speed through the water. These are required to convert relative wind speed and direction to true values.
c) Although the instrument package to be installed may include a separate sea temperature measurement, if a built-in ship thermo-salinograph exists, its data should be recorded.
d) If the ship's bridge meteorological measurements are available on the vessel's computer network, they should be logged, and the instrument locations included in the metadata.
e) A copy of the bridge event log; this is particularly useful when investigating anomalous data, revealing if the ship was hove to (e.g., for a CTD cast) or maneuvering and creating flow distortion, stack exhaust problems, etc.

Table 1: Accuracy, precision and random error targets for SAMOS.

Parameter	Accuracy of Mean (bias)	Data Precision	Random Error (uncertainty)
Latitude and Longitude	0.001°	0.001°	
Heading	2°	0.1°	
Course over ground	2°	0.1°	
Speed over ground	Larger of 2% or 0.2 m/s	0.1 m/s	Greater of 10% or 0.5 m/s
Speed over water	Larger of 2% or 0.2 m/s	0.1 m/s	Greater of 10% or 0.5 m/s
Wind direction	3°	1°	
Wind speed	Larger of 2% or 0.2 m/s	0.1 m/s	Greater of 10% or 0.5 m/s
Atmospheric Pressure	0.1 hPa (mb)	0.01 hPa (mb)	
Air Temperature	0.2°C	0.05°C	
Dewpoint Temperature	0.2°C	0.1°C	
Wet-bulb Temperature	0.2°C	0.1°C	
Relative Humidity	2%	0.5 %	
Specific Humidity	0.3 g/kg	0.1 g/kg	
Precipitation	~0.4 mm/day	0.25 mm	
Radiation (SW in, LW in)	5 W/m^2	1 W/m^2	
Near surface:			
Sea Temperature	0.1°C	0.05°C	
Salinity	0.1 psu	0.05 psu	
Current	0.1 m/s	0.05 m/s	

Notes: The above accuracy estimates are based on the goal to determine H_{net} in equation (1.1) to within ±10 Wm^{-2} on the monthly to seasonal time scales appropriate for climate studies. The reader should recognize that they are nominal values which apply to typical marine weather conditions from the tropics to mid-latitudes. They cannot be expected to apply in unusual or extreme conditions. In the Arctic, for example, if the air temperature is -40ºC, it makes no sense to measure relative humidity to 2%. Calculated bulk turbulent heat fluxes can incur errors from uncertainties in the measurements of temperature and wind speed in extreme conditions. Consider the ±10 Wm^{-2} goal arbitrarily apportioned equally between radiative and turbulent fluxes. 5 Wm^{-2} accuracy in the turbulent fluxes is less likely to be met when wind speeds exceed 15 ms^{-1} and highly unlikely above 20 ms^{-1}. This level of accuracy is also difficult to achieve in conditions where the 10-m air-sea temperature difference exceeds ±3ºC. What happens in a 50-kt gale in the Labrador sea in January is anybody's guess. However, very strong wind and/or extremely large sea-air temperature or humidity differences are sufficiently rare that long term averages of the fluxes should fall within, or close to, the desired target. This topic is discussed further in Appendix B3.

QR2. Installation (Location and Exposure)

On an otherwise uniform and relatively flat ocean, the ship is an obstacle that distorts the wind flow and air temperature, and shadows radiometers and rain gages. Thoughtful location of sensors on the ship can minimize errors due to ship influence.

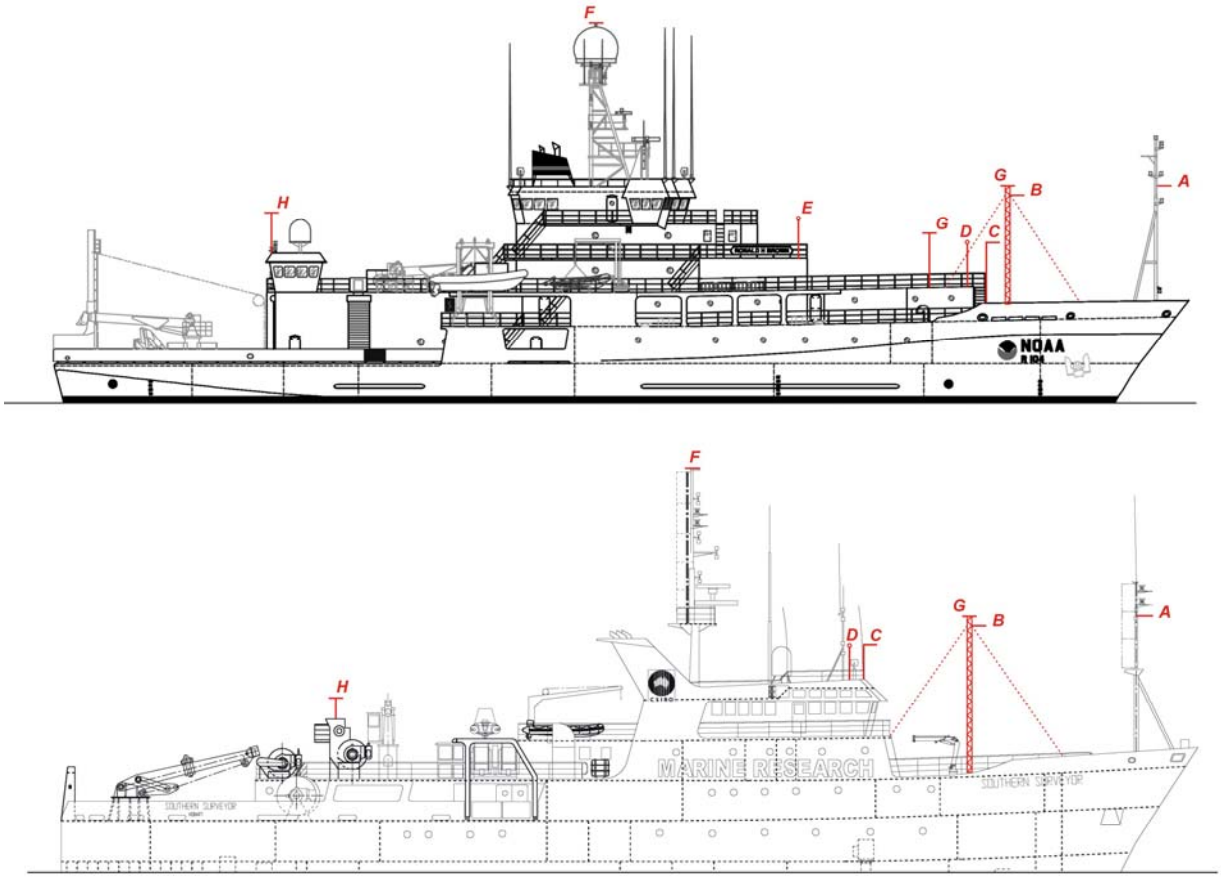

Figure QR1. Examples of ships with good foremast locations for instruments: R/V *Ronald H. Brown* (NOAA) and R/V *Southern Surveyor* (CSIRO). Locations A, B, etc., are described in the text.

Ideally, sensors should be exposed to the air before it has blown across the decks and superstructure. In Figure QR1, position A on a foremast is usually the best place for meteorological instruments. However, a tall enough mast may not exist or be unsuitable for regular climbing; on smaller ships such a mast may be swamped by seas over the bow. If practical and acceptable to the ship (operators, officers, technicians and crew), a guyed lattice mast could be specially installed on the foredeck for the instruments at B (see Figures QR1 and QR2).

A final option may be a pole above the wheelhouse at C in Figure QR1. This position will suffer from flow distortion and some thermal contamination from the foredeck, both of which will vary with relative wind direction. On the other hand, it provides better accessibility to instruments for maintenance, should this be an important issue. Location of instruments often

entails trade-offs and matters of judgment. If only one set of instruments is available, a forward facing support arm from A, B, or C will provide the best all-round exposure to relative wind. If two sets are provided, they should be installed on either side of the ship, at D or E for example, to improve exposure.

Figure QR2. Guyed mast installed on foredeck for good exposure of meteorological instruments.

In principle, radiation instruments need to be mounted so that surrounding objects do not cast shadows on them. On the restricted domain of a ship, this requirement is virtually impossible to achieve. For the two ships in Figure QR1, location F would serve, but such elevated sites are usually unsuitable because of prohibited access in rough weather, and proximity to RF antennae. Radiation instruments need careful leveling and regular attention to clean the domes. Compromise sites would be at G in the figure. At low viewing angles errors in the measurement are less important. Long- and shortwave instruments would normally be mounted as a pair on a rigid plate at the top of a pole attached, for example, to the rail around the wheelhouse roof. A gimbal mount would benefit the shortwave radiometer, but would need to be very carefully designed. If two sets of instruments are available, they should be widely separated to avoid coincident shadows.

For radiation instruments, but *not* those for wind speed or air temperature, a position well aft such as H may be used as a last resort, recognizing that the longwave signal may be significantly in error whenever the exhaust plume is above the pyrgeometer. More frequent washing of the domes may also be necessary to remove soot.

Barometers can be located within the bridge, a science lab, or can be mounted on a mast with other instruments. Whether inside or outside, it is important to ensure that the port for the barometer is located so as to avoid dynamic pressure fluctuations due to the wind, or if inside, free from a space that may be pressurised by, for example, air conditioning.

Rain gages are susceptible to wind effects that cause optical gauges to overestimate and funnel gauges to underestimate. The wind is deflected upwards when it encounters the ship, and

carries raindrops away from the funnel instead of falling in. The loss can be corrected to some extent providing the **relative** wind speed at or near the sensor is known. Thus, a location on the same mast as the anemometer is best.

If sea temperature is to be measured with a floating sensor, it should be trailed from the end of a light boom (or pole) as far forward and as far out as practicable, to avoid the bow wave.

Nearly all meteorological sensors, and particularly those for radiation, are susceptible to interference from the many sources of RF transmission aboard a ship. This should be borne in mind when locating the instruments, as noise in the signals can often be attributed to RF interference.

QR3. Documentation and Event Logging

The importance of documenting the location and serial numbers of all instruments deployed, and the date and time of any changes, cannot be overstated. Ideally, this should be an electronic document accompanied by digital photographs of the installation. The most useful photos are taken at sufficient distance to show the sensor in its environment, and possible obstacles to wind flow around it. A photograph from the wharf can also be helpful. This is also an opportunity to record the height of all instruments above the water, and above some ship datum (e.g., the deck below). Knowledge of instrument height is crucial for calculating bulk fluxes.

In addition, significant events that may affect the quality of the data should be recorded with the time in a daily log (e.g., cleaning radiometer domes, power failure, bird on anemometer). Information about the ship's speed, heading, position, etc., can be extracted from the link to the ship's network, but such eyewitness accounts are invaluable, particularly when trying to explain anomalous data.

QR4. Monitoring and Maintenance

The computer recording software should permit real-time display, in physical units, of the variables being logged. This may be as a list, a graphic display of time series, or both. This display should be monitored as part of a daily routine, and also from time to time as convenient. If paired sensors are installed, their values can be compared – if different by more than some amount (e.g., twice the specified instrumental accuracy), the reason should be sought. Whether a single or pair of sensors is installed, it is also useful to compare them daily with a handheld standard (e.g., an Assman psychrometer or portable barometer).

It is worth checking that the ship's navigation data are being recorded properly. A graphic display will also reveal anomalies in the measurements, such as spikes, noise, unreasonable values (e.g., air temperature (T) 75ºC, relative humidity (RH) 150%!). Such information should be logged and, as time permits, investigated. The first approach is usually to replace the sensor with a spare. If that does not solve the problem, replace the original and troubleshoot in the usual way.

The marine environment is hard on instruments mostly designed for use over land. Regular maintenance includes washing salt from radiometer domes, replacing the Gortex filter around humidity sensors, checking that the aspirator fan on the temperature/humidity instrument is working, that the rain gage funnel is not blocked (e.g., bird droppings). An expensive factory calibration intended to be valid for a year is useless if the sensor is crusted with guano.

Upward facing cable ties or metal spikes have been used to discourage birds from roosting on sensors, but with limited success.

QR5. Recording and Securing the Data

The computer date and time will be set to GMT (UTC) and the event log should also be referenced to GMT.

The recorded data will normally consist of the raw time series at the logger sampling speed, and a conversion to physical units via the instrument calibrations and transfer functions. This processing will often involve some computation involving several signals and sensors; for example, combining the three pyrgeometer signals for downward longwave radiation; or obtaining true wind from the measured relative wind and the ship's speed, course, and heading.

In many cases (SAMOS, for example), the meteorological data collected automatically by computer on the ship will be destined for use by scientists engaged in climate research elsewhere - modelers and analysts for example. The role of the shipboard operator is to maintain the quality of the data by monitoring the performance of the sensors, and making sure that all detail (e.g., time of radiometer dome cleaning, or a faulty instrument) is noted in the daily log. This individual should be provided with training to enable recovery of the system in the event of a computer crash; since extended time series are most valuable.

The capacity of the computer hard disc will be sufficient to hold several weeks' data, which should be backed up regularly according to normal computing practice. Every few days both raw and derived data should be written onto a CD or DVD, together with a copy of the metadata. If possible, an electronic copy should be made of the event log (e.g., in Word) and saved with the data and metadata.

Each vessel operator should establish a protocol for long-term archival of the meteorological observations with a national or international archive center. Data residing on a disk or tape in someone's desk drawer will not aid climate science, and the media will degrade with time. Archive centers are equipped, in most cases, to ensure the long-term viability of the data, event logs, and metadata on digital media. On a regular schedule, (at the end of each cruise, quarterly, etc.) all data and metadata should be forwarded to a national or international archive center.

FLUX MEASUREMENTS FROM SHIPS AND BUOYS

1. The Air-Sea Fluxes

1.1. *Introduction*

The dynamic coupling between the ocean and the atmosphere depends on the transfer across the interface of energy, momentum and freshwater. It is the fluxes of these quantities that we seek to determine experimentally from global networks of ships and moorings, to provide constraints on coupled models of the climate system, and for validation of similar observations from satellites. Producing these flux estimates will require measurements of traditional near-surface meteorological variables (wind speed, air temperature, humidity, water temperature) with more than sufficient accuracy to make them useful for numerous other applications.

The basic set of fluxes we consider are those of sensible and latent heat, of momentum (or wind stress), the shortwave and longwave radiative fluxes, and the freshwater flux.

1.2. *Turbulent fluxes*

Air-sea exchange of sensible heat (H_s), latent heat (H_l), and momentum (τ) occur predominantly by turbulent transport processes in the atmosphere. They are described by turbulence theory and may be obtained directly by measuring the fluctuating quantities and applying the covariance (or eddy-correlation) technique. This is a research tool, as yet unsuitable for routine use, which will not be discussed in this manual; rather, we will consider the bulk flux parameterization of the turbulent fluxes. When the situation changes, the manual will be updated accordingly.

1.3. *Radiative fluxes*

Shortwave fluxes are in the wavelength band 0.3 to 3 μm. Downwelling shortwave radiation at the surface ($R_{s\downarrow}$) has a component due to the direct solar beam, and a diffuse component scattered from atmospheric constituents and reflected from clouds. Upwelling shortwave radiation ($R_{s\uparrow}$) comes from reflection at the surface and the re-emergence of radiation backscattered from the upper ocean. In clear water, shortwave radiation penetrates to a depth of several tens of meters, influencing the thermal structure of the ocean surface layer. The ratio of downwelling to upwelling shortwave is the surface albedo (α), which depends on solar elevation, cloudiness and wavelength. For use in bulk algorithms, a single value of 0.058 for *broadband* albedo, based on the ratio of daily averaged upwelling and downwelling shortwave flux, has been found to be satisfactory.

Longwave fluxes range from 3 to around 50 μm wavelength. Downwelling longwave radiation ($R_{l\downarrow}$) originates from the emission by atmospheric gases (mainly water vapour, carbon dioxide and ozone), aerosols and cloud droplets. It is thus linked quite closely to the particular regional climate conditions. Upwelling longwave from the sea surface $R_{l\uparrow}$ depends on the ocean skin temperature and surface emissivity (ε), with a small contribution due to reflection of the downwelling component. Emissivity is wavelength-dependant, and a spectrally integrated value of 0.97 is commonly used. Longwave absorption and emission take place in about the top 0.5 mm of water.

1.4. *Freshwater flux*

The vertical density structure of the ocean surface layer determines its stability and mixing, which in turn has consequences for the transport of heat to and from the interface. Density is a function of both temperature and salinity, so that the freshwater exchange through evaporation (E) and precipitation (P) is an important component of the coupled system.

1.5. *Net surface fluxes*

The fluxes described above are illustrated in Figure 1.1. They are measured individually, and required separately to study various atmospheric processes. The *net* surface heat and freshwater fluxes are important quantities that prescribe the evolution of the coupled ocean/ atmosphere system for use in climate models. The net heat flux **into** the ocean surface is given by

$$H_{net} = -(H_s+H_l) + (R_{s\downarrow} - R_{s\uparrow}) + (R_{l\downarrow} - R_{l\uparrow}) - H_{rain} , \qquad (1.1)$$

where the second and third terms on the right-hand side are the net shortwave and longwave radiative fluxes, and the fourth term is the small heat contribution from rainfall (see section 2.8). H_{net} is the quantity for which the WOCE and TOGA accuracy goals of ± 10 Wm^{-2} were proposed, on monthly to seasonal time scales.

The net freshwater exchange (P-E) is usually expressed as mm of water in unit time. Note that E is H_l divided by the latent heat of vaporisation (see Appendix A).

2. Basic Variables Input to Bulk Flux Algorithms

2.1. *Introduction*

Bulk air-sea flux algorithms are generally of the form $F_x = C_x u(\delta_s - \delta_z)$, where F_x is the vertical flux of entity x (heat, moisture, momentum), u the wind speed, and δ the value of the corresponding meteorological variable (temperature, humidity, wind speed). Subscripts s and z refer to the value at the sea surface and at height z, so the quantity in parentheses is a sea-air difference of the particular variable, which depends upon the height of measurement. It is therefore common practice to refer all measurements to a "standard height" (usually 10 m above the sea surface), using knowledge of the vertical profile of the particular variable. C_x is an empirical transfer coefficient for entity x, determined from direct measurement (e.g., by the covariance method) and specified at the standard height. More detailed information on this subject is given in section 11.

Given a reliable value or functional form for C_x, the observational accuracy of F_x depends on the other quantities on the right hand side of the equation. In modern algorithms these will not necessarily be the values as measured; as discussed below, they may have been corrected for known error, reduced to standard height, or combined with other physical quantities. The required data set will consist of the state variables (temperature, humidity, and pressure), wind speed and direction, the radiative fluxes, and sea temperature at some specified depth.

The target net heat flux accuracy of ± 10 Wm^{-2} implies certain accuracies for the measured variables, as shown in Table 1, and discussed in Appendix B3. The TOGA-COARE process study demonstrated that, even for the research-quality instruments installed on survey vessels, these accuracies are only achievable with very careful attention to instrument location and performance, calibration and post-cruise scrutiny (details and references can be found in WCRP 2000). We consider some issues with the measurement of each variable:

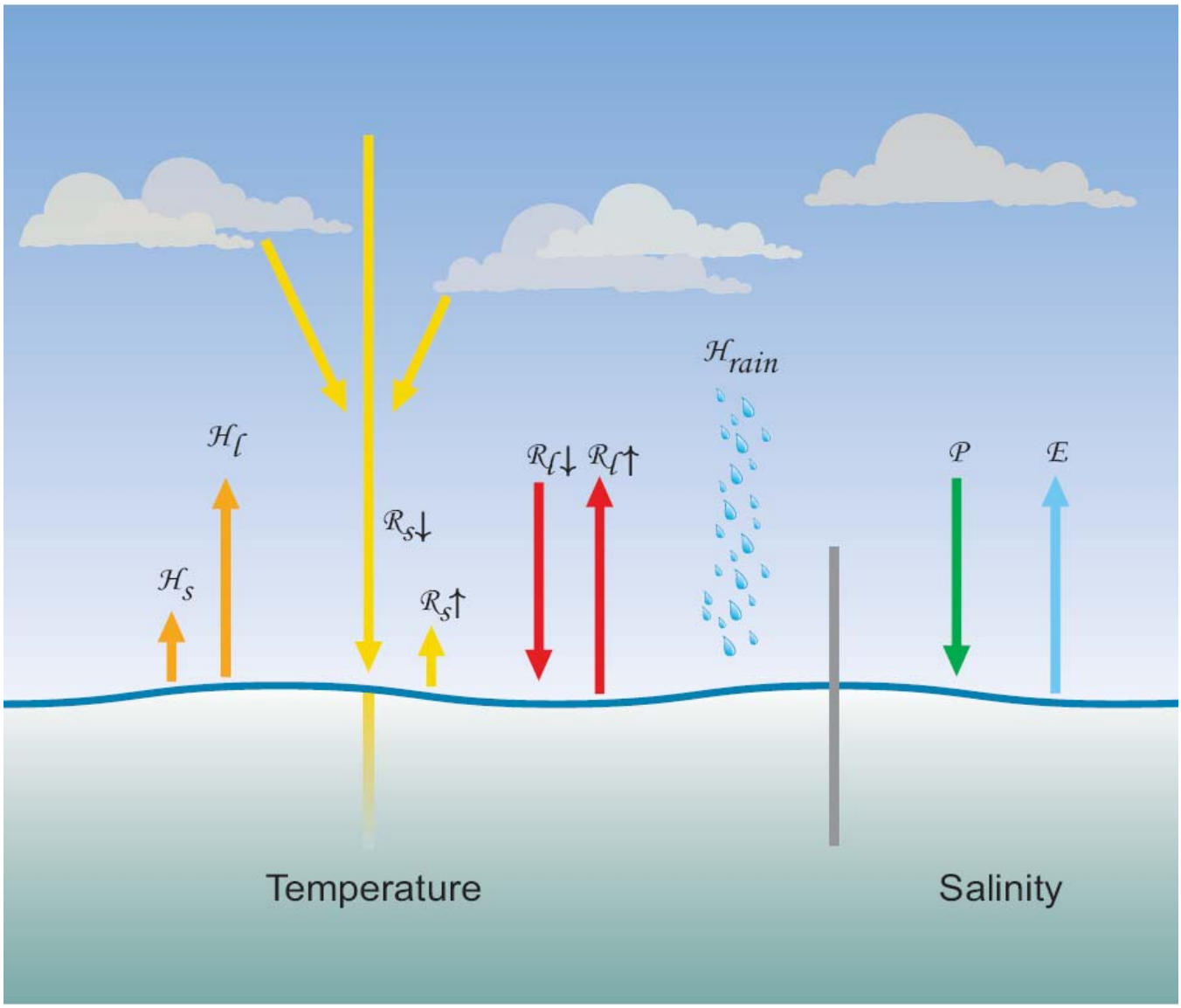

Figure 1.1. Schematic showing the net surface energy balance at the sea-air interface. H_s and H_l are the turbulent sensible and latent heat flux, R_s and R_l the shortwave and longwave radiative fluxes (upward or downward according to the arrows), H_{rain} the sensible heat contributed by rain, *P,* precipitation and *E,* evaporation. The gray bar separates heat and freshwater components.

2.2. *Air temperature*

The most usual causes of error in air temperature measurement are sources of anomalous heating; the sun and the ship. The temperature sensor is often installed within an enclosure that shades it from the sun but which relies on natural ventilation, i.e., through slots in the sides of the enclosure, as shown in Figure 2.1 (left). These may be effective in overcast conditions or strong winds; but in light winds and strong sun, the temperature in such a simple housing has been shown to rise several degrees above the true air temperature. To achieve the accuracy cited in Table 1, the sensor element must be within a specially designed, shielded and ventilated enclosure such as the one illustrated in Figure 2.1 (right). Even such an arrangement is ineffective if the system is poorly located. The ship itself is a massive source of heat, and

almost any location aft of the bow will measure air that has passed over some area of warm steel. Usually, the best location is high on a foremast (e.g., A in Figure QR1), if one exists. Experiments that rely on continuous and accurate measurement of air temperature (and other meteorological quantities) will often duplicate instrument packages on port and starboard, taking data from the sensors most favourably exposed to the wind. Even so, the wind will sometimes be directly over the stern of the ship and the data will have to be discarded. Thus, relative wind direction is a critical part of the data record.

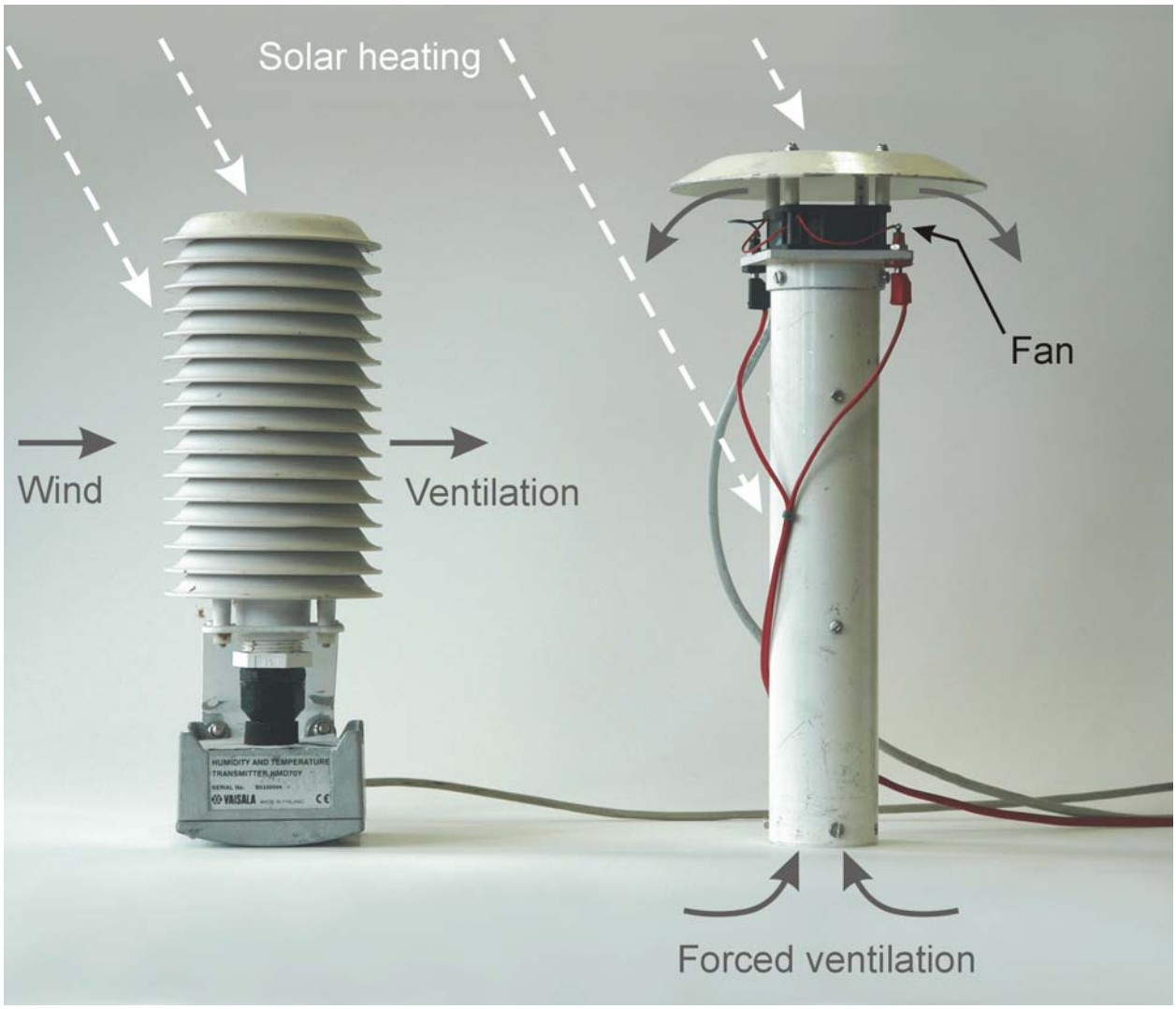

Figure 2.1. Temperature/humidity screens; left with natural ventilation; right with double screening and forced ventilation.

2.3. *Humidity*

Atmospheric humidity is variously specified by the partial pressure of water vapour (e, mbar or equivalently hPa), vapour density (ρ_v, gm^{-3}), specific humidity (q, g/g of moist air), mixing ratio (r_v, g/g) or relative humidity (RH=100 e/e_s) where e_s is the saturation vapour pressure at air temperature T_a. At a particular ambient humidity, reducing air temperature reaches the point where e equals e_s. This is known as the dew-point T_d. Formulae to convert

between these various definitions of humidity are given in Appendix A, as are empirical equations for e_s as a function of T_a.

Humidity sensors in common use are described in section 3.3. Depending on the particular measuring principle the output may be any one of the above definitions of humidity. Some sensors are more suited to use at sea than others, and most need periodic maintenance to remove salt deposited on the sensor or the filter provided to protect some sensors. Some systems combine air temperature and humidity sensors in the same package, so they are subject to the same conditions of ventilation and screening from solar heating. Conversion between some forms of humidity, for example from *RH*, requires the temperature of the air surrounding the humidity sensor. Since water vapour is a conservative quantity, the corresponding error in the water vapour measurement is less severe than an error in temperature when the latter is obtained from the collocated sensor.

2.4. *Atmospheric pressure*

Pressure is one of the state variables which define the thermodynamic properties of the atmosphere. It varies with elevation above sea level and slowly with synoptic weather changes. The World Meteorological Organization (WMO) target accuracy for pressure measurement is ±0.1 mb. In boundary layer and climate studies, pressure most commonly appears in the calculation of dry and moist air density (needed for air-sea flux calculation), and in humidity conversions; it also appears in the psychrometer equation (see Appendix A). Under "normal" synoptic conditions (i.e., no hurricanes or severe storms), pressure at sea level lies between about 990 and 1030 mb, with a diurnal variation (the atmospheric tide) of around ±3 mb in the tropics, less at higher latitudes. Relative to "standard" sea level pressure of 1013.25 mb, the above range typically represents a ±2% difference in air density or specific humidity. Pressure near the surface varies with height by roughly 0.1 mb per metre, so overall it's seldom the most severe source of error in flux calculation, providing the barometer is installed in such a way as to avoid the effects of dynamic pressure. With increasing demands for accuracy in climate applications, it is wise to include the measurement of pressure and to document the actual location of the barometer.

2.5. *Wind speed and direction*

Accurate wind data are important because, as shown above, the fluxes calculated using a bulk algorithm are directly proportional to the wind speed. Thus, any error in wind speed will carry through to the latent and sensible heat fluxes. For momentum flux (or wind stress), the difference term ($\delta_s - \delta_z$) represents the wind speed *relative to the surface*, so the flux is proportional to u^2. In fact, it increases rather faster than the square of the wind speed, because the exchange coefficient for momentum also increases with wind speed. Wind stress is also an important factor in determining the atmospheric stability, again affecting both scalar and momentum fluxes. The need for care in determining true ambient wind cannot be emphasized too strongly. As indicated in section 5.2, the location of the wind/direction sensors is critical to minimise errors caused by wind flow distortion around the ship.

Wind speed and direction are taken together, partly because they are often both obtained from a single instrument, but also because they are measured relative to the ship and must be combined with the ship's heading, course, and speed to arrive at the true wind vector (the correct equations with which to combine these vectors are given in Appendix A). The demands on

accuracy of the ship's velocity are therefore equivalent to those of the anemometer measurement, a fact not always appreciated. It is thus necessary to record the ship's navigational data stream together with the meteorological data, and to document whatever information is available on the accuracy of the various components. The appropriate wind speed to use in bulk flux algorithms is that relative to the ocean surface; i.e., taking account of the surface current. This introduces another source of uncertainty, because the water velocity at the interface itself is very seldom measured. There are two ways in which conversion from relative to true wind can take some account of the surface velocity: by combining the ship motion in Earth coordinates (e.g., from GPS) with currents from the ship's ADCP, or by using the Döppler-log/gyro which measures the ship's motion through the water. Data reports should indicate which method has been used; both incur additional sources of instrumental error, and furthermore the measured currents are at considerable depth (of order 10 m). Fortunately, in many cases current is a small fraction of the wind speed, so its contribution to the error is also small, but in light winds it can be significant.

2.6. *Sea surface temperature*

Historically, sea surface temperature was understood to be the temperature measured from a ship by whatever means available, and reported as SST irrespective of the depth of measurement. We now know that temperature in the ocean surface layer can vary with depth by an amount that is significant in the context of accurate bulk flux determination. It is the temperature of the sea-air interface itself that physically determines the magnitude of the turbulent heat fluxes and also the outward flux of longwave radiation. At the same time, these fluxes produce a cooling at the interface, the so-called "cool skin" of order 1 mm thick and typically a few tenths of °C.

In moderate to strong winds the water below the skin will be well mixed, and its "bulk" temperature will vary little in the vertical. During the day, however, penetration and absorption of solar radiation can produce a diurnal warm layer below the cool skin. Under clear skies and with light winds, as found in tropical oceans, this layer may be a few °C higher than in the bulk below. "Sea surface temperature" may thus vary with depth, as shown in Figure 2.2, and for the purposes of flux calculation, the temperature value should always be accompanied by the depth at which it was measured (e.g., $SST_{(d)} = 18.3^{o}_{(4.5\ m)}$). As indicated in section 3.6, this depth can be ambiguous. The characteristics of the ocean surface mixed layer are discussed in Price et al. (1986), and the physics of the cool skin and diurnal warm layer is given in Fairall et al. (1996a).

Traditional bulk transfer coefficients have usually been determined using a bulk sea temperature. However, newer algorithms use transfer coefficients determined with respect to the interface value. The true interface temperature cannot be measured with present technology, but the measurement of an infrared radiometer (at a few μm depth) comes close; and is sometimes available from shipboard or satellite sensors. Also, models of both the cool skin and diurnal warm layer, which enable skin temperature to be estimated from a bulk measurement at known depth, are becoming more reliable.

The TOGA program specified an accuracy of ±0.3ºC for SST over a 2 x 2 degree region as a target for validation of space-borne radiometers (WCRP 1985). An error of 0.3ºC changes sensible and latent heat fluxes calculated with a bulk flux algorithm by 2 Wm^{-2} and 10 Wm^{-2} respectively, for typical climatic conditions in the tropics. The past decade has seen the development of several high-resolution infrared radiometers for shipboard deployment that achieve 0.1ºC accuracy.

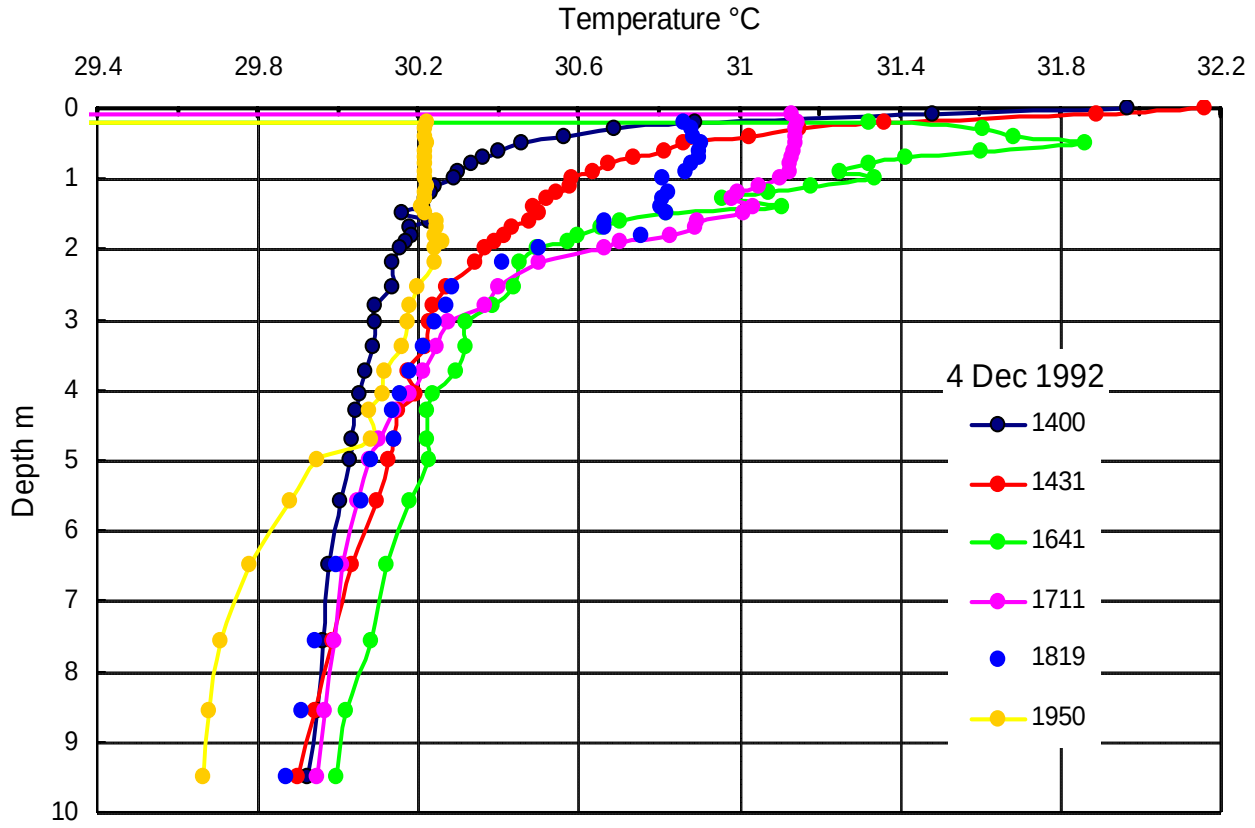

Figure 2.2. Profiles of sea water temperature measured during the TOGA COARE program with a near-surface undulating towed sensor, known as Seasoar. The different symbols denote the (local) time of the profile. The strong temperature increase near the surface is caused by solar heating. Later in the afternoon, the surface mixing is eroding the warm layer.

2.7. *Radiation*

Besides direct application in equation (1.1), the net radiative fluxes ($R_{s\downarrow}$- $R_{s\uparrow}$) and ($R_{l\downarrow}$- $R_{l\uparrow}$) are also used in bulk algorithms for models of the oceanic mixed layer temperature profile and to estimate SST. For these reasons they are increasingly being measured routinely aboard ships and moorings.

On a clear day at low and middle latitudes, $R_{s\downarrow}$ is the dominant component of surface heating, peaking in the vicinity of 1000 Wm^{-2}. Thus, any deterioration in performance of the measuring instrument can lead to significant error in determining the net flux, and the thermal and density structure of the ocean mixed layer. Studies of cloud-radiation interaction, currently in their infancy, will need to distinguish between the direct and diffuse components of $R_{s\downarrow}$.

Over tropical oceans $R_{l\downarrow}$ is determined largely by very high humidity in the boundary layer, with little diurnal variability or effect from clouds (typically $R_{l\downarrow}$ ~350-400 Wm^{-2}); at higher latitudes and under clear skies, $R_{l\downarrow}$ is significantly lower. The warm water of the tropics can emit 450 Wm^{-2} of thermal energy, cooler waters of higher latitudes correspondingly less. ($R_{l\downarrow}$- $R_{l\uparrow}$) is therefore the difference of two fairly large quantities, and typically of order 50 Wm^{-2}.

Accurate measurement of both $R_{s\downarrow}$ and $R_{l\downarrow}$ requires an unobstructed hemispheric view of the sky, which is virtually impossible to achieve onboard ship while retaining access to the instruments for maintenance. In the case of $R_{s\downarrow}$, shadowing by the highest parts of the ship, masts, funnel, antennae and the like, is the main difficulty. Instrumental problems have plagued the measurement of $R_{l\downarrow}$ for some years, partly associated with the fact that sources of thermal radiant energy are ubiquitous. These issues are dealt with in detail in sections 3.7, 6.6, and Appendix C.

2.8. *Precipitation*

Rainfall, particularly during convective storms, is perhaps the "patchiest" of all meteorological variables. Single point measurements from ships and buoys are generally less relevant for climate models than area-averaged values or spatial characteristics. Nevertheless, accurate point measurements over the ocean are invaluable for validating satellites and radar which *do* obtain spatial rainfall patterns, but must be calibrated against ground truth. Currently such validation is mostly obtained from rain-gauges located on islands and atolls, which have been found to distort the rainfall field.

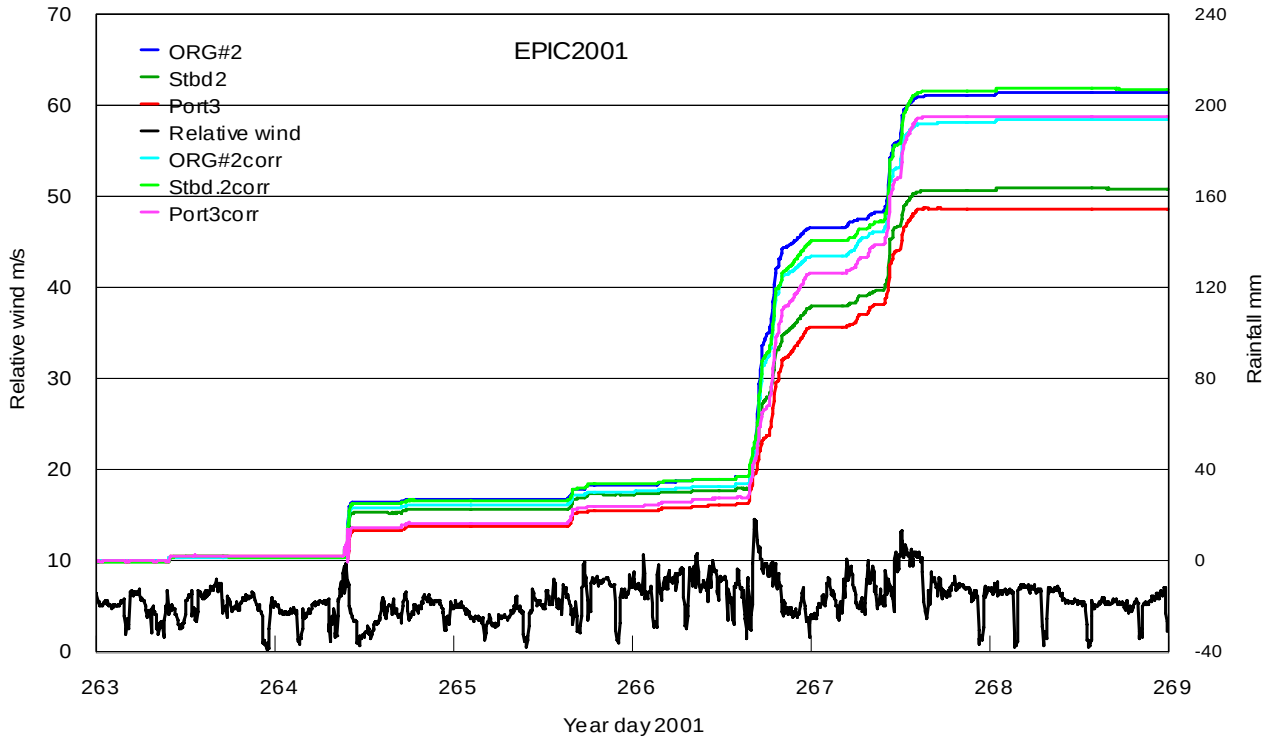

Figure 2.3. Cumulative rainfall measured by optical and funnel rain gages on a ship, before and after wind correction. The ORGs overestimate slightly when the raindrops are blown through the optical path at an angle to the vertical (dark and light blue traces). Siphon gauges underestimate when strong winds are distorted up over the ship and deflect raindrops away from the funnel (dark and light pairs of red and green traces). The black curve is the relative wind speed. Rainfall events started around days 264.4, 265.7, 266.6, and 267.3.

The main problem in measuring rainfall from ships (and to a lesser extent from buoys) using the traditional funnel gauge is error due to wind flow distortion that can lead to under-estimation depending on the location of the gauge. The problem has been studied, using an array of gauges distributed around the ship, and correction schemes devised which can improve the accuracy of rain measurement, to within 10-15%, as shown in Figure 2.3. Operationally, it is important to ensure the rain gage is well exposed and near the location where relative wind speed and direction are recorded. A well-positioned gauge adjacent to a wind instrument is better than several gauges scattered around the ship. The range of rainrates observed, from drizzle registering less than 1 $mmhr^{-1}$ to tropical storms producing 200 mmh^{-1} (often accompanied by strong winds) also presents challenges for rain-gauge design (see section 3.8).

As shown in equation (1.1), the net air-sea heat flux includes a component of sensible heat from rainfall. Heat exchange with the ocean can be calculated from the rain rate and the temperature of raindrops, usually assumed to be close to the wet-bulb temperature at sea level. In the case of tropical deep convection it has been found that raindrops are about 0.2ºC cooler than this temperature. Over extended periods, the contribution is small, but during heavy storms it can be several hundred Wm^{-2} and a significant component of a daily average net flux (Figure D2). Note that the momentum flux imparted to the ocean by raindrops may also be non-negligible.

3. Bulk-Flux Meteorological Sensors

3.1. *Introduction*

In this section we consider the types of sensors in common use at sea for measuring atmospheric temperature, humidity, wind speed, pressure, and sea temperature. The sensor is the part of a measuring instrument that is directly exposed to the entity being measured, and whose characteristics respond in a predictable way to changes in that entity (e.g., resistance of a platinum wire to temperature). Other important components of the measuring system are the sensor housing and any associated electronics or recording equipment. These sensors have been developed mainly for observations over land, and their use on ships and buoys has required some adaptation. At the very least they need protection from the highly corrosive environment of salt air and spray, which usually means that the housing has to be specially designed for marine applications. It may also be important to take account of platform motion, and systems on long-term moorings may need modification for low power consumption. Sensors evolve continuously in the research and commercial environment; for use in either testing new physical principles of measurement or to quantify some newly significant entity (e.g., a trace gas transferred across the air-sea interface), and with the advance of measurement technology.

There are often several choices of sensor for each variable, the most suitable for a particular application depending on several factors, including the required accuracy and resolution, frequency response, and overall convenience of operation. Atmospheric variables fluctuate on time scales from below 0.1 seconds to several hours. Rapid sampling, typically at 20 Hz or more, is required to obtain the turbulent fluctuations of wind, temperature and humidity for eddy correlation or inertial dissipation determination of the fluxes. These methods are not considered in this handbook, in which we focus on the observations required to calculate *bulk* fluxes. A sensor responds to a step change exponentially, the time taken to reach $1-1/e$ (≈ 0.632)

of the final value being its *time response*. By virtue of their mass, most bulk sensors have a time response of many seconds, and to avoid aliasing are sampled at about once per second. The resulting data are then time-averaged over suitable periods from a few minutes to one hour to reduce unsteadiness. We note, however, that some fast-response instruments (e.g., sonic anemometers) have become sufficiently stable that, if deployed for other purposes, they can also provide reliable long time averages.

3.2. *Temperature*

Sensors commonly used to measure atmospheric temperature are thermocouples, platinum resistance thermometers (PRTs), thermistors, and mercury-in-glass thermometers. The latter are still used operationally in handheld instruments such as Assman psychrometers and the sling thermometers used by observers who file ships' weather reports, as well as in some fixed thermometer screens. Accuracy depends on the quality of the thermometer and the care with which the observer reads it. High-quality Assman thermometers can be read to 0.1°C. Being free from instrumental errors, their value in the present context is to verify data from the electronic measuring systems installed on the ship by taking careful "spot" readings at a location free from ship influence (Figures 3.1 and 3.4).

The other three types of sensors lend themselves to automatic, continuous data logging. Thermocouple systems have the disadvantage of low output voltage, and for absolute measurement require a reference "cold" junction. Good-quality PRTs are very stable, and with careful calibration, accuracy of about 0.01°C can be achieved, although their typical resistance of 100 ohms requires a high-resolution resistance bridge. PRTs are the temperature sensors most commonly used in high-quality commercial instruments. Both thermocouples and PRTs can be easily configured for differential measurement, which can improve the measurement accuracy of the wet bulb depression when they are used in a psychrometer (see next section).

Thermistors are semi-conductor devices with much higher resistance values (typically 3000 ohms) than PRTs, making the measurement of resistance changes easier. Unlike the linear response of PRTs, the larger signal comes at the expense of nonlinearity. Formerly, they were prone to uncertainties of stability and calibration, but guaranteed interchangeability of ±0.1°C is now available from some manufacturers, and micro-processor technology enables their logarithmic response to be linearized.

Radiometric air temperature sensors are just starting to be used (Minnett et al. 2005) and are likely to become more common in the future. Being non-invasive, they have some advantages over traditional methods but validation against high-quality *in situ* air temperature measurements have yet to take place.

3.3. *Humidity*

The traditional instrument for atmospheric humidity measurement is the psychrometer, consisting of a pair of thermometers, one being covered with a moist wick. Air drawn over the thermometers evaporates the moisture, cooling the wick until the evaporation rate is in equilibrium with the atmospheric water vapour. This *wet bulb depression* is understood from thermodynamic theory, and described by the psychrometer equation given in Appendix A. Handheld sling or Assman psychrometers use mercury-in-glass thermometers, the former achieving ventilation by rapid movement through the air, while the Assman is equipped with a spring-wound or electrically driven fan which draws air over the thermometer bulbs. The basic

accuracy of 0.1ºC for both wet and dry bulb thermometers leads to an uncertainty of 0.20 g kg^{-1} in specific humidity or bout 1% in *RH*. To achieve this, the wick must be moistened (but not flooded) with distilled water, washed from time to time to remove salt, and changed after a period of use.

Figure 3.1. Measuring wet and dry bulb temperatures with an Assman ventilated psychrometer. The use of the forward chock as a sampling location ensures good exposure and some shielding from the sun.

For automatic data logging, psychrometers can be constructed using either PRTs or thermocouples as the sensing elements. Accurate measurement requires adequate airflow over the thermometers to ensure full wet bulb depression, and that they be well shielded from solar radiation. This is best achieved by using a double heat-reflecting shield, as illustrated in Figure 2.1 on the right, with the air drawn over it *and* through the space between the shields at a rate of at least 4 ms^{-1}. With PRTs in a differential bridge, temperature resolution of ±0.01°C is possible, and with care, specific humidity accuracy of 0.05 g kg^{-1}.

Most ships are provided with a pair of wet and dry thermometers in a naturally ventilated screen, which are read by the bridge officers for the bridge log, and in the case of ships participating in the Voluntary Observing Ships (VOS) program, for the hourly weather observations transmitted to shore. The example shown in Figure 3.2 is in a well-exposed location, but the screen design is poor leading to inadequate ventilation of the wet and dry-bulb

thermometers. In sunny conditions the temperature inside the box could be several degrees above ambient and the air-flow through the box is insufficient to achieve the full web-bulb depression and thus overestimate the humidity. Observations from this unit during mostly overcast

Figure 3.2. Example of the installation of wet and dry bulb thermometers.

Figure 3.3. A more usual type of screen to house the wet and dry bulb thermometers read hourly by the bridge officers. It is also well exposed, and all four sides are louvered to allow free airflow to the thermometers.

conditions are given in Figure 3.4. The more usual type of screen, with louvres all round to improve air flow to the thermometers is shown in Figure 3.3. Nevertheless, under clear sky with light winds even this screen could become much warmer inside than the ambient.

Thin-film polymers which absorb or desorb water as the relative humidity changes are the most common humidity sensors currently used on research vessels at sea. Early versions of these sensors often failed at very high humidity, but recent developments have largely overcome this problem and improved their accuracy and stability of calibration. The polymer usually forms the dielectric of a capacitance in a circuit that provides an electrical output proportional to relative humidity. Conversion to mixing ratio, specific or absolute humidity requires the temperature of the air surrounding the dielectric, often using a collocated PRT. The best quoted accuracy is ±2% *RH* (or ±0.3 g kg^{-1} at 20°C and 70% *RH*). For accurate measurement these temperature/*RH* sensors are ventilated and screened as for the psychrometer. There is also a Gortex filter around the sensing element that must be changed or washed to remove salt.

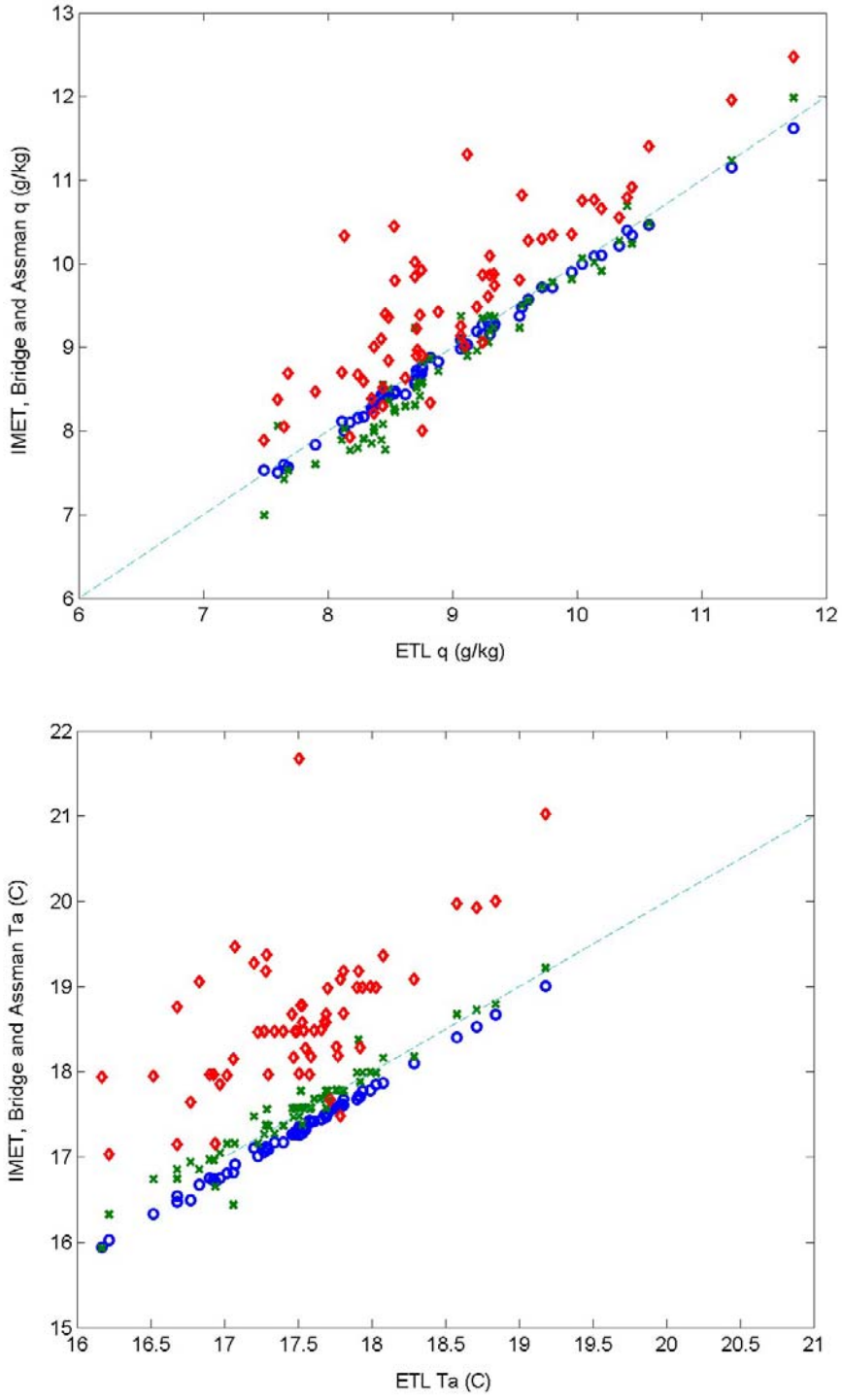

Figure 3.4. Comparison between a high quality T/RH sensor used by ESRL (formerly ETL) and: (green crosses) an Assman psychrometer; (blue circles) the ship's IMET system; (red diamonds) the wet and dry bulb thermometers read by the bridge officers hourly for their weather reports.

The dew-point hygrometer incorporates a mirror that is maintained, by optical and electronic feedback, at the temperature, T_d , where moisture or ice just condense on its surface. Using the relationships in Appendix A, this dew point can be converted to any of the other units. It is an absolute instrument, not well suited for operational use at sea, but often carried as a secondary standard to calibrate other sensors. Best-quoted accuracy for a dew-point instrument is ±0.2°C, which converts into an uncertainty in *RH* of ±1%.

Humidiometers that measure the absorption of ultraviolet (Lyman-α) or infrared radiation by water vapour respond to rapid changes in humidity and are used for eddy-correlation flux measurement. Currently they are not sufficiently stable to be suitable for routine measurement of long time series.

3.4. *Atmospheric pressure*

Ships monitor atmospheric pressure routinely to include in their daily weather reports, transmitted on the Global Telecommunication System (GTS) for use by national weather forecasting institutions. The barometer is normally located on the bridge. The proper installation and operation of mercury barometers at sea has proven very difficult, and they are now rarely used aboard ships. Modern aneroid barometers with a digital readout have a resolution of 0.1 mb and are relatively stable, but require checking against standard instruments from time to time. However, for applications requiring continuous time series of pressure to be recorded, solid state sensors with high resolution and long-term stability of 0.1 mb are now available. Whether they are located inside the wheelhouse or outside, it is important to ensure that the port for the barometer is located so as to avoid dynamic pressure fluctuations due to the wind, or if inside, free from a space that may be pressurised by, for example, the ship's air conditioning. Special inlet ports designed to overcome dynamic pressure fluctuations from the wind are available, for connection to the barometer via a plastic tube.

3.5. *Wind speed and direction*

For average wind speed and/or direction over some time period, cup (or propeller) anemometers and wind vanes are usually the most convenient. Some operational designs will withstand continuous exposure to stormy conditions, but there are also more sensitive instruments intended for research work. Apart from mechanical strength, the difference is reflected in their starting speed and distance constant (response time converted to run of wind). A sensitive cup anemometer will start from rest in a breeze of 0.3 ms^{-1} and have a distance constant less than 1 metre.

For best accuracy (typically 1%), cups must be calibrated individually, although calibration in the steady horizontal flow of a wind tunnel can be misleading when the instrument is exposed to the natural fluctuating wind. In such a situation, cup anemometers usually overestimate for two reasons; the rotor responds more quickly to an increasing wind than to the reverse; and in a wind gust with a vertical component, shielding by the upwind cup is reduced. Numerous studies have been made of these effects. Propellers have poor response to off-axis wind direction, but this is normally overcome by mounting them on the front of a wind vane. The one instrument thus measures both wind speed and direction. Otherwise, a cup anemometer/wind vane pair is often mounted at opposite ends of a horizontal bar. Ideally, the wind direction sensor should have a complete 0 to 360˚ response. However, some instruments use a potentiometer that has a finite deadband (≤10°), in which case care must be taken to ensure

that readings in this deadband are infrequent and do not corrupt the average reading. The orientation of the 0/360 degree transition relative to the centreline of the ship is an important item of metadata, to ensure correct calculation of true or ocean-relative winds.

As noted above, sonic anemometers, which are commonly used for fast-response applications in the research environment, have become sufficiently stable to enable observation of long time series. They have many advantages: they have no moving parts; less distortion to the wind flow than cups or propellers; they obtain the total wind vector; and some have an air temperature output. Sonic anemometers are likely to become more widely used at sea as the more robust, and less costly, models appearing on the market prove their suitability and gain acceptance.

3.6. *Sea temperature*

The so-called "bucket" sea temperature is aptly named. An open cylindrical container, usually insulated and equipped with a mercury-in-glass thermometer, is attached to a line and cast from the after deck to collect a sample of water. Allowing for some change during the time it takes to read the thermometer, this procedure produces spot values of a well-mixed sample of surface water every hour or so, probably to an accuracy of 0.5ºC depending on atmospheric conditions. As described in section 2.6, this frequency and accuracy are no longer adequate for the calculation of research quality air-sea heat fluxes; furthermore, disturbance by the ship makes it uncertain what depth the sample represents. Some of the errors in bucket measurements of sea temperature are predictable and can be corrected, and routine bucket temperatures from VOS still form an important part of the climatic record.

On some research vessels, a thermosalinograph measures the temperature of engine cooling water near the intake port. The basic accuracy of the instrument is a few 0.001ºC and the flow sufficiently large that spurious heating from inside the ship is not significant. The depth of the intake is known but it is usually well aft. It has been found that, because of the pattern of flow along the hull, the water entering the intake may have originated from some shallower depth ahead of the ship. With a well-mixed surface layer, at night for example, the difference may be small, but in daytime if there is a significant vertical temperature gradient near the surface due to light winds and solar heating, it can be several tenths of a degree.

A better arrangement is when the thermosalinograph has its own intake port and pump near the bow of the ship. There is still some uncertainty about the effective depth of measurement, particularly with the ship pitching in heavy seas when there is also the danger of the intake breaking the surface. Often the thermosalinograph is turned off in port and in some coastal conditions to prevent fouling of the sensors by oil and other contaminants.

Another class of sensors is attached inside the hull of the ship and these sensors measure some sort of average temperature over the surface layer, providing they are located well below the water line.

Some research cruises measure sea temperature close to the surface by trailing a sensor (usually a thermistor) mounted at the end of a length of plastic hose, or a rope with an internal conductor. One type is known as a "Seasnake". It is towed from a light boom near the bow of the ship and extends as far out as practicable, preferably outside the bow wave. Underway in slight seas, the hose will follow the surface at a depth of 5-10 cm, but in heavier seas will often become airborne. This can be overcome to some extent using streamlined weights.

Comparisons with ships' thermosalinographs at night, and when the surface layer is well mixed to a considerable depth, indicates that the Seasnake is capable of 0.1ºC accuracy. During the day it captures nearly all the daytime surface warming, but is below the cool skin regime. In persistent stormy conditions it may have to be brought inboard and stowed to prevent its destruction. When the ship stops, it normally sinks, even if not weighted, but under these conditions the water temperature is contaminated by the ship in any case.

During the past decade, a number of high-resolution infrared (IR) radiometers have been developed for use at sea. This instrument is normally mounted forward on a siderail of the ship, high enough to view the sea surface outside the bow wave. Its view is a narrow cone operating within spectral bands in the range 8-12 μm, similar to the channels of space-borne IR radiometers. The view angle to the undisturbed surface will depend on the geometry of the ship, and is usually between 30º and 60º to the vertical. SST is obtained from the measured radiance and surface emissivity, which is a function of view angle, and a correction made for reflected sky radiation using a second radiometer pointed skyward at the same angle (which is covered during rain). Depending on sky conditions and atmospheric water vapour content, this correction can vary from near zero to at least 1ºC. Some instruments self-calibrate the radiometer sensor using internal blackbody targets at different temperatures. The most sophisticated examples of this type of instrument claim SST accuracy of 0.1ºC. However, combined with estimates of the cool skin from recent models, a Seasnake is the more economical option.

3.7. *Radiation*

Because of its dominant role in the Earth's energy budget, much attention has been given to the study of solar and terrestrial radiation components, their intensity, spectral characteristics and distribution. In the course of this, accurate instruments and methodology have evolved, often requiring precise directional pointing, meaning that they can only be operated from a completely stable platform. This requirement precludes their routine deployment from ships and moorings. The following describes instruments currently suitable for marine studies.

Downwelling shortwave and longwave radiation are measured with a pyranometer and a pyrgeometer, respectively. These instruments are physically similar, both accepting broadband, whole-sky radiation through a hemispherical dome with the relevant spectral transmission characteristics (Figure 3.5). Solar radiation passing through the glass dome of the pyranometer impinges on a flat thermopile with a blackened upper surface. The instrument is so constructed, using two concentric domes to overcome convection within the instrument, that the thermopile output has a linear response to the radiative intensity. Accuracy of the instrument is usually quoted as 2%. The pyrgeometer works by determining its own thermal balance, combining the contributions from dome and case temperatures with longwave radiation through the silicon dome which is detected with a thermopile. There are thus three output signals to be recorded and combined externally using the pyrgeometer formula (Appendix A). An alternative method provided by the manufacturer, using an internal compensating circuit to provide just a single output signal, is to be avoided since it severely degrades the potential accuracy of the instrument from about 3% to worse than 20%. Both radiation instruments are vulnerable to the many sources of electromagnetic interference aboard ships, since the domes leave the thermopile unscreened. Pyrgeometer domes also suffer from problems of shortwave leakage.

Ideally both instruments should be in a location with an unobstructed horizon-to-horizon view in any direction, but shipboard it is virtually impossible to avoid shadowing of the

instruments while still maintaining accessibility for maintenance. At sea, the domes become contaminated with salt and soot and need washing frequently. The shadowing problem means that the pyranometer location is usually a compromise. The instruments shown in Figure 3.5 are quite well exposed at position G (Figure 6.1) and duplicated for increased reliability. In less favourable exposure, the pairs could be separated far enough to avoid being covered simultaneously by the same shadow. With their relative locations carefully documented, shadows can usually be diagnosed and flagged from the data record. In the case of pyrgeometers, the effect of IR flux contamination by objects in the field of view is analysed in Appendix C.

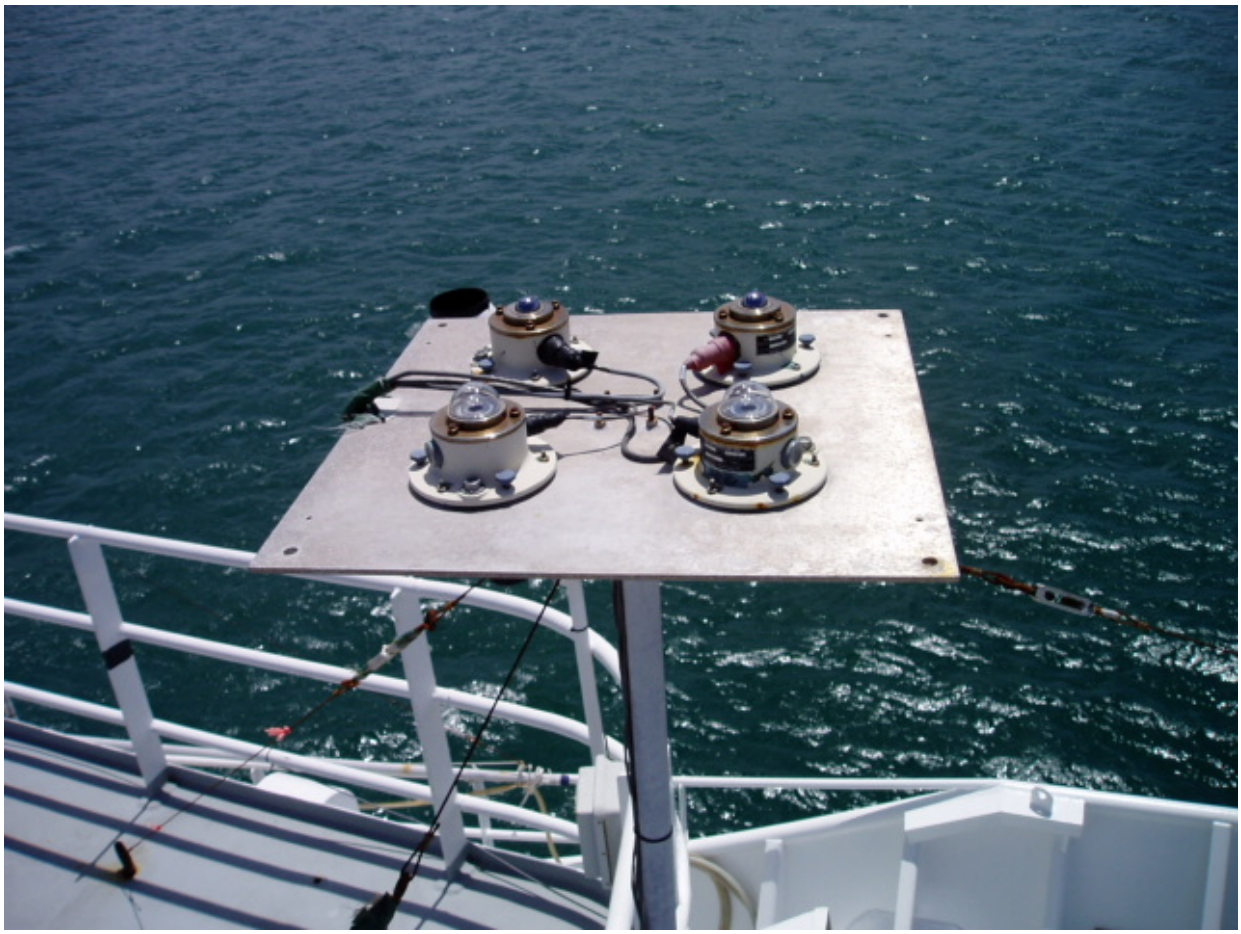

Figure 3.5. Example of duplicated pyranometer and pyrgeometer sensors mounted on a ship at position G (see Figure 6.1).

Platform motion is also a potential source of error when radiation instruments are used at sea. For correct measurement, the instruments must be horizontal, but both ships and buoys can roll through several degrees or take on a systematic lean caused by wind force or poor trim. The severity of the error depends on the inherent stability of the particular platform, but also on factors such as cloudiness, latitude, season and time of day. It is less severe for the pyrgeometer, since any sea in the field of view would be close to the near-surface air temperature. A possible solution is to set the instruments on gimbals but, unless very carefully designed, gimbals introduce other problems due to damping and phase variations. The better arrangement would be a dynamic system, such as a servo-controlled platform whose stability is achieved by feedback from a motion sensor, but so far such an arrangement is not available.

Regular dome cleaning may not be sufficient to overcome erroneous measurement. A recent observation of condensation on the inside of a pyranometer dome, despite the provision of a desiccant within the instrument, was found to reduce the output by about 100 Wm^{-2}. The probability that this phenomenon would be noticed is small because the instruments are usually mounted well above eye level. This example prompts the question of whether condensation inside the domes of pyrgeometers may be the cause of anomalous signals found with those instruments also. Because of the interference filter deposited inside pyrgeometer domes, condensation would not be seen but perhaps suspected if found in an adjacent pyranometer.

Over land or on a fixed platform at sea, diffuse radiation is measured by fitting the pyranometer with a "shadowband", set to shield the sensing element from the direct solar beam as it tracks across the sky. Unstable platforms preclude the use of a fixed shadowband, but measurements of the diffuse component have been made from shipboard using a rotating shadowband which, whatever the relative position of the sun, casts a shadow on a fast-response radiation sensor once per revolution. The diffuse signal produced by the shadowband is determined from the time series, and is unambiguous under clear skies but under broken cloud can be difficult to recognise. The fast-response sensor is usually of poor accuracy and stability, and so is continuously referenced to a regular pyranometer during the non-shadow periods.

The essential steps that must be taken to ensure the required accuracy from radiation instruments are careful data acquisition, a well-exposed location, frequent washing of the domes, regular replacement of the desiccant, and calibration before and after each deployment.

3.8. *Precipitation*

Traditional rain gages measure the rain falling into a funnel of known area. For automatic recording, either a weighing system is used, or a tipping-bucket rain gage in which the funnel discharges to a pair of buckets in a "see-saw" arrangement which flips over at every 0.1 mm of rainfall. Neither of these methods is feasible on the unsteady platform of a ship or buoy. The most common rain gage in this case is the siphon gauge in which the funnel discharges to a reservoir that fills to its capacity (about 50 mm of rain), when it siphons automatically and then starts filling again. An electronic sensor keeps track of the level of water in the reservoir.

Rain gages used at sea must handle rain rates up to around 200 mm hr^{-1}, which would be an extreme tropical storm. A heavy rainstorm in mid-latitudes might produce instantaneous rain rates of 50 to 100 mm hr^{-1}, but more commonly, rain rates are between 1 and 20 mm hr^{-1}. All funnel gauges lose catch in strong winds, when the gauge deflects airflow so raindrops are carried past the funnel. This phenomenon is exacerbated at sea by wind flow distortion over the entire bulk of the ship. The siphon gauge also misses rain while the instrument is siphoning. A rain gage intended to overcome both of these problems has been developed by the Oceanographic Institute at Kiel, but is not yet fully proven (Hasse et al. 1998).

Optical rain gauges (ORGs) measure *rain rate* by detecting raindrops falling through an optical path. One system measures extinction of a light beam by the raindrops; another measures the intensity of scintillations caused by raindrops passing through the semi-coherent infrared beam from a light-emitting diode. Rainfall amount is obtained by integrating the rain rate. ORGs must be calibrated against a funnel gauge in natural or simulated rainfall. Their main drawback is that the light path has a particular (and arbitrary) direction relative to the rainfall,

whose vertical component is thus uncertain. Some indication of errors due to this uncertainty may be obtained by mounting two ORGs orthogonally (Figure 3.6).

Figure 3.6. Example deployment of optical rain gauges. A pair of sensors is mounted with their axes oriented at 90º to each other. This geometry helps with the wind correction procedure.

Disdrometers are primarily intended for the measurement of drop size and drop distribution in rainfall. The most usual is an acoustic device that converts the sound of the impact of raindrops hitting the sensor surface into an electrical signal related to the size of the drop. Continuous recording of the size and number of drops provides a time series of rain rate and total rainfall by integration. Disdrometers are still regarded as a research tool and are seldom used operationally on ships.

4. Measurement Systems

The sensors described above and their physical shortcomings and potential for poor exposure, represent only one aspect of the possible sources of error in the final dataset. Between the actual sensor and the raw data record there is a hierarchy of stages, each of which is capable of degrading the accuracy of the measurement. Figure 4.1 (left) illustrates a typical measurement system, comprising the sensor, which is presumed to have an analogue output signal, analogue amplifier/filter unit, multiplexer, analogue to digital converter, data logger, data processing and archiving system.

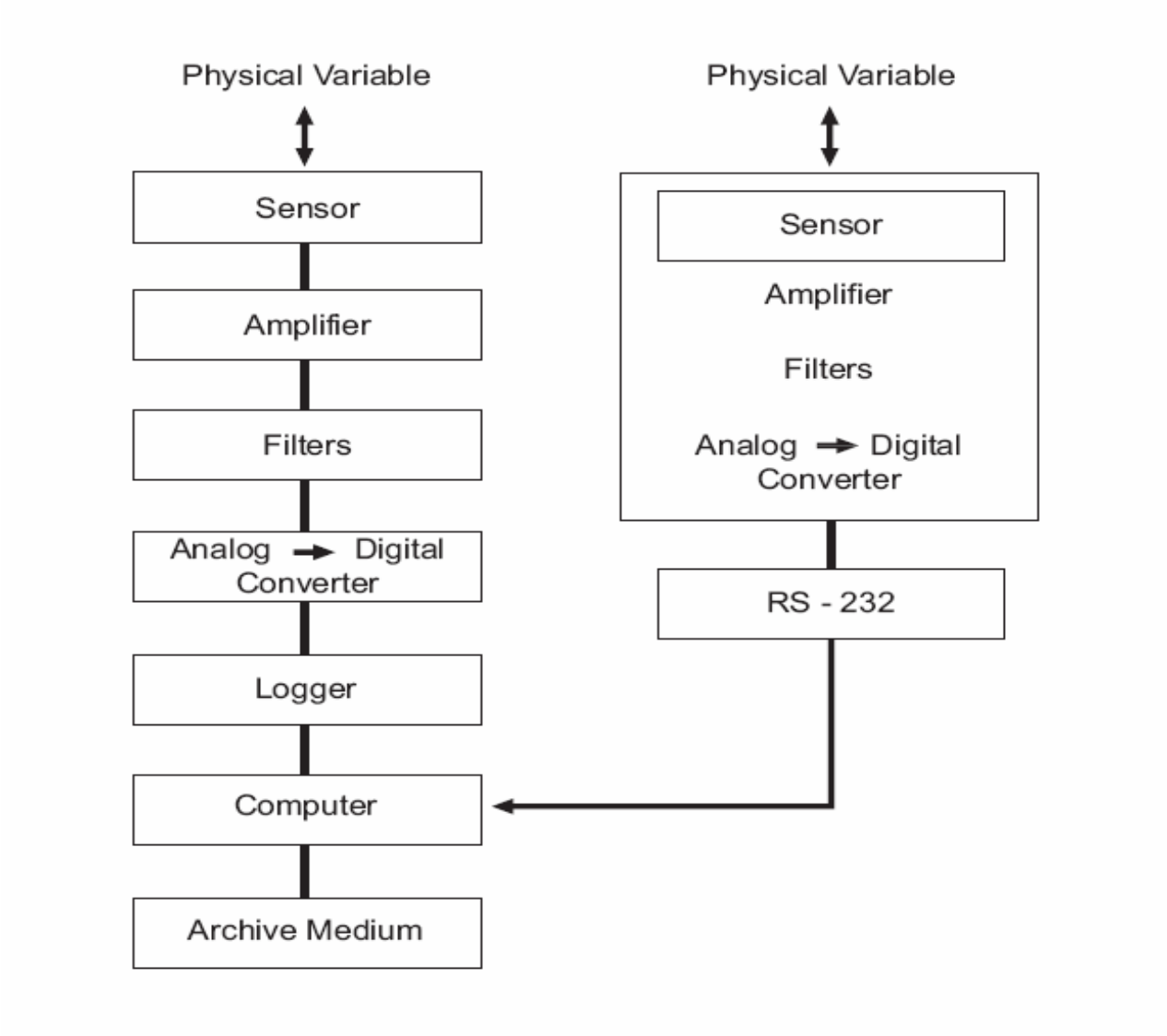

Figure 4.1. Schematic of components of a measurement system. The left part of the diagram shows a conventional sensor-to-acquisition component cascade; the right part shows an example where a fully digital sensor is used.

Whereas each component is a discrete unit with known characteristics (calibration, gain, etc.), it should in principle be possible to combine these to determine the overall transfer function of the system. In reality, individual errors, together with electronic noise and offsets produced by connecting the units together, often combine to produce an overall uncertainty that exceeds what is acceptable. The most critical part of the signal processing system is what takes place between the sensor and its conversion to digital form; i.e., the analogue stages and the digitization prior to recording. Providing that the bit resolution of the logger and subsequent computer hardware are adequate, the digital record will retain its accuracy through ensuing manipulation.

It is therefore good practice to calibrate the system as a whole from sensor to digital record, and repeat this as often as practical to verify that offsets do not change with time.

Ground loops are easily created when many instruments are distributed around a ship, and may change when the load on the line power changes. Most research vessels provide "clean" power which is isolated from the surges produced by starting large electric motors, and should be used when available. These problems are minimized in some instruments where integrated circuit technology enables the analogue signal processing, and conversion to digital mode, to be packaged together with the sensor (Figure 4.1; right). In this case the instrument output is already in digital format (e.g., RS232) and an overall system calibration is implicit.

If it is not possible to log all information (meteorological sensors, navigation information, etc.) on the same system, particular attention must be paid to synchronising the time stamps. In any case, the time reading used by the logging should be checked periodically.

5. Particular Problems on Ships and Buoys

5.1. *Introduction*

Land-based meteorologists seeking an observing site for research studies or operational use will try to select an area free of local anomalies such as buildings, trees or surface inhomogeneity. They aim to avoid features that may introduce local gradients of the quantities (temperature, humidity, wind speed and direction) that would make the recorded data unrepresentative of the surrounding region. They normally have a choice of candidate locations, and are able to distribute measuring instruments to avoid mutual interference. Furthermore, the land does not move around.

A ship represents a challenging measurement platform. It is a local heat island and a bulky obstruction to the ambient wind flow. When the ship is steaming, it disturbs the ocean surface layer and when hove to transfers heat to the surrounding water, so that a water temperature measurement close to the hull is always uncertain. A ship is a forest of tall obstacles, masts, funnels, cranes, and communication antennae which severely restrict the exposure of instruments and cast shadows on radiometers. Moored buoys and meteorological stations on pilings can have similar problems

5.2. *Wind flow distortion*

Because of the height dependence of all meteorological variables in the surface layer, and the need to reduce all observations to "standard" height (usually 10 m), it is important to know the average height of each sensor above the sea surface. Except in very calm weather this is difficult to determine at sea, and a measurement made at the wharf must be accepted. However, in blowing over the ship the wind is deflected upward, so that the true height from which the air measured by the sensor originates is unknown. There are also consequences for the measurement of rainfall using siphon gauges as described in section 3.8. Particularly in strong winds, and when the ship speed augments the true wind, the upward flow carries raindrops away from the funnel instead of falling in. As for the wind measurement itself, flow distortion by the ship not only creates uncertainty in the height of origin upwind, but also changes the wind speed (and often direction) by accelerating the wind around the obstacle of the ship. Obviously, errors in both wind speed and direction measurement affect the true wind calculation, and hence the bulk fluxes (Figure 5.1).

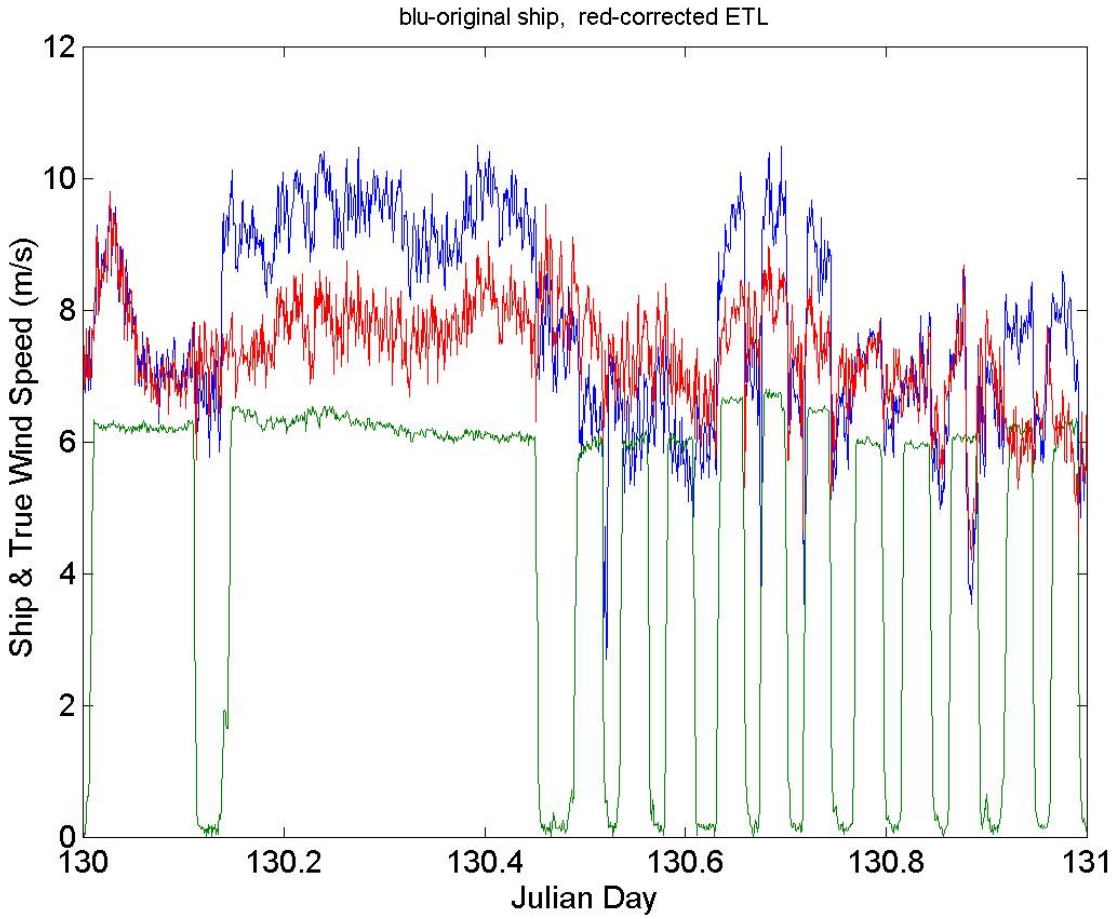

Figure 5.1. Illustrating the effects of flow distortion by the ship's structure on the determination of true wind speed. On this day the ship steamed in a star pattern performing a series of CTDs, which required the ship to stop periodically (ship speed is the green line) and change course at the vertices of the star. Such a course change occurred after the stop at 130.13. The red trace shows true wind speed computed from a research anemometer mounted well forward on the foremast (at A in Figures QR1 and 6.1). This anemometer has a flow distortion correction applied. The blue trace shows true wind speed computed from the ship's anemometer mounted to the port of the foremast, with no flow distortion correction. The course change alters the flow distortion pattern and thus the relative wind; the effect on the uncorrected anemometer is apparent in the blue trace.

Correction for wind distortion is seldom attempted due to lack of knowledge at this stage. From simple aerodynamic considerations, the deflection will be less severe when wind blows directly over the bow than abeam, when the ship represents a larger obstacle. The effect of wind distortion can be quantified with wind tunnel, water flume or computational fluid dynamics (CFD) model experiments. Studies have already been made of the air flow distortion around a number of research vessels. Figure 5.2 is such a CFD simulation of particle trajectories for wind flow head on to NOAA's R/V *Ron Brown*. The effect caused by the central superstructure is particularly dramatic; the upstream wind of about 12 ms^{-1} at around standard instrument height is lifted by two decks and decelerated to around 5 ms^{-1}.

It is necessary to establish the wind field around various generic ship designs and determine corrections as a function of wind incidence angle to the ship. Meanwhile, we emphasize the importance of documenting the location of anemometers (with photographs), and the height of all measuring instruments above some reference level on the ship (e.g., the foredeck). The height of the reference level relative to the sea surface is also needed. The planned flow distortion studies provide the opportunity for retrospective correction providing sensor locations are properly documented.

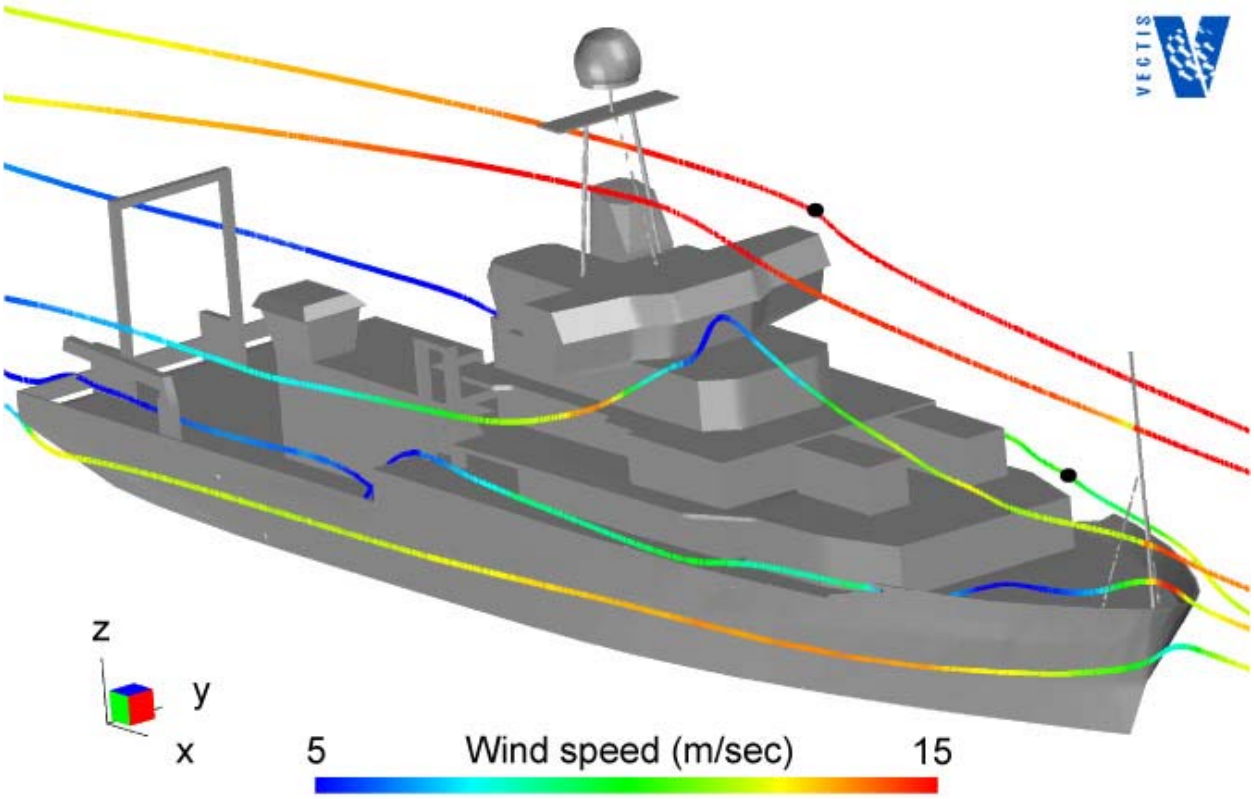

Figure 5.2. CFD simulation of wind flow around R/V *Ron Brown*. Positions of two funnel rain gages are shown as black dots on particle trajectories that pass through them, showing the flow deflected sideways and upward at each site. Other trajectories originate 100 m upwind on the centreline of the ship, at heights of 5, 7, 9, and 15 m above the sea surface. The colours represent wind speed and scale from 5 to 15 ms^{-1}. Courtesy Ben Moat.

5.3. *Sea spray and salt contamination*

Even without strong winds and flying spray, instruments at sea become coated with a layer of salt which needs cleaning periodically, especially from the domes of radiometers. Temperature and humidity sensors must be well shielded from salt contamination, which would directly affect the measurement by absorbing and desorbing water vapour. All electrical connections and electronic instruments outside must be enclosed in sealed boxes. Signal cables

must be protected against damage, such as that due to chafing on sharp edges. There have been cases where a slight, barely noticeable nick in the jacket of a cable allowed salt to corrode the copper conductor and cause an intermittent fault which was almost impossible to locate.

In rough weather, even the largest research vessels pitching into swell will send spray surprisingly high over the ship. This spray is sometimes detected in rain-gauge records.

5.4. *Ship and buoy motion*

The irregular motion, rolling and pitching, of ships and buoys produce various effects on measuring instruments. There is no such thing as "level" on a ship, unless it is produced by a stabilized platform as is done for some radar installations, or naval guns. Instruments for which orientation is important, such as radiometers and anemometers, must be set up with reference to the axes of the ship.

Except in extreme conditions, a ship will typically pitch through ±3º, and roll through ±10º (Class 2 without stabilizers) or ±5º (Class 1 with stabilizers). The effect of this motion on radiation measurements is less severe for the diffuse shortwave and downwelling longwave than for the direct solar beam. For the latter, providing that the motion is symmetrical about zenith, experiments have shown that for rolls of 10º amplitude at a zenith angle of about 50º, the largest error was 2%; thus for low latitudes and modest seas, the effect of platform roll may not be too serious for radiation measurement. Even at mid-latitudes, more severe seas causing greater roll tend to be associated with bad weather and cloudiness, reducing the absolute radiance which is also mostly diffuse. However, a persistent tilt of only 5º has been found to produce errors much greater than 5%. Such tilt angles may be caused by misalignment of the instrument relative to the ship, or by the ship listing due to poor trim or a strong wind abeam.

The effect of pitching on the meteorological sensors is to move them up and down through a gradient of the quantity they are measuring. The vertical motion at the bow of the ship (the preferred location for many sensors) can be several metres in rough weather. The frequency of pitching motion is irregular, but typically has a period of a few seconds, of the same order as the time constant of the sensor. Thus, the measurement is some sort of average over the sensor path, assumed to be at an average height close to the one determined at the wharf. The height of measurement is thus subject to yet one more uncertainty. Fortunately, in more moderate conditions the vertical motion is less and at typical instrument height, the gradient of most boundary layer variables is relatively small.

Wind sensors are affected directly since the ship motion creates a complicated apparent wind pattern relative to the instrument. In section 2.5 we discussed determining the mean true wind speed from the relative wind speed (i.e., accounting for the heading and vector motion of the ship). However, pitch and roll may produce second-order errors in true wind speed when non-ideal wind sensors are used. For example, with cup anemometers the motion acts like a continuous sequence of vertical wind gusts on the rotor's imperfect cosine response. Because sonic anemometers measure all three instantaneous components of the wind vector, it is possible to continuously correct for pitch, roll, and other ship motions. This correction produces the most accurate true wind vector measurements but requires an additional system to provide all of the motion information. Such systems are now entering the research vessel fleet in an effort to improve the accuracy of ADCP measurements of current profiles, but have yet to see general application to wind measurements.

5.5. *Exhaust contamination*

On a ship it is unavoidable that periodically the stack exhaust plume will cross the location of the meteorological sensors. The impact of the exhaust is most severe on temperature, humidity, and radiation sensors downwind from the stack. One may also expect contamination problems with any optical sensor (e.g., optical rain gages, radiometers). The likelihood of exhaust contamination is lessened by locating sensors as far forward of the vessel stack as possible (e.g., in Figures QR1 or 6.1, positions A and B for temperature or G for radiation sensors).

The exhaust plume will result in shadowing errors for shortwave radiation sensors. The impact on longwave radiation sensors is caused by the exhaust plume, being a heat anomaly, resulting in overestimated downward longwave readings. Also, the plume will deposit soot on the radiometer domes, so frequent cleaning of the domes is essential if the radiometers are aft of the stacks.

Abrupt changes in temperature and humidity are caused by the exhaust plume. Figure 5.3 shows the abrupt rise in air temperature, and consequent reduction in relative humidity, that occurs when the exhaust plume on the R/V *Meteor* passes these sensors. In this case, although the sensors are forward of the stack, the relative wind is from astern, causing sensor contamination. One would expect that similar problems would occur with dew-point or wet-bulb temperature sensors.

For all measurements affected by the stack exhaust, the ship-relative wind can be used to eliminate suspect values. In the case of temperature and humidity sensors positioned forward of the stack, but above the wheelhouse, upward of 25% of these measurements will be in error when the relative wind is from the stern (typically when the ship is manoeuvring at low speed). Even sensors on a bow mast can be affected by the exhaust when the relative winds are from the stern, but the range of relative wind angles that will result in sensor contamination is reduced as sensors are placed farther forward of the stack.

5.6. *Electrical problems*

Lightning and buildup of static electrical charge must be considered as a source of damage and interference. Use of plastic instrument cases that accumulate rather than bleed off static charge is not advised. The ship's own power system may present challenges in the form of uncertain grounding, potential between neutral and ground, and surges and level fluctuations, especially during port call or when generators are shifted on- and off line for servicing.

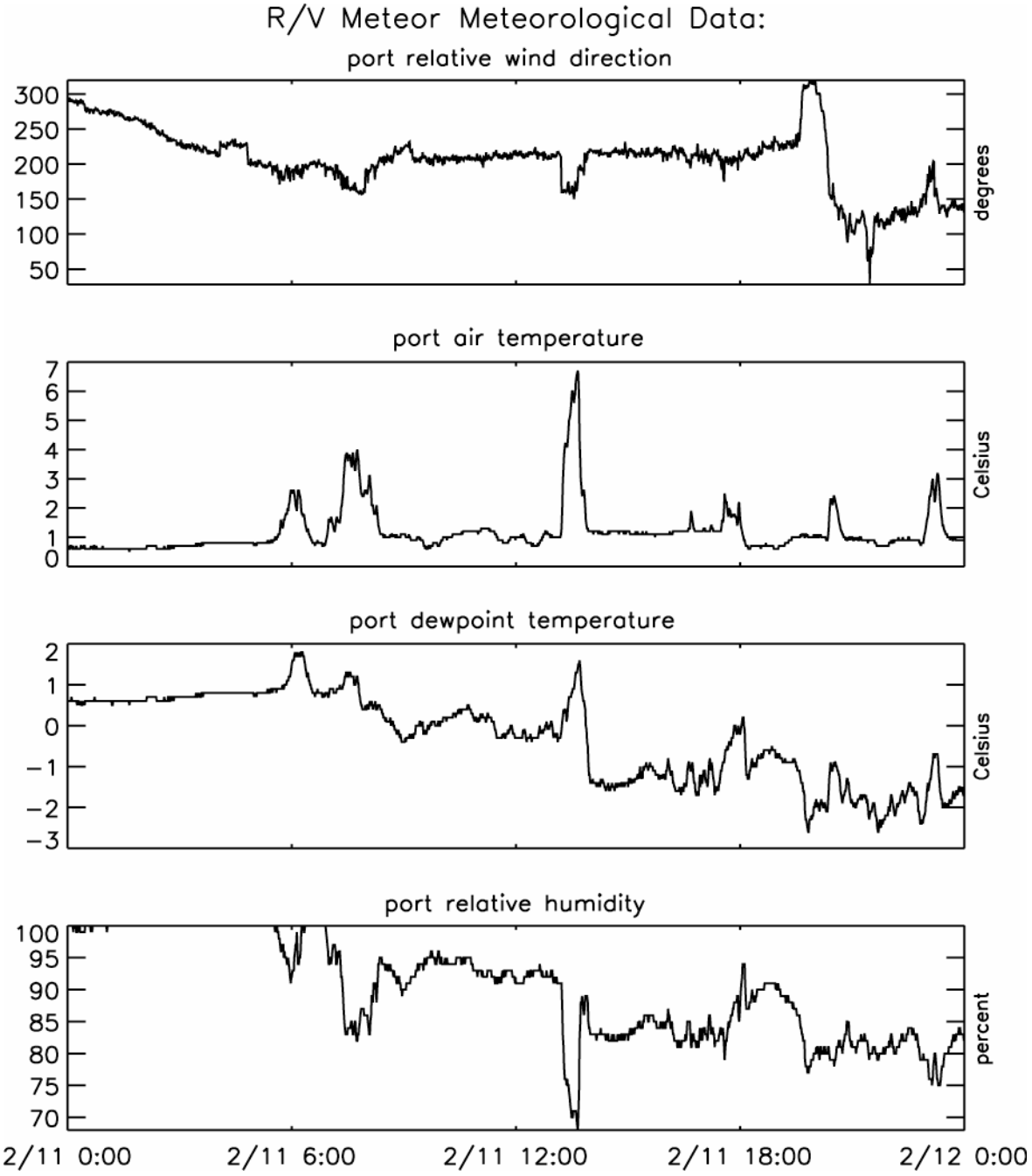

Figure 5.3. One-minute sampled relative wind direction, air and dewpoint temperature, and relative humidity from the scientific instrument system on the R/V *Meteor*. Data are all from the portside sensors collected on 11 February 1990. The increases in air and dewpoint temperature and the decrease in relative humidity occur when the relative winds are from the stern (~160-200˚), indicating contamination of the sensors by the vessel exhaust.

6. Location of Instruments

6.1. *Introduction*

Location of the sensors on the ship is the most critical aspect for accurate measurement of the basic meteorological variables, and therefore of the fluxes. The particular difficulties of making these measurements aboard an unstable, bulky obstacle were noted in sections 3 and 5. In general, meteorological instruments should be located forward on the ship, ahead of the engine and air-conditioner exhausts. The ideal position would be high on a forward mast, high enough to be above spray when the ship pitches in heavy seas. Because ships are various shapes, sizes, and have different appendages, such decisions must be made on a ship-by-ship basis. But there are principles, mostly common sense, which can help minimize defective observations. They are illustrated in relation to typical ships in Figure 6.1.

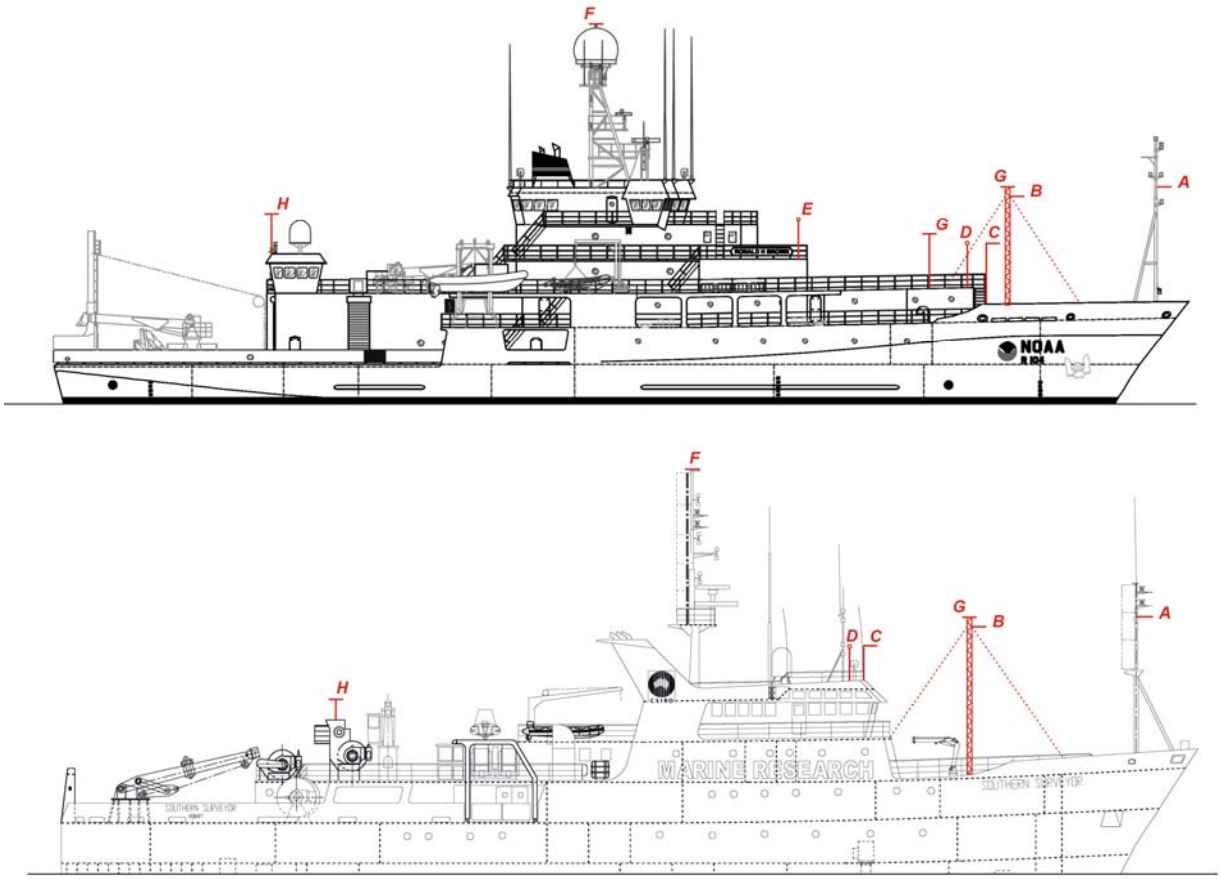

Figure 6.1. Examples of ships with good foremast locations for instruments: R/V *Ronald H. Brown* (NOAA) and R/V *Southern Surveyor* (CSIRO). Locations A, B, etc., are described in the text of section QR2, where this figure is repeated.

6.2. *Temperature*

The temperature sensor should be as far forward as possible to avoid heat contamination from the ship. Again, this is impossible when the wind is from astern, so duplicate sensors to port and starboard provide better data recovery. The temperature sensor should be shielded and ventilated, but care must be taken to ensure that there is no possibility of sea spray being drawn into the air inlet. Although the mainmast may have a well exposed site for wind instruments and be clear of sea spray, it is usually a poor location for temperature sensors that can then "see" large areas of the deck.

6.3. *Humidity*

As described above, water vapour measurement is little affected by wind and thermal distortion caused by the ship. It is important that the temperature of air surrounding the sensor is recorded, and since the two measurements are commonly made in the same package the more stringent exposure requirements of the temperature sensor ensure that the humidity sensor is also well exposed. The location must, however, permit access to the humidity element for periodic maintenance. If a psychrometer is being used, it will also be necessary to top up the water reservoir with distilled water from time to time.

6.4. *Wind speed and direction*

The most important requirement of the wind sensors is that they should have no obstruction upwind. A single speed/direction set can be mounted on a forward-facing arm from a foremast, or high on the mainmast. With only one set of instruments, there will always be a sector astern over which the relative wind will be in error. If two wind sets are available, it is good practice to mount one on each side of the ship, and give preference to whichever has the best exposure to the relative wind.

Note that even an object **behind** the anemometer will cause some disturbance to the wind, the error scaling with the size of the object. Thus, mounting a sensor high on the top of a mast or pole is a good location. If mounted on an arm facing forward from the mast, it should be at least 5 mast diameters forward. However, a horizontal boom in front of the bow is not a good place because, with the bulk of the ship behind, it is not possible to go far enough forward to measure undisturbed flow.

6.5. *Sea temperature*

The location of a ship's thermosalinograph and its inlet port are usually outside of the investigator's control. Ideally, as noted above, the port should be in the bow at sufficient depth (e.g., about 5 m) so that it does not break the water surface. A hull sensor should similarly be mounted inside the bow. A Seasnake-type sensor should be towed from a point as far forward and as far out as practical, intending that the sensor will spend much of its time outside the ship's bow wave. For the same reason, infrared radiometers for SST measurement, when available, are mounted as far forward and as high as possible (on the wheelhouse roof for example) so that their view is of an undisturbed ocean surface.

6.6. *Radiation*

Upward-facing radiometers need an all-round, horizon-to-horizon view with minimal obstruction by parts of the ship, which would cast shadows on the pyranometer and be a source

of thermal radiation for the pyrgeometer. Possible locations are the top of the mainmast or foremast, providing they are accessible at sea under moderate weather conditions so that the domes can by cleaned periodically, and the desiccant replaced. In some cases installing water jets, controlled from a convenient tap on the deck, has been successful in cleaning domes without climbing an instrument mast at sea. The pair of instruments is normally mounted together on a single aluminium plate, and levelled. If the masts prove impractical, the plate can be mounted on the top of a rigid galvanized metal pipe (e.g., a scaffolding tube or thick water pipe), clamped in some way to a convenient rail, perhaps above the wheelhouse.

Shadows can often be diagnosed by installing a second pyranometer, separated widely enough from the first that they are not covered by common shadows (see section 3.7). Both pyranometers and pyrgeometers are 'cosine' detectors, so objects near the horizon have a much smaller effect than objects overhead. Appendix C describes the error in a pyrgeometer measurement when it receives thermal radiation from parts of the ship unavoidably in its field of view. In a real-life example, pyrgeometers mounted in position G (Figure 6.1 top ship) "see" an area 6 m × 1.5 m of the bulkhead 10 m aft on deck 3, and 16 m × 2.5 m of the bridge 16 m aft. If the sky and bulkhead temperatures are as given in Figure C1 (lower panel), by interpolating the upper curve we can estimate that these two barriers would produce errors of 1 Wm^{-2} and 3 Wm^{-2}, respectively. According to the middle curve on each diagram, the foremast, 16 m forward, has negligible effect.

6.7. *Rainfall*

The difficulties of making accurate measurements of rainfall on ships, and the strong dependence on location of the instruments, have been described above. Funnel gauges should not be mounted in a location of strong upflow, such as on a rail just above the side of the ship or above the wheelhouse, where they will lose catch. Rain gages located on the aft part of the ship may overestimate by catching water that has accumulated on the superstructure. Once again, the best location is on a foremast. If that becomes too crowded, a position on the foredeck near the centre-line of the ship will help avoid updraughts.

Because wind information is used to correct both funnel and optical rain gages, a location near the wind sensor is preferred.

7. Instrument Calibration

While the absolute accuracy of an atmospheric measurement is the result of the cumulation of errors in each step of the measurement/archival process, it is clear that the calibration of the sensor is the starting point. The operator of a ship observation system must establish (and document) a routine for regular replacement and recalibration of each sensor in use, at least once a year and preferably before and after each cruise. The routine will involve having a stock of precalibrated sensors onboard to replace those that are away for calibration, or any found to be faulty or performing poorly while in operation.

The calibration facility used should be traceable to a national standard. The system operator may choose to rely on factory calibrations (i.e., regular maintenance/calibration by the manufacturer of the sensor), a secondary calibration laboratory, or maintain an in-house calibration facility. For institutions with one or two research vessels, an in-house calibration facility is unlikely to be cost-effective. Reputable manufacturers of meteorological equipment

(e.g., Vaisala, Rotronic, ATI, Gill, R.M. Young, Eppley, Kipp and Zonen) have large, well-equipped facilities, calibrate thousands of instruments every year, and usually represent a solid standard. In some cases secondary calibration laboratories provide more comprehensive information that may be useful. For example, the NOAA Climate Monitoring and Diagnostics Laboratory (Boulder, Colorado) can provide cosine-response curves for pyranometers and dome-heating correction coefficients for pyrgeometers. A pyranometer with a poor cosine response curve could be retired or relegated to the emergency backup shelf.

Regardless of the approach, the process must include keeping a documentation record of the calibration and deployment history of each sensor. It is important to realise that seemingly identical sensors from a production line may differ sufficiently in their calibrations to be significant in the context of the accuracies of Table 1. So when sensors are switched, this history will ensure that the correct calibration is associated with the active sensor. In view of the many possible hazards to sensors deployed on ships which have been described in the above sections, and which may remain undetected particularly on long voyages, it is good practice to calibrate both before and after the deployment. Gradual deterioration of a sensor may thus be detected and corrected, perhaps by simple linear regression, to improve data accuracy.

8. Intercomparisons

8.1. *Portable standards*

While it is sometimes justified to equip laboratories that handle large numbers of instruments with standard calibration facilities, or in some cases to carry calibration equipment onboard ship, this is usually impractical. In any case, not every ship could be so equipped, which would lead to non-uniformity of data quality. With many ships involved in a cooperative project such as SAMOS, it is feasible to verify the operational instruments installed against a common set of portable secondary standards. These are instruments whose calibration is traceable to a recognised standards laboratory. They can be operated alongside the ship instruments in a realistic field situation, on part of a regular cruise for example, and recorded independently of the ship's system. The portable standard can be rotated around several ships, and verify not only the performance of the ship sensors, but the measuring system as a whole, from instrument location to recorded data.

8.2. *Replication of sensors*

It has been noted above that there are benefits in having duplicate sensors on opposite sides of the ship, to deal with the range of relative wind direction or the shielding of radiometers. However, there are times when both sets of instruments might be reasonably well exposed, and expected to agree fairly closely. The ability to compare their measurements, and to analyze any differences between them, is a further advantage. While it is not always feasible to have two sets of instruments in operation, it is good practice to carry a complete set of spare, freshly calibrated sensors, ready to replace the operational ones in the event of failure. However, except for trouble-shooting purposes, replication of sensors should not normally be done at the expense of exposing a freshly calibrated spare unit. The intermittent loss of data through unfavourable wind or sun direction is usually less important than having a data time series cut short by instrument failure on a long cruise.

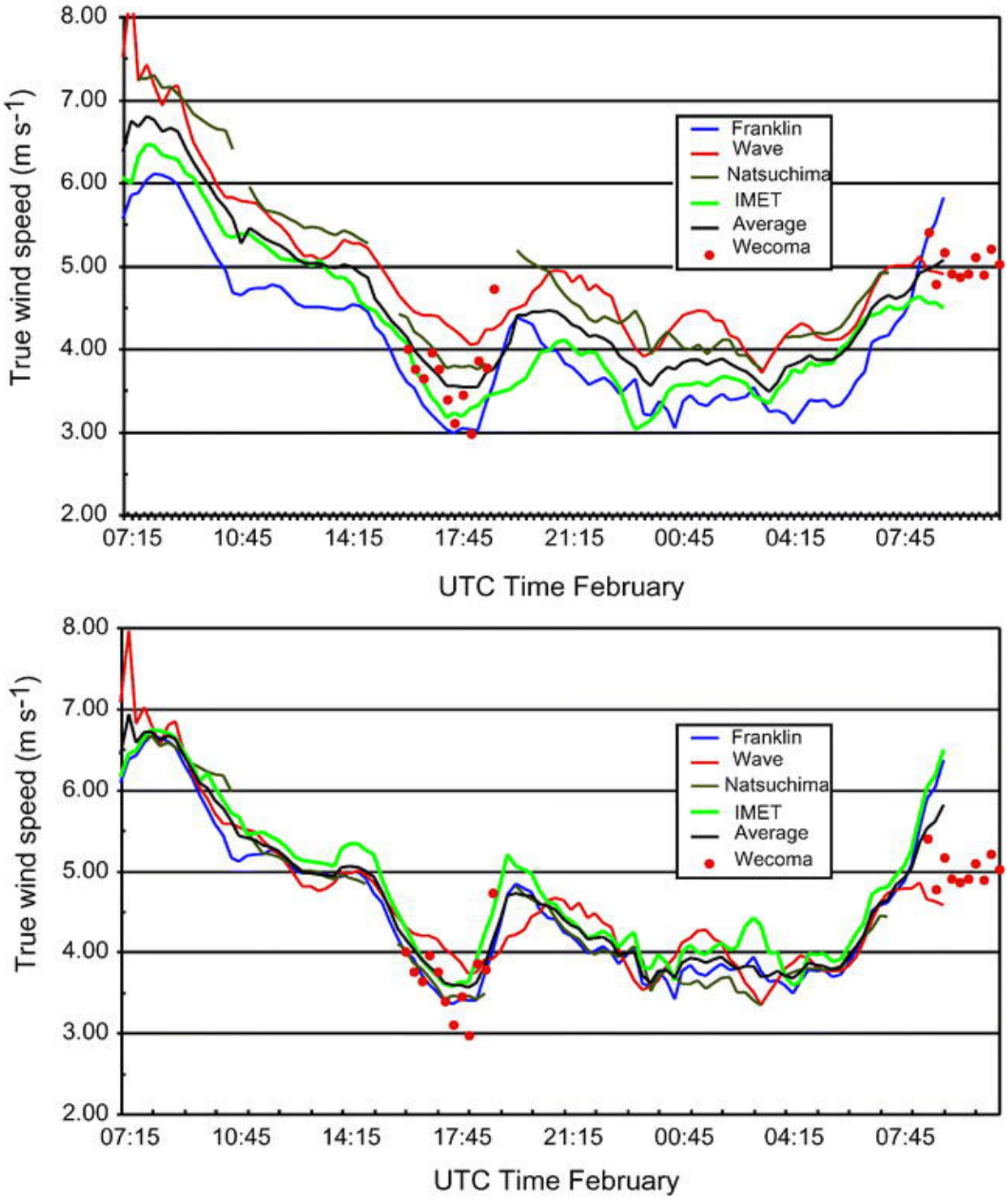

Figure 8.1. Field intercomparison of ship true wind speed measurements from TOGA COARE. Three ships ran side-by-side for about one day in the vicinity of the WHOI IMET mooring; a fourth ship (Wecoma) transited the area on two occasions. The raw comparison (upper panel) showed mean differences between platforms. Each platform was then corrected by that difference with the lower panel showing the new comparison. The corrected wind speeds were used for flux calculations for the entire experiment.

8.3. *Field intercomparisons*

Field intercomparisons between sets of instruments on different platforms should be made whenever the opportunity presents itself. During TOGA-COARE such comparison periods were scheduled as part of the operation plans of ships and aircraft, and there were also other occasions when platforms in the same vicinity could compare measurements. The quality of surface meteorology and flux datasets resulting from COARE is due in large measure to these field intercomparisons, and their careful analysis (Figure 8.1). This alerted participants to several potential sources of measurement error, and has influenced methodology in many subsequent air-sea measurement campaigns. For example, the ship used for deployment and retrieval of the Woods Hole Oceanographic Institution (WHOI) ocean reference moorings is equipped with a set of high-quality meteorological instruments, and stands off the mooring for a few days at either end of a deployment while the old and new buoy instruments are compared with those on the ship.

Note that the scheduled intercomparison periods must be long enough, typically 24 hours or more, to give statistically meaningful results.

8.4. *Manual observations*

In the same way that ship's officers preserve their skills in the use of a sextant to check the ship position in case GPS fails, it is prudent for meteorological observers to remain familiar with observation techniques before the days of SAMOS. The reason is not so much to fill in data should the automatic system fail, but as an aid to monitoring the health of the sensor array and signal processing system. There are at least four "traditional" observations that should be made regularly for this purpose.

a) Temperature/humidity. Use of the Assman psychrometer is referred to in sections 3.2 and 3.3, and little needs to be added. The Assman is preferred over the sling psychrometer because it usually has superior thermometers, and they can be read while the instrument is held *in situ*. This has the advantage that short-term fluctuations in temperature (in light wind, convective conditions for example) may be averaged visually. If possible, the instrument should be stored outside air-conditioned space for quicker equilibration with ambient conditions. Along with the precautions described in section 3, it is critical to note the time of reading to the minute for comparison with the automatically logged value.

b) Sea temperature. The traditional measurement is of the "bucket" temperature. The nature and probable accuracy of this method is referred to in section 3.6. A bucket measurement may be impossible from very large vessels, but most research ships possess such an insulated bucket. Its size is important; too small, and the water sample will change temperature before it can be read; too large and it will be heavy and awkward to handle. The technique is to throw it forward and out from the ship, and bring it in when level with the observer. Several casts are needed to ensure that the bucket is close to the water temperature. Obviously, the temperature should be read as soon as possible after bringing it onboard, but timing is not so critical because sea temperature does not fluctuate as rapidly as air.

c) Wind speed. The traditional estimate of wind speed at sea is by observation of its effect on sea state. Unlike cup and acoustic anemometers, the Beaufort scale (Table E1) does not break, fuse or rust and is independent of ship speed and heading. In recent years the various sea state descriptions have been refined by comparison with careful instrumental wind measurements.

As indicated in sections 2.5 and 5.2 there are several potential sources of error in the true wind measurement, from instruments measuring wind and ship speed, the calculation from relative wind, and flow distortion. It is almost impossible to estimate the true wind by "feel", so the Beaufort scale enables the observer to judge, within a couple of ms^{-1}, whether the logged wind speed is within reasonable limits.

d) Downwelling radiation. Except under special conditions, short-term variability in solar and IR radiative fluxes, especially due to cloudiness, make these signals the most difficult to check with spot observations. There are various parameterizations for radiative fluxes, based on surface air temperature and humidity combined with visual observations of cloud fraction, but these are too uncertain to be of use in this context. However, reliable models of these fluxes for a *cloud-free sky* may be used to check the radiation observations for this particular condition. The IR flux [see equation (1.1)] may be written $R_{l\downarrow} = \varepsilon_{e0}\sigma T_a^4$, where T_a is the air temperature (Kelvin) and ε_{e0} an effective emissivity for clear skies for which Brunt (1932) proposed a 2-parameter form $\varepsilon_{e0} = A + B\sqrt{q_a}$. From a database of several cruises, Hare et al. (2005) determined A and B as linear functions of latitude φ, such that

$$R_{l\downarrow} = \left[\left(0.52 + \frac{0.13}{60}|\varphi|\right) + \left(0.082 - \frac{0.03}{60}|\varphi|\right)\sqrt{q_a}\right]\sigma T_a^4 . \qquad (8.1)$$

The pyrgeometer output, being a combination of three temperature signals, is vulnerable to stray thermal contamination, but equation (8.1) can provide a check to within ±10 Wm^{-2}.

Clear-sky parameterizations for solar flux are also available, but require atmospheric profiles of certain constituents, and involve strong dependencies on location and season, making them too complex for checking the pyranometer. However, knowledge that the solar flux falls identically to zero at night (note, a standard pyranometer will normally read a few Wm^{-2} negative at night), and takes a maximum clear-sky value around 1100 Wm^{-2} in the tropics, enables the observer to identify unreasonable values in most situations.

9. Documentation (Metadata)

9.1. *Introduction*

Careful documentation of the sensor installation, calibration practices, and known data faults is an essential task of the person responsible for maintaining a shipboard meteorological system. These metadata are crucial to the future application of the observations; a detailed example of a metadata structure is given in Appendix G. The importance of documenting the calibration and deployment history of each instrument cannot be emphasized too strongly. In the chaos that sometimes accompanies replacement of a faulty sensor, it is easy to postpone and eventually forget to note the circumstances. This can subsequently lead to puzzling features in the air-sea flux time series that can never be resolved with certainty. Similarly, it is sometimes unavoidable that the location of the sensor is less than optimal. Providing that the location is carefully documented, ideally supported by digital photographs, seemingly anomalous data from that sensor can often be explained, and in some cases, corrected. Equally, data from a sensor known to be very badly exposed for a given relative wind direction can be flagged as erroneous without fearing that the information is being lost. The following indicates details and incidents

that should be recorded (with date and time) in an event log during the cruise, and if possible transcribed into an electronic document. This, and the digital photos, will be part of the metadata to accompany the measurements.

9.2. *The basics*

- Time convention (preferably GMT [UTC])
- Recorded units of observations (preferably SI)
- Ship name
- Data sampling rates
- Averaging or calculation methods (e.g., true wind vs. ocean-relative winds)

9.3. *Sensor calibration and history*

- For each instrument, the make, model and serial number.
- The date and source of each calibration (indicates stability of sensor)
- Sensor dates of deployment period
- Incidents during deployment period (maintenance, repairs, mishaps--e.g., swamped by wave over bow)

9.4. *Instrument location*

- Description of main support (e.g., foremast, forward rail above wheelhouse)
- Position w.r.t. main support (e.g., 1.2 m to port or stbd., 0.8 m forward)
- Position w.r.t. ship's centreline (e.g., 2.5 m to port or stbd)
- Distance from bow
- Height above the water, and/or height above some ship reference (e.g., 15.3 m above foredeck)
- Height above the deck immediately below the sensor
- Any significant object that may affect the exposure of the instrument (e.g., Inmarsat dome on rail 2 m to port; after installation large instrument box mounted 1 m forward)

9.5. *Digital photographs*

Rough sketches in the logbook of the locations of instruments, with heights and salient dimensions with respect to the ship, are extremely helpful. It would be even better to have digital schematics of the vessel (top and side view) showing instrument locations (similar to Figure 6.1). Together with digital photographs of the installations, these enable the analyst to assess the overall quality of the ensuing measurements, and provide valuable information on the likely cause of any suspect data.

Close-up photographs of the instrument itself can sometimes be helpful in detecting instrument faults (e.g., damaged cables), but are most useful when taken at a distance sufficient to show the sensor's environment and possible obstacles to airflow around the sensor; in the case of radiation sensors, objects or installations likely to cast a shadow. If possible, after installation, photographs should be taken from the wharf, as in Figure 9.1 of the NOAA research vessel *Ronald H. Brown*. If written documentation were lost or mislaid, having the plans of the ship (e.g., Figure 6.1), together with such photographs, would enable the heights of the instruments, and their relative positions, to be estimated reasonably well.

Figure 9.1. Meteorological instruments on the foremast of the NOAA ship *Ronald H. Brown*; a) below the upper cross-arm is a covariance package. The sensor of the sonic anemometer is well exposed, although the instrument boxes below and behind it represent a greater obstacle to airflow than is desirable; b) close-up of the bulk flux instrument package. From left to right on crossarm: optical rain gage; T/RH sensor with forced ventilation; second T/RH sensor in naturally ventilated screen; siphon rain gage; propeller anemometer and wind vane unit. Below these instruments can be seen a laser wave-height sensor aimed forward of the bow and a second sonic anemometer.

10. Securing the Data

10.1. *Introduction*

All data and metadata should be stored in a manner that will preserve the information for current and future scientists. This requires each operator to establish a protocol for managing the output from their sensor system. A detailed data protocol should include plans to store the observations, metadata, and event log on digital media during each cruise and to ensure the long-term availability of the observations at a national or international archive center.

10.2. *Data storage*

The computer date and time should be set to GMT (UTC). The event log should also be written in GMT, although some relationships (cloud-radiation forcing, for example) make more sense when analysed in local solar time. It is often helpful if the difference between local time and GMT is noted (but note that ship time, i.e., the time to which the ship's clocks are set, may differ from local solar time).

The recorded data will normally consist of the raw time series at the logger sampling speed, and a conversion to physical units via the instrument calibrations and transfer functions. This will often involve some computation using several signals and sensors; for example, combining the three pyrgeometer signals for downward longwave radiation, or obtaining true wind from the measured relative wind and the ship's speed/course.

In many cases (SAMOS, for example) the meteorological data collected automatically by computer on the ship will be destined for use by scientists (e.g., modelers and analysts) engaged in climate research elsewhere. The role of the shipboard operator is to maintain the quality of the data by monitoring the performance of the sensors, and making sure that all detail (e.g., roosting birds, or a faulty instrument) is noted in the daily log. This individual should be provided with training to enable recovery of the system in the event of a computer crash, since extended time series are most valuable.

The capacity of the computer hard disk will be sufficient to hold several weeks' data, which should be backed up regularly according to normal computing practice. Every few days both raw and derived data should be written onto a CD or DVD, together with a copy of the metadata. If possible an electronic copy should be made of the event log (e.g., in Word) and saved with the data and metadata.

10.3. *Data Archival*

"Archiving" is a term that is rather poorly utilized in the climate community. Simply storing the observations collected on a cruise on a DVD or other digital media and placing this on a shelf does not constitute archival of the data.

As part of an ocean observing system, the mission of a national or international archive center is "to acquire, preserve, and provide access to data in perpetuity." High-priority objectives include integrity and completeness of the archives. Essential functions include constant monitoring of data streams, accounting for all files and records, and frequent checks of accuracy. Metadata are equally important since they ensure that the maximum information can be derived from the data. Archive centers must have maintenance strategies that protect the data as storage media and systems change. Data stewards must constantly guard against changes in

formats and software that could make accessing the data more difficult, more costly, or even impossible. Since important collections are seldom static, a significant effort is required to integrate new metadata, add improvements and corrections to the data, and make additional related historical archives easier to access (Hankin et al. 2005). This effort goes beyond the capability and resources of most vessel operators.

Each vessel operator should establish a data pathway whereby meteorological observations are transferred from the vessel to a national or international archive center. The pathway may be direct, with copies of all data sent by the operator to the archive center on digital media to a pre-defined schedule (e.g., after each cruise, quarterly, annually). Alternatively, the data can flow through a specialized data center (e.g., the SAMOS data center), which will ensure the observations arrive at an appropriate archive center. Establishing an archive protocol will ensure that the investment in time and money that goes into collecting the observations will not only benefit current scientists, but those 10, 20, or even 50 years in the future.

11. Bulk Flux Algorithms (and the atmospheric surface layer)

Bulk flux algorithms enable the turbulent air-sea fluxes (sensible heat H_s, latent heat H_l, and momentum τ) to be calculated from the measured difference between the values of the corresponding bulk meteorological variable (temperature t, humidity q, wind speed u) at height z and at the sea surface. The simple form of the bulk air-sea flux equation given in section 2.1 is repeated here for convenience

$$F_x = C_x u(\delta_s - \delta_z), \tag{11.1}$$

where F_x is the vertical flux of entity x (heat, moisture, momentum), u the wind speed, and δ the value of the corresponding bulk meteorological variable (temperature, humidity, wind speed).

This equation suggests that C_x can be determined by measuring the surface fluxes by whatever means possible, together with the mean physical variables. During the second half of the 1900s, many such determinations were made using profile, covariance and dissipation techniques for the fluxes. Many of these employed atmospheric boundary-layer relationships between the fluxes and the (stability-dependent) vertical profiles of each variable, which had been determined over uniform sites on land and were subsequently applied over the ocean. To compare observations taken in different situations, these relationships are used to reference all measured values to the "standard" height of 10 m, and to define the transfer coefficient as a "neutral" value. The neutral value would give the same flux had the measurement been made at 10 m height under conditions of neutral atmospheric stability, and is normally represented by $C_{x10\,n}$.

From this early work the exchange coefficient for momentum (or drag coefficient) was found to increase at higher wind speeds. A relationship suggested by Smith (1980), $C_{D10\,n}=(0.61+0.063U_{10\,n})\text{x}10^{-3}$, appears also to fit more modern data sets (Yelland et al. 1998, Drennan et al. 2005). The exchange coefficients for the "scalar" variables, sensible and latent heat, seemed to be fairly constant; for example, Large and Pond (1982) found for sensible heat $C_{H10\,n} = 1.13\text{x}10^{-3}$ (unstable conditions), 0.66 (stable conditions) and for moisture $C_{E10\,n} = 1.15\text{x}10^{-3}$. Reviews by Smith (1988,1989) concluded that $C_{H10\,n}=1.0\text{x}10^{-3}$ and $C_{E10\,n} = (1.2\pm0.1)\text{x}10^{-3}$ for winds between 4 and 14 ms^{-1}. At that stage there were few measurements

below 4 ms^{-1} or above 14 ms^{-1}, and only recently has a clear increase of $C_{E10\,n}$ as winds increase been observed (Fairall et al. 2003). Values outside these limits were best regarded as extrapolations from the mid-range wind speeds where data were more plentiful. Further, as wind speed and atmospheric stability were usually the only variables considered, other variables such as sea state which might affect the air-sea exchange process were simply absorbed into the exchange coefficient.

The uncertainty in behaviour of the transfer coefficients, and the consequent limits to accuracy with which the fluxes could be calculated, became unacceptable as the sensitivity of climate models to the fluxes was recognised, particularly from efforts to couple ocean and atmospheric models. New bulk formulae were developed, incorporating better and more complete physical descriptions of the air-sea exchange process. The following is a brief account of the direction that these algorithms followed. To aid readability, in the context of profiles we have ignored the distinction between temperature and potential temperature, and the possible complication of a displacement height. However, such details may be found in WCRP (2000) and standard texts (e.g., Garrett 1992; Kraus and Businger 1994).

The way in which the bulk meteorological variables (t, q, u) change with height above the sea surface depends on atmospheric stability, and is well known. The dimensionless profiles of the variables are given by Monin-Obhukov similarity theory (e.g., Businger et al. 1971)

$$\frac{\kappa z}{u_*}\frac{\partial \bar{u}}{\partial z}=\phi_m\,;\quad \frac{\kappa z}{t_*}\frac{\partial \bar{t}}{\partial z}=\phi_t\,;\quad \frac{\kappa z}{q_*}\frac{\partial \bar{q}}{\partial z}=\phi_q \qquad , \tag{11.2}$$

where κ (= 0.4) is von Karman's constant, and the scaling parameters (u_*, t_*, q_*) are defined with reference to the surface fluxes

$$-u_*^2=\frac{\tau}{\rho}\,,\quad -u_*t_*=\frac{H_s}{\rho C_p}\,,\quad -u_*q_*=\frac{H_l}{\rho\lambda}\quad . \tag{11.3}$$

ρ and C_p are air density and specific heat, respectively, and λ the latent heat of vaporisation. The dimensionless profiles φ_x are functions of the atmospheric stability ζ (= z/L), where

$$-L=\frac{T_v}{g\kappa}\frac{u_*^2}{\left[t_*\left(1+0.61q\right)+0.61tq_*\right]} \tag{11.4}$$

is the Monin-Obhukov stability length (the height at which contributions to atmospheric turbulence by shear stress and buoyancy flux are roughly equal). The buoyancy flux is the quantity in square brackets, T_v [= $T(1+0.61q)$] is the virtual temperature of the air, and g is the acceleration due to gravity. Over the ocean, particularly in the tropics, the contribution of moisture to buoyancy is significant. Experiments over land have established formulae for the dimensionless profiles of the form

$$\phi_m=(1-\alpha\varsigma)^{-\beta}\quad for\ \varsigma<0\quad \text{unstable boundary layer} \tag{11.5a}$$

$$\phi_m=(1+\gamma\varsigma)\quad for\ \varsigma>0\quad \text{stable boundary layer}\,, \tag{11.5b}$$

where α, β and γ are empirically determined constants (see, e.g., WCRP 2000). The observations also support the assumptions that

$$\phi_t=\phi_q=\phi_m^2\quad for\ \varsigma<0;\quad \phi_t=\phi_q=\phi_m\quad for\ \varsigma>0\,. \tag{11.6}$$

Both unstable and stable forms of the dimensionless profiles (11.2) can be integrated between the surface and measurement height z

$$u_z = u_0 + \frac{u_*}{\kappa}\left(\ln\frac{z_u}{z_o} - \psi_m\right); \quad t_z = t_0 + \frac{t_*}{\kappa}\left(\ln\frac{z_t}{z_{0t}} - \psi_t\right); \quad q_z = q_0 + \frac{q_*}{\kappa}\left(\ln\frac{z_q}{z_{oq}} - \psi_q\right), \qquad (11.7)$$

where u_0, t_0, q_0 are the surface values, and the stability functions ψ_χ are integrals of the dimensionless profiles φ_χ. In neutral conditions the ψ_χ are zero and the profiles take the familiar logarithmic form. The heights for the wind and scalar measurements can be different; the denominators are the surface roughness lengths for each variable.

Certain aspects of these land-based equations differ when applied over the ocean. Over land $u_0 \equiv 0$, whereas the water surface is mobile. Physically, the correct wind velocity to use when calculating sea-air transfer is relative to the water surface, so when u_z is measured with respect to Earth coordinates (e.g., using GPS) the surface current, u_0, should be subtracted vectorially (but see comments in section 2.5). Also, since the humidity at the air-sea interface, q_0, is calculated as the saturation vapour pressure (svp) over pure water at the SST (Clausius-Clapeyron relationship), it must be reduced by 2% to allow for the reduction of svp over saline water at 34 psu (Kraus and Businger 1994).

Comparing equation (11.7) with the formal bulk flux equation (11.1) for the case of momentum,

$$\frac{-\tau}{\rho} = u_*^2 = C_D\left(u_0 - u_z\right)^2, \qquad (11.8)$$

we see that the drag coefficient can be expressed as $C_D = \kappa^2\left(\ln\frac{z_u}{z_0} - \psi_m\right)^{-2}$, (11.9)

whence the 10 m neutral value $C_{D10n} = \kappa^2\left(\ln\frac{10}{z_0}\right)^{-2}$. (11.10)

This emphasizes the important point that the neutral drag coefficient is directly related to the wind roughness length z_0 – the two are interchangeable. If the roughness of the sea surface can be specified, for example by a physically based wind/wave relationship or a well-founded empirical parameterization, the above equations can be solved to obtain the wind stress.

From classical studies in fluid mechanics, surface roughness and wind stress are related through the dimensionless roughness Reynolds number $R_r = u_* z_0 / \nu$, where ν is the kinematic viscosity of air. When $R_r > 2.0$ the surface wind regime is said to be aerodynamically "rough" and for $R_r < 0.13$ it is "smooth", with R_r approaching a constant value of about 0.11 as wind speed decreases. Over the ocean, these limits on R_r correspond to 10 m wind speeds of about 8 ms^{-1} and 2 ms^{-1}, respectively; in between is a transition regime between rough and smooth flow.

On the basis that the ocean roughness results mainly from gravity waves generated by wind stress, Charnock (1955, 1958) proposed that $z_0 = \alpha_c u_*^2 / g$, where g is the acceleration due to gravity and α_c is Charnock's "constant". However, the wide range of values found for α_c

signal that wind/wave characteristics are more complicated than this simple relation suggests. Smith (1988) proposed that the entire smooth to rough flow regime be written,

$$z_0 = \frac{\alpha_c u_*^2}{g} + 0.11\frac{\nu}{u_*} \quad , \tag{11.11}$$

but this only fits the data if α_c is allowed to vary. The transfer coefficients for heat and moisture depend on both the momentum roughness length, and those for temperature and humidity, which can be similarly parameterized as $R_t = u_* z_{0t} / \nu$ and $R_q = u_* z_{0q} / \nu$. By considering physical transfer processes across the interface using surface renewal theory, in which small eddies transfer heat intermittently between the bulk and the ocean surface, Liu et al. (1979) determined empirical relationships between R_r, R_t, and R_q. This approach is the basis of some modern bulk algorithms, which solve equations for the fluxes, profiles and atmospheric stability iteratively. The bulk algorithm developed for community use in the TOGA-COARE experiment (Fairall et al. 1996b, 2003) is described in Appendix B.

In recent years, the imperatives of climate research that set the 10 Wm^{-2} goal for net air-sea flux measurement have also led to greatly improved measurements, extending the wind speed range over which the exchange coefficients are valid. There remain difficulties at high winds (> ~20 ms^{-1}) when spray droplets contribute to the transport of heat and water vapour, for which reliable parameterizations have yet to be developed. At very low winds, equation (11.1) predicts vanishing fluxes at zero mean wind. In reality, this limit is usually associated with variable, gusty winds which transport energy and stress even when the vector mean wind is zero (Bradley et al. 1991). Godfrey and Beljaars (1991) avoid this problem by introducing a "gustiness" velocity, u_g, proportional to the convective scaling velocity for the atmospheric boundary layer W_*, (Deardorff 1970) where

$$W_*^3 = \frac{g}{T}\left[\frac{H_s}{\rho C_p} + 0.61 T \frac{H_l}{\rho \lambda}\right] z_i \quad , \tag{11.12}$$

so that $u_g = \beta W_*$, the constant β to be determined empirically. (11.13)

The sea state (wave characteristics) and surface current also modify fluxes, the surface currents, by changing the wind shear. A current moving in the same direction as the wind will result in smaller surface fluxes, while currents running counter to the wind will increase them. A situation can be imagined in which changing tidal currents cause variation in the fluxes under a constant wind. The magnitude of the vector difference of the wind and the surface current should replace wind speed in flux calculations, with the stress in the direction of the vector difference.

There have been many approaches to parameterize the influence of waves on surface stress. Most agree that the stress is larger when the wind waves (waves supported by the local winds) are relatively steep. This effect can be explained in terms of wave age (which has several different definitions), and usually parameterized through the drag coefficient or Charnock's parameter [α_c in equation (11.11)]. For example, short and sharp waves that initially form when there is sufficient wind over a smooth surface have a much larger drag coefficient than very tall, long and gently rolling waves. There is no convincing evidence that waves influence transfer coefficients for heat and moisture.

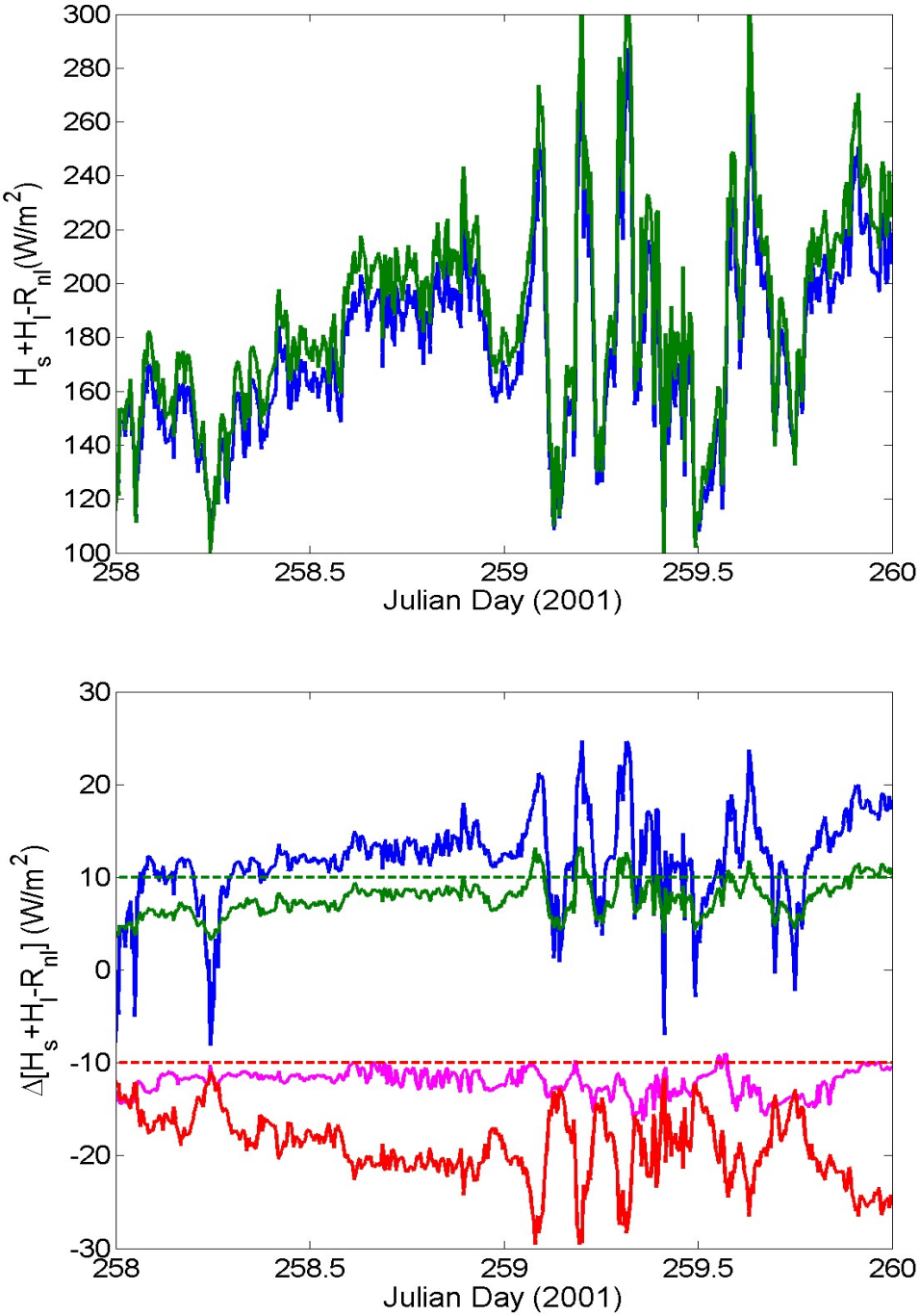

Figure 11.1. Sensitivity of bulk flux calculations to algorithm and input data; time series of sum of sensible, latent, and net longwave fluxes. Upper panel: COARE 3.0 (C3 blue) and Large and Pond 1982 (LP green). Lower panel: LP - C3 (blue), C3(Ts-0.5) - C3(Ts) (red), C3(qa-0.5) - C3(qa) (green), and C3(U - 0.5) – C3 (mauve).

The influence of swell, waves produced by distant winds and not supported by the local winds, is more controversial. Wind waves tend to propagate in a direction parallel to the wind vector. Swell propagating in other directions has been observed to cause large variability in the traditional drag coefficient, which cannot be explained in terms of wave age. An alternative approach, which considers wave-related modifications in a similar manner to the current modifications discussed above rather than the drag coefficient, has shown promise for both wind waves and swell, and is an area of ongoing research. Figure 11.1 looks at the **ocean heat loss terms** in equation (1.1) to examine the effect of different algorithms or small biases in the data. The upper panel is computed using two of the best known bulk flux algorithms, Large and Pond (1982; LP) and COARE 3.0 (Fairall et al. 2003, C3). These are from different eras and contain different functions and assumptions, so this is not intended to evaluate them, but rather to provide natural differences in calculated fluxes. We consider the two consecutive but contrasting days of Figures D1 and D2 with wind speeds in the range 3-6 ms^{-1}.

The lower panel shows the difference between LP and C3 (blue trace). LP produces greater ocean cooling, by around 10-15 Wm^{-2} on the steady day, but more variable and as much as 25 Wm^{-2} on the convective day. The other three traces indicate the effect of a realistic error (an electronic signal offset or calibration error for example) in the input data to the COARE 3.0 flux algorithm. The ±10 Wm^{-2} target accuracy is indicated by the green- and red-dashed lines. An error in specific humidity of -0.5 g kg^{-1} (drier air) will increase latent heat flux and hence produce too much ocean cooling, by around 10 Wm^{-2} in this example (green trace); an error that reduces true wind speed by 0.5 ms^{-1} will reduce both latent and sensible heat loss totalling 10 Wm^{-2} (mauve trace); a -0.5ºC error in sea temperature affects sensible and latent heat, and also reduces the outgoing longwave radiation, the three effects together assigning around 20 Wm^{-2} too much warming of the ocean (red trace).

These figures assume that only one of the input variables is in error, while the other two are exact. In practice this is unlikely, hence the more stringent accuracy requirement given in Table 1. Note also that use of the routine ship weather observations, which Figure 3.4 showed can contain significant errors, will not produce air-sea fluxes of sufficient accuracy for climate studies without careful analysis and corrections to the observations.

Appendix A - Useful Formulae, Parameters, and Conversions

Studies of the atmospheric and oceanic surface layers, and the transport of energy and matter across the interface between them, involve the dynamic and thermodynamic properties of the respective fluids, air and seawater. The following equations and values are frequently needed in the analysis following measurements of the state variables, air temperature, pressure, density and moisture content. In some cases they are not strictly rigorous - simplifications are made by neglecting small quantities, insignificant in the present context. More complete derivations are given in Andreas (2005). Comprehensive discussions of atmospheric thermodynamics can be found in standard texts, e.g., Garratt (1992), Bohren and Albrecht (1998).

A1. Equations of State

Temperatures in degrees Kelvin are denoted by T and in Celsius by t, where $T = t + 273.16$ K.

Quantities relevant to the thermodynamic properties of moist air are:

The universal gas constant	$R = 8.3145$	(J mol^{-1} K^{-1})
Molecular mass of dry air	$m_a = 0.028965$	(kg mol^{-1})
Gas constant for dry air	$R_a = R/m_a = 287.05$	(J kg^{-1} K^{-1})
Molecular mass for water vapour	$m_v = 0.018015$	(kg mol^{-1})
Gas constant for water vapour	$R_v = R/m_v = 461.5305$	(J kg^{-1} K^{-1}) .

From the ideal gas law we obtain the

Density of dry air $\rho_a = (p - e)/R_a T$ (kg m^{-3}) ,

with temperature T in kelvins and (p - e) pressure in Pascals (100 Pa = 1 mb). Note, to compute the *dry air* density we must remove the pressure contribution of water vapour from the pressure gauge reading. At standard temperature (273.15 K = 0°C) and pressure (101325.0 Pa = 1013.25 mb) ρ_a = 1.2922 kg m^{-3}.

The behaviour of water vapour in the atmospheric surface layer approximates that of an ideal gas so that the

Water vapour density $\rho_v = 100\, e/R_v T$ (kg m^{-3}) ,

where, traditionally in meteorology, e is the partial pressure of water vapour in millibars (mb). The vapour density is also referred to as the ***absolute humidity***.

Other ways of specifying the water vapour content in a sample of moist air are the

Mixing ratio $r = \rho_v / \rho_a = 0.622e/(p - e)$, (kg kg^{-1} of dry air) ,

where the factor 0.622 = m_v/m_a , and the barometric pressure p and e are in the same units.

Specific humidity $q = \rho_v / \rho = 0.622e/(p - 0.378e)$, (kg kg^{-1} of moist air) ,

where the factor 0.378 = (1 - m_v/m_a), and the density of moist air

$$\rho = \rho_a + \rho_v = 100\, p/(R_a T(1 + 0.61q)) \quad \text{(kg m}^{-3}\text{)} .$$

The factor 100 converts from mb to Pa, and 0.61 = (m_d/m_v-1). The quantity $T(1+0.61q)$ is called the ***virtual temperature*** T_v , which is the temperature that air of given pressure and density would have if it were completely free of water vapour.

Saturation vapor pressure $e_s = 6.1121\,(1.0007 + 3.46x10^{-6}\,p)\,\exp(17.502\,t\,/(240.97 + t))$ (mb), where t (°C) is air temperature**,** and p (mb) is atmospheric pressure. This empirical expression is valid above pure water between -20° and 50°C (Buck, 1981).

Some relationships below require a value of the *saturation vapor pressure* (svp).

Above seawater the svp is depressed to $e_{sea} = e_s\,(1 - 0.000537S)$ (mb),

where S is salinity (psu). If S = 35 psu, $e_{sea} = 0.981e_s$ or roughly 2% less than over pure water.

Relative humidity $RH = 100(e/e_s)$ *as* % ; *or* (e/e_s) *as a fraction* .

Dew point T_d : for given *e, T_d* may be obtained by inverting the *svp* equation; however, most often T_d is measured (see section 3.3) and *e* calculated by putting *t = Td* (°C) in the *svp* equation.

Specific heat of dry air at constant pressure is given by the polynomial,

$$C_p = 1005.6 + 0.0172t + 0.000392t^2 \qquad (\text{J kg}^{-1}\ ^\circ\text{C}^{-1})$$

valid in the range ±40°C and for barometric pressures around one atmosphere. The temperature dependence is weak, and a constant value of 1006 J kg^{-1} °C^{-1} is usually adequate.

Latent heat of vaporization $\lambda_v = (2.501 - 0.00237t)\times 10^6$ (J kg^{-1}),

with the constant value 2.50×10^6 J kg^{-1} being accurate enough for most purposes in the surface layer.

Psychrometric equation $e = e_s(t_w) - \dfrac{m_a}{m_v}\dfrac{C_p}{\lambda_v}(t - t_w)\,p$ (mb),

where $e_s(t_w)$ is the *svp* at wet-bulb temperature t_w , $(t - t_w)$ is the ***wet-bulb depression*** and p the barometric pressure. The factors before the parentheses are known as the ***psychrometric constant***. Using the constant values quoted above, and combining with p = 1013.25 mb (the standard atmosphere at sea level), the practical psychrometer equation is usually written

$$e = e_s(t_w) - 0.66\,(t - t_w) \qquad (\text{mb}),$$

where t and t_w are referred to as dry-bulb and wet-bulb temperatures (°C), respectively.

Kinematic viscosity of dry air

$$\nu_a = 1.326\times 10^{-5}\,(1 + 6.542\times 10^{-3}t + 8.301\times 10^{-6}t^2 - 4.840\times 10^{-9}t^3)\ (\text{m}^2\ \text{s}^{-1})$$

valid for the temperature range t = ±50°C.

Dry adiabatic lapse rate $\left(\dfrac{\partial t}{\partial z}\right)_{\theta = const.} = -\dfrac{g}{C_p} = -\Gamma_d = -0.0098\ ^\circ\text{C m}^{-1}$

where θ is the potential temperature.

Potential temperature, θ, is the temperature an air parcel with absolute temperature t (K) at height z would have if brought adiabatically to the sea surface. From thermodynamic considerations, we obtain:

$$\theta = t + \frac{g}{C_p} z \ .$$

Calculation of the sensible heat flux using the bulk equation (1.1) should therefore use the potential temperature difference

$$\Delta\theta = t_{sea} - t_{air} - 0.0098z$$

with sea and air temperatures in °C and z the height of the air temperature measurement (m).

A2. Ice-Related Expressions

Latent heat of fusion of ice $\lambda_f = 0.334 \times 10^6$ (J kg^{-1})

Saturation vapor pressure over ice (or snow)

$$e_s = 6.1115\,(1.0003 + 4.18x10^{-6}\,p)\exp(22.452\,t/(272.55 + t)) \quad \text{(mb)}$$

valid for $-50° \le t \le 0°$ (Buck, 1981)

Specific heat of ice $c_{pice} = -114.19 + 8.1288T + 3.421T\exp[-(T/125.1)^2]$ (J kg^{-1} K^{-1}).

A3. Radiometry

The following values of albedo and emissivity of the ocean surface were obtained during the TOGA-COARE campaign, and are broadband and isotropic.

Short-wave albedo of sea surface	$\alpha = 0.055$	
Long-wave emissivity of sea surface	$\varepsilon = 0.97$	
Stefan-Boltzmann constant	$\sigma = 5.670 \times 10^{-8}$	(Wm^{-2}K^{-4})
Pyrgeometer equation	$R_{l\downarrow} = V/s + \sigma T_c^4 + B\sigma(T_c^4 - T_d^4)$	(Wm^{-2})

with thermopile output V (μV) and calibration factor s in μV/(Wm^{-2}), T_c and T_d temperatures (K) of the instrument case and dome, respectively, and B a factor representing the IR transmission and absorption characteristics of the dome. For a given instrument, s will be given but B may not, in which case the value $B = 3.5$ is a fair average.

Outgoing long-wave radiation $R_{l\uparrow} = \varepsilon\sigma T_s^4 + (1-\varepsilon)R_{l\downarrow}$ (Wm^{-2}) ,

where T_s is the ocean surface temperature (K), ε (= 0.97) is its emissivity and σ (= 5.67x10^{-8}) is the Stefan-Boltzmann constant.

A4. Barometer Correction

Near the surface, atmospheric pressure falls at about 0.12 mb m^{-1} as height increases. Since we need the value near the surface and the barometer is usually on the bridge some tens of metres higher, we make a correction based on the hydrostatic equation for the atmosphere,

$$\frac{1}{\rho_a}\frac{\partial p}{\partial z} = -g$$ where z is height, p is pressure and g is the acceleration due to gravity.

Introducing the ideal gas law, integrating this expression from observation height to the surface and simplifying, we have for the surface pressure

$$p_s = p\exp(gz / R_a T),$$

where p is the observed pressure at height z, R_a is the gas constant for dry air, and T (K) is a reference temperature (e.g., at z = 10 m). For example, if the pressure at a barometer height of 30 m was 1000.0 mb, with g = 9.81 ms^{-2}, R_a = 287.05 $Jkg^{-1}K^{-1}$ and T = 290 K, p_s = 1003.54 mb.

A5. Conversions

1 nautical mile (nm) = 1.852 km by definition.

1 knot = 1.852 $kmhr^{-1}$ = 0.51444 ms^{-1}.

1 standard atmosphere = 1013.25 mb.

Standard gravity g = 9.80665 ms^{-2}.

An average latent heat flux of 100 Wm^{-2} evaporates 3.456 mm water per day.

A6. Gravity

Acceleration due to gravity*, g* (ms^{-2}) is calculated as a function of latitude at sea level by the expression

$$g = 9.78033(1 + (0.0053\sin^2\phi - 5.8\times10^{-6}\sin^2 2\phi))\ \ (\mathrm{m\ s^{-2}})$$

or by the polynomial

$$g = 9.7803267715\times(1 + c1\sin^2\phi + c2\sin^4\phi + c3\sin^6\phi + c4\sin^8\phi)\ \ (\mathrm{m\ s^{-2}}),$$

where c1 = 0.0052790414
c2 = 0.0000232718
c3 = 0.0000001262
c4 = 0.0000000007.

These two methods agree to four places of decimals. They give g = 9.7803 and 9.8322 ms^{-2} at the equator and the poles, respectively. The standard value 9.80665 ms^{-2} is given at latitude ~ 45.5°.

A7. Relative Wind Conversions Aboard Ship

Conversion of Relative to True wind speed and direction

"True" wind and direction will be defined as being in Earth-relative coordinates.

Directions follow the meteorological convention – "northerly" winds are *from* the north, "easterly" *from* the east.

Then, cog = ship's course over ground from GPS
sog = ship's speed over ground from GPS
head = gyrocompass heading, north = 0° east = 90°
rels = relative wind speed
reld = relative wind direction, 0° over bow, 90° over starboard

relsn = rels.cos(head+reld) northerly component of relative wind
relse = rels.sin(head+reld) easterly component of relative wind

sogn = sog.cos(cog) north component of ship speed
soge = sog.sin(cog) east component of ship speed

un = relsn-sogn northerly component of true wind (-ve sign because wind dir. "from").
ue = relse-soge easterly component of true wind (-ve sign because wind dir. "from").

dirt = mod(atan2(ue,un)+360,360) true wind direction
$ut = (un^2 + ue^2)^{1/2}$ true wind speed

Notes. The above implies that angles are expressed in degrees. Some computer software requires that angles be expressed in radians, and entering degrees can generate bewildering results. In this case angles should be multiplied by the factor rdcon = *pi*/180 (*pi* = 3.14159).

The atan2 function is commonly available in software such as Matlab, Fortran, Excel, etc. It computes, in our case, the arc tangent of *un/ue*, returning an angle in the range *–pi* to *+pi*, expressed in radians, using the signs of *un* and *ue* to compute the quadrant of the result. If the calculation is done by hand, care must be taken to resolve the ambiguity of the *arctan* function.

Conversion of relative to water-relative wind speed and direction

Certain applications, in particular air-sea flux calculation, require the wind speed relative to the surface water [see section 2.5 and equation (11.7) et seq.]. We call this the "water-relative" wind. When the near-surface current speed and direction (Earth-relative) are available (e.g., from a surface mooring) this current can be resolved into north and east components cn and ce. These would normally be in the oceanographic convention "to". Then, having acknowledged this unusual convention, the true wind components can be converted to water-relative, and the water-relative wind speed $uw = [(un+cn)^2 + (ue+ce)^2]^{1/2}$ which is equivalent to $(u_z - u_0)$ in equation (11.7).

Alternatively, uw may be obtained by replacing *cog* and *sog* with course and speed from the ship's 2-axis Döppler-log and gyro-compass, as follows:

uf = forward speed from Döppler-log
us = side-slip to starboard (positive)

head = gyro-compass heading, north = 0° east = 90°
rels = relative wind speed
reld = relative wind direction, 0° over bow, 90° over starboard

relsn = rels.cos(head+reld) northerly component of relative wind (as before)
relse = rels.sin(head+reld) easterly component of relative wind (as before)

sown = uf.cos(head)-us.sin(head) north component of ship speed
sowe = uf.sin(head)+us.cos(head) east component of ship speed

unw = relsn-sown northerly component of water-relative wind (-ve sign, wind dir. "from")
uew = relse-sowe easterly component of water-relative wind (-ve sign, wind dir. "from")

dirw = mod(atan2(uew,unw)+360,360) water-relative wind direction
$uw = (unw^2 + uew^2)^{1/2}$ water-relative wind speed ,

where again uw is equivalent to $(u_z - u_0)$ in equation (11.7).

The above comments regarding the mode of angles and use of atan2 apply.

These issues and other aspects of the reporting of true wind are discussed in considerable detail by Smith et al. (1999). Program codes for calculating true (earth-relative) winds can be obtained from http://www.coaps.fsu.edu/woce/truewind/.

A8. Height Adjustment

The variation with height of wind speed, temperature, and water vapour content in the atmospheric surface layer (their profiles), depend on surface conditions and thermal stability, as described in section 11. There are two main reasons for needing to estimate the value of any of these variables at a height other than that at which it was measured; adjustment to standard reference height (10 m) to relate to other experiments (e.g., comparing $C_{D10\,n}$ and $C_{E10\,n}$); and when inter-comparing instruments at different heights and on different platforms. The latter is of particular importance in the context of procedures for the SAMOS initiative and this Handbook (see section 8.3).

Based on the principles of Monin-Obhukov similarity theory, equation (11.7) defines the three profiles, in the familiar "log-linear" form. The critical assumption is that the fluxes, or equivalently the M-O scaling parameters (u_*, t_*, q_*), are constant with height within the surface layer. In neutral conditions, the logarithmic profiles are specified by their slope (u_* etc.) and intercept on the height axis (z_0 etc.). In diabatic conditions the $\Psi(z/L)$ term [also dependent on the fluxes; see equation (11.4)] produces an increasing departure from logarithmic with increasing height and thermal instability (or stability). Thus, for a convenient averaging period (e.g., 30 min or 1 hour), profiles can be constructed when the fluxes and the roughness lengths are known. This can be achieved with modern advanced and validated bulk flux algorithms.

The profiles shown in Figure A1 are derived from meteorological data obtained from the IMET instruments aboard R/V *Revelle* during a 27-hour inter-comparison with the WHOTS mooring 100 km north of Hawaii. The COARE Version 3.0 bulk algorithm was used to calculate the fluxes, roughness lengths and stability-related parameters needed in equation (11.7).

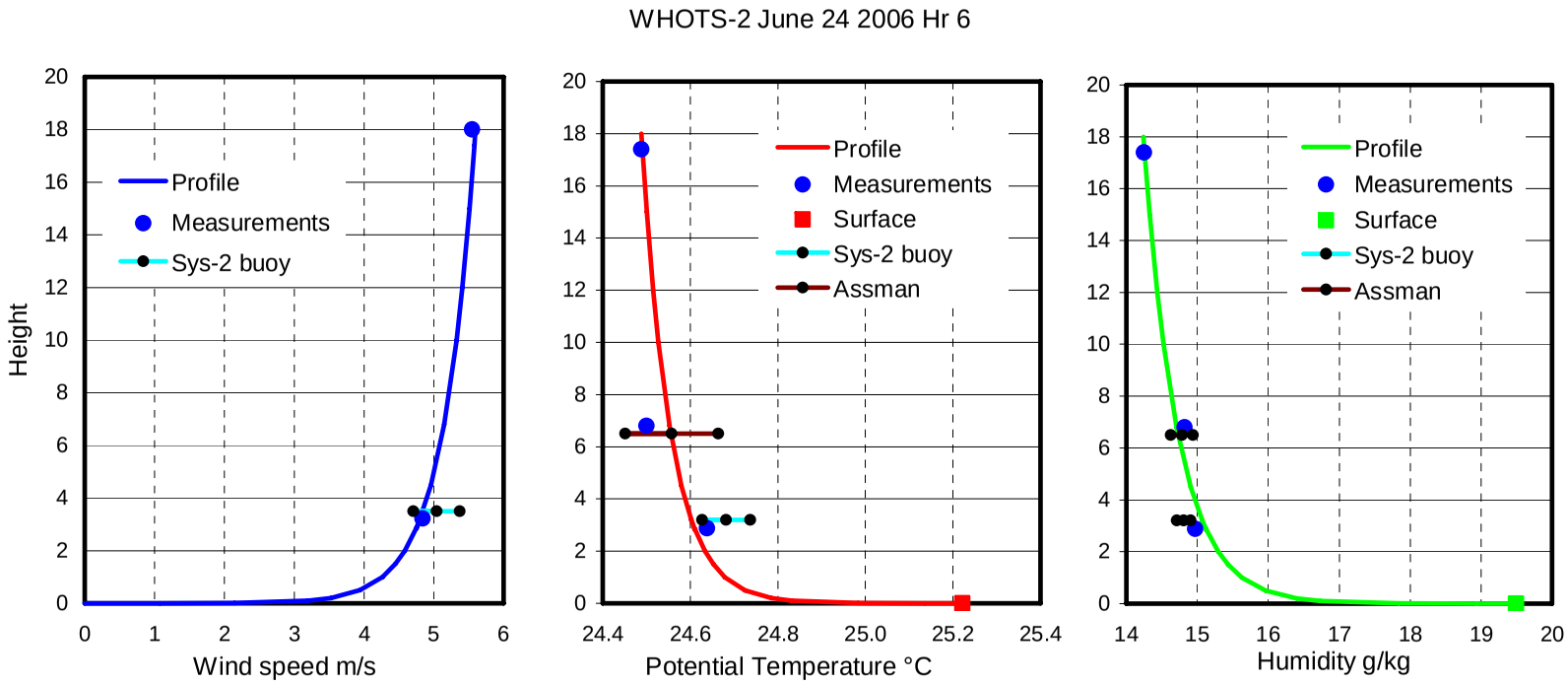

Figure A1. (Data courtesy Bob Weller). Example of need for height adjustment when comparing measured values at various levels above the sea surface. The ship's anemometer was at 18 m on the foremast, and the temperature/humidity sensor at 17.4 m. Temperature and humidity were measured with an Assman psychrometer through a forward chock at 6.8 m height (see Figure 3.1). The ship was standing about 0.25 nm downwind of the WHOI buoy, which had two wind sensors at 3.22 m above the sea surface and two temperature/humidity sensors at 2.88 m. The ship and buoy data points are hourly averages; the Assman values are spot readings. The profiles were constructed from flux/gradient parameters calculated using Version 3.0 of the COARE bulk flux algorithm, and used in equation (11.7), as follows;

Parameter	u_*	t_*	q_*	z_o	z_{ot} , z_{oq}	ψ_m	ψ_t , ψ_q	z/L
Units	ms^{-1}	C	g kg^{-1}	m	m			
Value	0.184	-0.026	-0.192	4.75e-5	7.74e-5	0.705	1.257	-0.427

Surface values (u_0, t_0 and q_0) were 0 ms^{-1}, 25.22 °C, and 19.57 g kg^{-1} respectively; $\kappa = 0.4$.

Their values for this particular one-hour period are given beneath the figure, to acquaint the reader with the typical magnitude and sign of these symbols that feature in the theoretical development. A z/L of -0.4 is moderately unstable, but not in the realm of convective conditions.

The algorithm input data consisted of the wind speed and temperature/humidity measurements near the top of the foremast, the thermo-salinograph sea temperature from 5-m depth, and other relevant variables (barometric pressure, short- and long-wave radiation). The surface temperature and humidity values in the figure are extrapolated from 5 m to the surface using models of the cool skin and diurnal warming. No surface current data was available, so u_0 was taken to be zero. A linear height scale is used to illustrate more clearly the characteristics of near-surface profiles over the ocean. Because the sea is very "smooth" compared with land surfaces (typically, z_0 over grassland is 0.01 m), most of the sea-air difference occurs in the lowest 1-2 metres. Note that the profiles in Figure A1 have each been produced from just two measurements (at the top of the mast and the sea surface) and with the benefit of knowledge gained from many decades of boundary layer study over land sites.

We can now compare measurements from the same local regime, but at different heights, in this case by a hand-held Assman psychrometer and from the buoy that has been *in situ* for a year. The buoy is equipped with two independent meteorological systems – for clarity we illustrate only one. Without allowing for the height difference the buoy wind speed would have seemed almost 1 ms^{-1} too low compared with the ship's ultrasonic anemometer. The profile indicates that at buoy height (2.88 m) the potential temperature is 0.15ºC higher, and the specific humidity 0.73 g kg^{-1} higher, than at the top of the foremast (17.4 m). After a year of unattended operation both the potential temperature and specific humidity measurements by the buoy during this hour agree remarkably well with the height adjusted ship instruments. The differences from the profile were 0.03ºC and 0.12 g kg^{-1}, well within the accuracy targets in Table 1. The role of the Assman psychrometer is to validate the ship's temperature and humidity instruments (see section 8.4). For this hour agreement is within 0.05ºC and 0.11 g kg^{-1}, better than the resolution of the thermometers.

For the purpose of illustration, from the 27 hours available for this intercomparison we have selected an hour with reasonable overall agreement. The horizontal bars indicate the variability of the measurements; the centre dot in each case being the average difference over the 27 hours (the bias) with the bars indicating ±1 standard deviation. Variability is due mainly to the separation between the ship and the buoy, and also the different sampling strategies of the ship and Assman. Nevertheless, with the possible exception of the buoy humidity, the comparisons on this day were within the goals of Table 1, possibly aided by the fact that conditions were fairly steady. We make the point, however, that intercomparison periods should run for at least 24 hours to overcome the sampling problem.

It was convenient for us to perform this height analysis using the COARE flux algorithm. However, we emphasize that any model (or combination of models) of air-sea exchange that produces values for the fluxes, the roughness parameters, and the atmospheric stability is capable of relating an observation at a particular height in the surface layer to any other height (e.g., standard 10 m) through the use of equation (11.7).

Appendix B – The TOGA-COARE Bulk Flux Algorithm

B1. History and Features

In 1993, as part of the TOGA-COARE Air-Sea Interaction (Flux) Working Group activity, Chris Fairall, Frank Bradley and David Rogers began development of a bulk air-sea flux algorithm for use by the COARE community. The purpose was to ensure that the bulk flux results from every measuring platform were derived from identical assumptions, physical functions and computational methods. Faced with the challenging target of net heat flux accuracy of 10 Wm^{-2}, any disagreements would be due to the basic observations, not differences in the bulk algorithm. In some respects, the same situation applies to the SAMOS initiative.

The COARE algorithm had to take account of the light wind, strongly convective conditions found in the region of the tropical Pacific warm pool. It was based on the model of Liu, Katsaros and Businger (1979), hereafter referred to as LKB, which used the formalism of Monin-Obhukov similarity theory for the atmospheric surface layer, solving equations (11.2) to (11.7) iteratively for the surface fluxes. The velocity roughness was specified by the Charnock/Smith expression (11.11), and the scalar roughness lengths from relationships between the velocity and scalar roughness Reynolds numbers given by LKB. Independent estimates of α_c (= 0.011) and the gustiness parameter, β (= 1.20) in equation (11.13) were made from covariance and dissipation flux measurements made during COARE. The *unstable* profile functions were a blend of the Kansas functions, ψ_k, near neutral (Businger et al. 1971) with a form, ψ_c, that obeys the theoretical scaling limit in highly convective conditions (Fairall et al. 1996b). The *stable* forms were as determined for Kansas.

At Version 2.5b the COARE bulk flux algorithm was made generally available (Fairall et al. 1996b). Its major shortcomings were that the exchange coefficients were based on less than 1000 hours of directly measured fluxes and solely on COARE data, and so was effectively "tuned" to tropical conditions with few wind speed observations greater than 10 ms^{-1}. Clearly, the algorithm needed to be generalized for more global applications and tested against a much broader dataset. By 1999 Fairall's group at NOAA/ESRL [Earth System Research Laboratory; formerly Environmental Technology Laboratory (ETL)] had undertaken cruises in all ocean basins (Fairall et al. 1997). From these a flux database of over 7200 h was assembled, including 800 h with wind speeds in excess of 10 ms^{-1}, and 2200 h at high latitudes. It was augmented with 94 h of high wind data from the HEXMAX experiment (De Cosmo et al. 1996). A subset of these data were used to refine the algorithm as Version COARE 3.0, and it was tested against the entire database (Fairall et al. 2003).

Codes are available at ftp://ftp.etl.noaa.gov/user/cfairall/bulkalg/cor3_0/ and accompanied by a "readme" description. Inputs required are time series of the meteorological variables, together with the height (or depth) of measurement; i.e., date, time, wind speed, air temperature and humidity, sea temperature, downward short- and long-wave radiation, rainfall, latitude, longitude. The radiation data are required for the calculation of ocean surface warming, the ship's position for gravity and the solar time.

Features of Version 3.0 are as follows:

1. Below 10 ms^{-1} the Charnock parameter in equation (11.11) retains the value (α_c = 0.011), but above 10 ms^{-1} takes a simple wind speed dependence based on data from various sources (e.g., Hare et al. 1999).

2. The Liu et al. (1979) scalar roughness relationship has been replaced with a much simpler one that fits both the COARE and HEXMAX databases, $z_{0t} = z_{0q} = 5.5 \times 10^{-5} R_r^{-0.6}$.

3. A gustiness factor [equations (11.12) and (11.13)] is calculated in the flux loop, using $\beta = 1.25$ determined from COARE measurements, and applied as $\sqrt{(u^2 + u_g^2)}$ to avoid singularity as u→0.

4. An empirical constant in the *convective* portion of the scalar profile function has been optimized to match direct profile observations (Grachev et al. 2000).

5. The Kansas *stable* profile functions (Businger et al. 1971) have been replaced by those from Beljaars and Holtslag (1991), which compare well with new profile data taken over the Arctic ice cap (Persson et al. 2002) and appear to be a better fit at extreme stability.

6. The stability iteration loop uses a bulk Richardson number parameterization as a first guess (Grachev and Fairall, 1997), thus reducing calculation time and making the algorithm more attractive for use in numerical models.

7. SST (skin temperature) can be obtained from measurements at depth, using models of the diurnal warm layer and cool skin (see section 2.6, Fairall et al. 1996a and Wick et al. 2005). The models require downwelling long- and short-wave radiation data; values for broadband surface albedo and ocean emissivity are taken as 0.055 and 0.97, respectively (from COARE observations). These optional models are not used if SST is obtained using an infrared or microwave radiometer.

8. An option has been included to allow the velocity roughness to be calculated from wave parameters. We have taken two models from the recent literature that are wave age and/or wave slope based. Oost et al. (2002) requires the wave period to be specified, and Taylor and Yelland (2001) need both wave period and significant wave height. However, these schemes have not been tested with reliable wave measurements.

9. The so-called Webb correction (Webb et al. 1980) to latent heat flux arises from the requirement that the net dry mass flux be zero. The latent heat flux is therefore formulated in terms of mixing ratio, the fundamentally conserved quantity, instead of specific humidity. However, the model returns the mean Webb velocity, which can be used to compute Webb corrections for any trace gas or particle fluxes measured simultaneously.

10. The momentum and sensible heat fluxes due to rainfall are calculated (Caldwell and Elliott, 1971; Gosnell et al. 1995).

B2. Examples of COARE 3.0 Performance

The essence of the bulk flux scheme is the specification of roughness lengths or, equivalently, of the 10-m neutral transfer coefficients. Version 3.0 is based on averaging thousands of data points; in Figure B1 the actual data are shown with the model. An example of the model's ability to yield the correct values, on average, for fluxes is shown in Figure B2, where both model-derived and measured latent heat fluxes have been composited in wind speed bins (the lines denote means and the symbols denote medians). The agreement is excellent from 0 to 20 m/s. Another way to view the state of the transfer coefficients is to ratio with the Version 3.0 specifications (Figure B3). Here the ESRL (ETL) data are shown as points with statistical uncertainties in the mean quantity. The dashed lines are the transfer coefficients used by the two major operational weather forecast centers (NCEP and ECMWF). NCEP recently replaced their

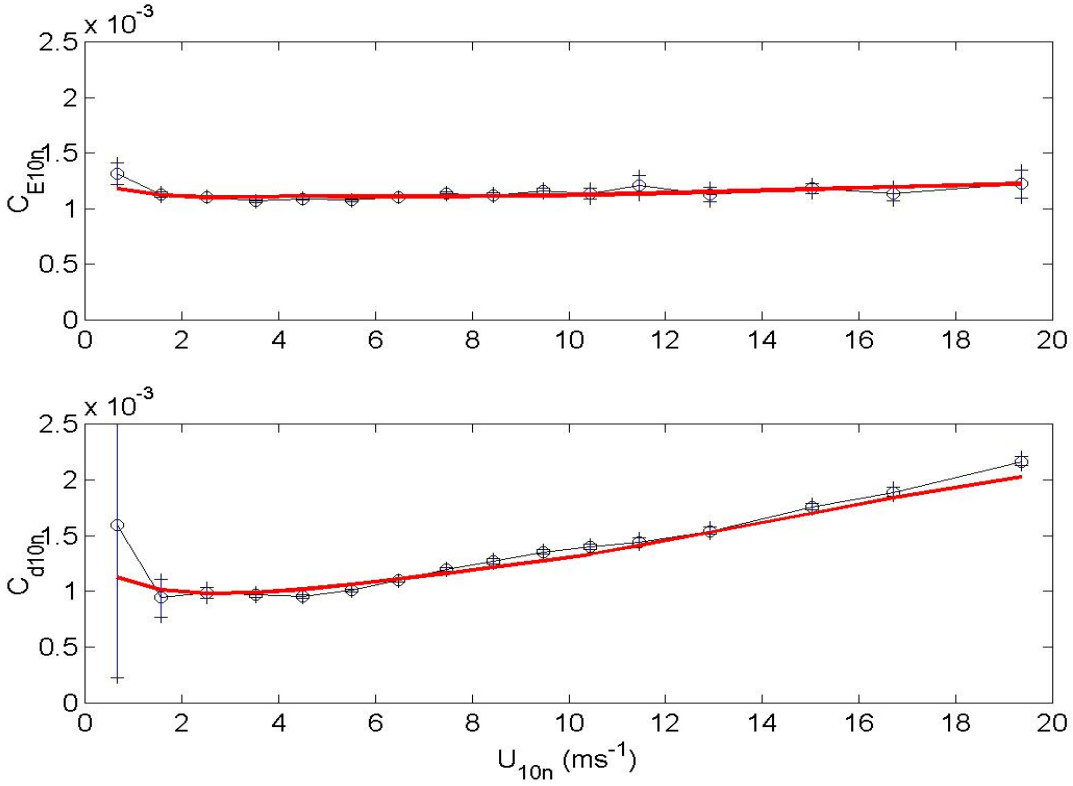

Figure B1. Wind speed dependence of the momentum (lower panel) and scalar transfer (upper panel) coefficients for COARE versions 3.0 (solid line) and measurements (thin line with circles).

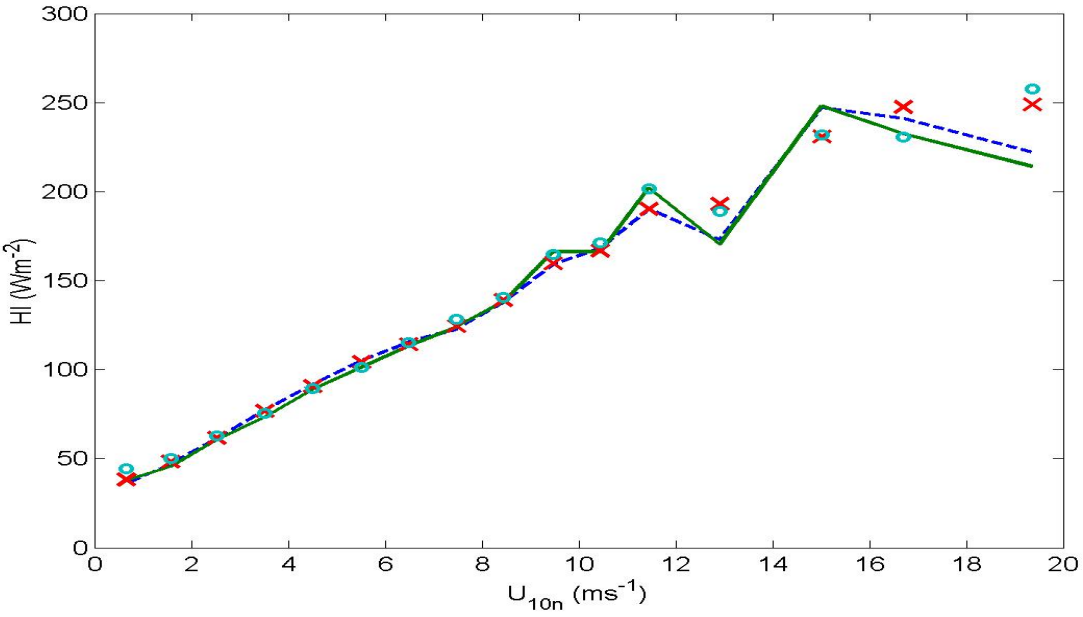

Figure B2. The average of covariance and ID latent heat fluxes computed in 10-m neutral wind speed bins. Mean values are shown by lines and medians by symbols: the solid line and circles are measured fluxes, and the broken line and crosses are calculated with COARE 3.0.

model (labeled 'old' in the figure) with a derivative of the COARE 2.5 model. The operational parameterizations are now within 10% of the ESRL (ETL) data and the COARE algorithm for wind speeds from 0 to 20 m/s.

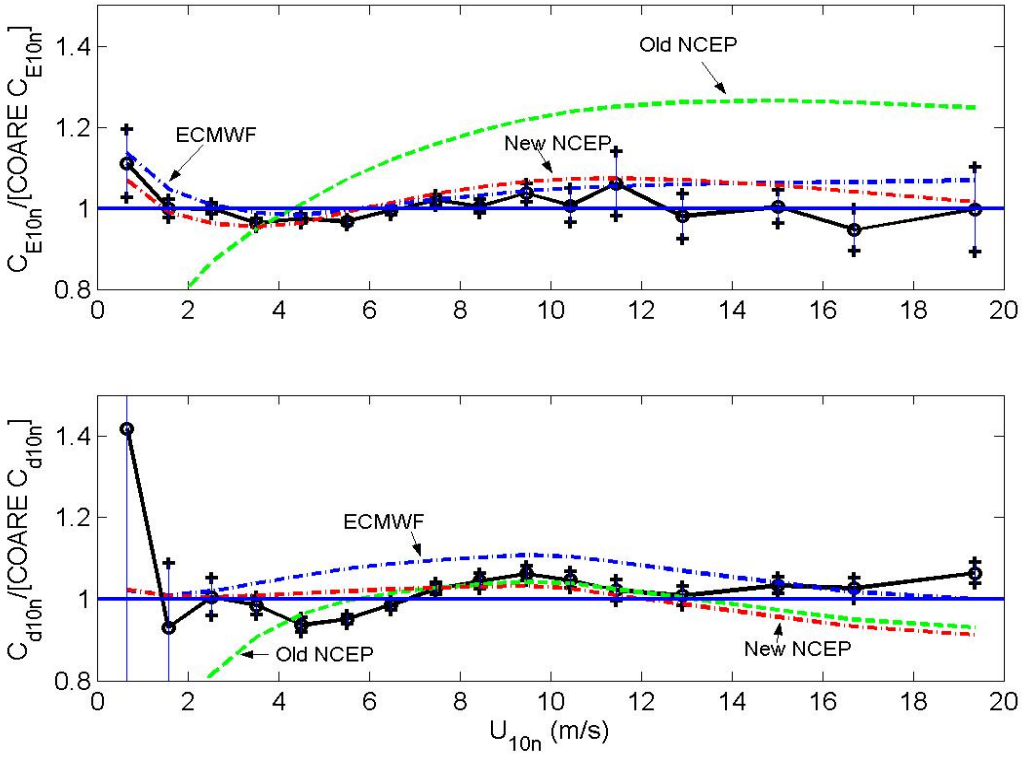

Figure B3. The average wind speed dependence of 10-m neutral transfer coefficients divided by the COARE 3.0 values (Upper panel, $C_{e10\,n}$; lower panel $C_{d10\,n}$). The dashed lines are NCEP and ECMWF formulae (as labeled); the solid line with symbols is the average ESRL (ETL) data.

B3. Estimate of Turbulent Flux Errors

If we want to determine the value of some variable, x, then we perform a 'measurement' with an instrument that provides an estimate of the value, x_m. A simple method to illustrate the relationship between what we want and what we get is a linear form with a bias (offset) and a slope,

$$x = bias + slope * x_m = x_m + bias + (slope - 1) * x_m . \qquad \text{(B3.1)}$$

The bias represents a persistent offset in the device and the (slope-1) corresponds to a persistent percentage error in each measurement. In principal, the bias and slope can be determined by a laboratory calibration and subsequently removed as a source of error by correcting the device output. To actually use the device on a ship, we ship it from the calibration facility, mount it somewhere in an environment that may be quite different (variable and influenced by flow distortion, heat island, etc.), connect it to data-logging system and operate it for a time period on the order of a year. Thus, the correct bias and slope corrections to be applied to this one-year record now must be considered uncertain. In many cases, we may need to apply *in situ*

calibration or intercomparison methods to constrain these uncertainties to meet our guidelines (see Table 1) as discussed in detail in the previous sections.

A second aspect of measurement uncertainty must be considered when dealing with geophysical variables, which vary considerably with space and time. Typically, we are interested in *statistical* properties of the variables, such as the mean, standard deviation, or frequency spectrum. For climate purposes, the one-month average temperature at a particular location is of more significance than the instantaneous temperature at any specific time. If we now consider the variable to be a function of time, *x(t)*, then we are interested in estimating the intrinsic mean of the variable, μ_x, or its standard deviation, σ_x. At a given place and time, we can take a sample of the time series of *x* and compute the average of *x* (denoted $<x>$) over some time interval, Δt.

$$< x >_{\Delta t} = \frac{1}{\Delta t} \int_{t}^{t+\Delta t} x(t)dt \ . \qquad \text{(B3.2)}$$

However, this particular average is only an estimate of the intrinsic mean – there is uncertainty in the estimate. This is analogous to asking 100 people how they will vote (a sample) to try to guess the outcome of an election. You cannot expect the 100 people you happen to poll to give exactly the same result as the 1 million that vote in the election. We can compute how uncertain our estimate of μ_x is by using normal statistics theory

$$\mu_x = < x >_{\Delta t} \pm \frac{\sigma_x}{\sqrt{\Delta t / \mathrm{T}_x}} \ , \qquad \text{(B3.3)}$$

where T_x is the decorrelation time scale for *x*. Suppose you make a measurement of *x* at a specific time, then the decorrelation time is how long you must wait before a subsequent measurement will be independent of the previous one. Another way of stating it is "how long do you have to wait before *x* changes by about σ_x?" Thus, the quantity inside the squareroot symbol in equation (B3.3) is essentially the number of independent samples contained in the time interval Δt (analogous to the 100 people we sampled in our poll). For climate applications, the trick is to make the number of independent samples so large (or, Δt so long) that the sampling uncertainty term in equation (B3.3) become negligible. Of course, we are still left with the residual errors caused by uncertainty in the bias and slope errors of the instrument.

To examine uncertainty in fluxes, we begin with an approximation to the net surface energy budget equation (1.1) as the sum of sensible and latent heat plus the net radiative flux components.

$$H_{net} = -H_s - H_l + R_{sn} + R_{\ln} . \qquad \text{(B3.4)}$$

The uncertainty in the net flux, δH_{net}, is estimated as

$$(\delta H_{net})^2 = (\delta H_s)^2 + (\delta H_l)^2 + (\delta R_{sn})^2 + (\delta R_{\ln})^2 . \qquad \text{(B3.5)}$$

If we want the net flux uncertainty on the order of 10 Wm^{-2} and, for example, we allow each term to contribute equally, then the individual terms would have to be accurate to 5 Wm^{-2} (i.e., 4*25 = 100). The uncertainty of each term is computed by expanding the fundamental

computation relationship as a series of partial derivatives of the fundamental measured variables (x, y, z…) that go into the estimate of the flux terms. The uncertainties of each of those variables (δx, δy, δz…) gives an expression for the total error

$$(\delta F)^2 = (\frac{\partial F}{\partial x}\delta x)^2 + (\frac{\partial F}{\partial y}\delta y)^2 + (\frac{\partial F}{\partial z}\delta z)^2 ... \qquad \text{(B3.6)}$$

For a turbulent heat flux, we use equation (11.3), $F_x = -u_* x_*$ and represent each scaling parameter in terms of measured variables:

$$u_* = C_d^{1/2}(\varsigma)S \quad -x_* = C_x^{1/2}(\varsigma)(X_s - X_z) = C_x^{1/2}(\varsigma)\Delta X \,. \qquad \text{(B3.7)}$$

Using (B3.7) in (B3.6) we have done the derivatives and expanded each system of equations for stress, sensible heat, and latent heat. This involves combining all common terms resulting from the stability length derivative before squaring. We will spare you the 25 pages of fascinating algebra and show just a few examples of the results. To do this, we created an error computation program (*bulk_err_3.m*) where all of the algebra is coded without a single error. This program is accessed with a simple driver program (err_drive.m) in which basic conditions and the accuracy of the measurements are specified. The accuracies are expressed as an offset and slope uncertainty for a linear measurement relationship

```
ue=[.2 .03];%'true' wind speed relative to sea surface
te=[.3 0];%sea-air temperature difference
qe=[.3 0];%sea-air humidity difference
```

In this example, the wind measurement is uncertain by a 0.2 ms^{-1} offset plus 3% of the reading. In this case it is the wind error relative to the surface so it includes errors in the anemometer, the surface current, and the true wind computation. Here we assume that the sea-air temperature difference and the sea-air humidity difference suffer only from offset errors.

We have run the program for tropical conditions. The program graphs the errors as a function of wind speed for different values of the sea-air temperature difference. In the TOGA COARE field program in the tropical western Pacific, the typical wind speed was 5 ms^{-1} and the sea-air temperature difference was 1.5 C. These figures yield an uncertainty in bulk sensible flux of 1.5 Wm^{-2} and latent heat flux of 7 Wm^{-2} for a total uncertainty of the combined turbulent fluxes of about half our allowed total. Errors in the radiometric components account for most of the remainder.

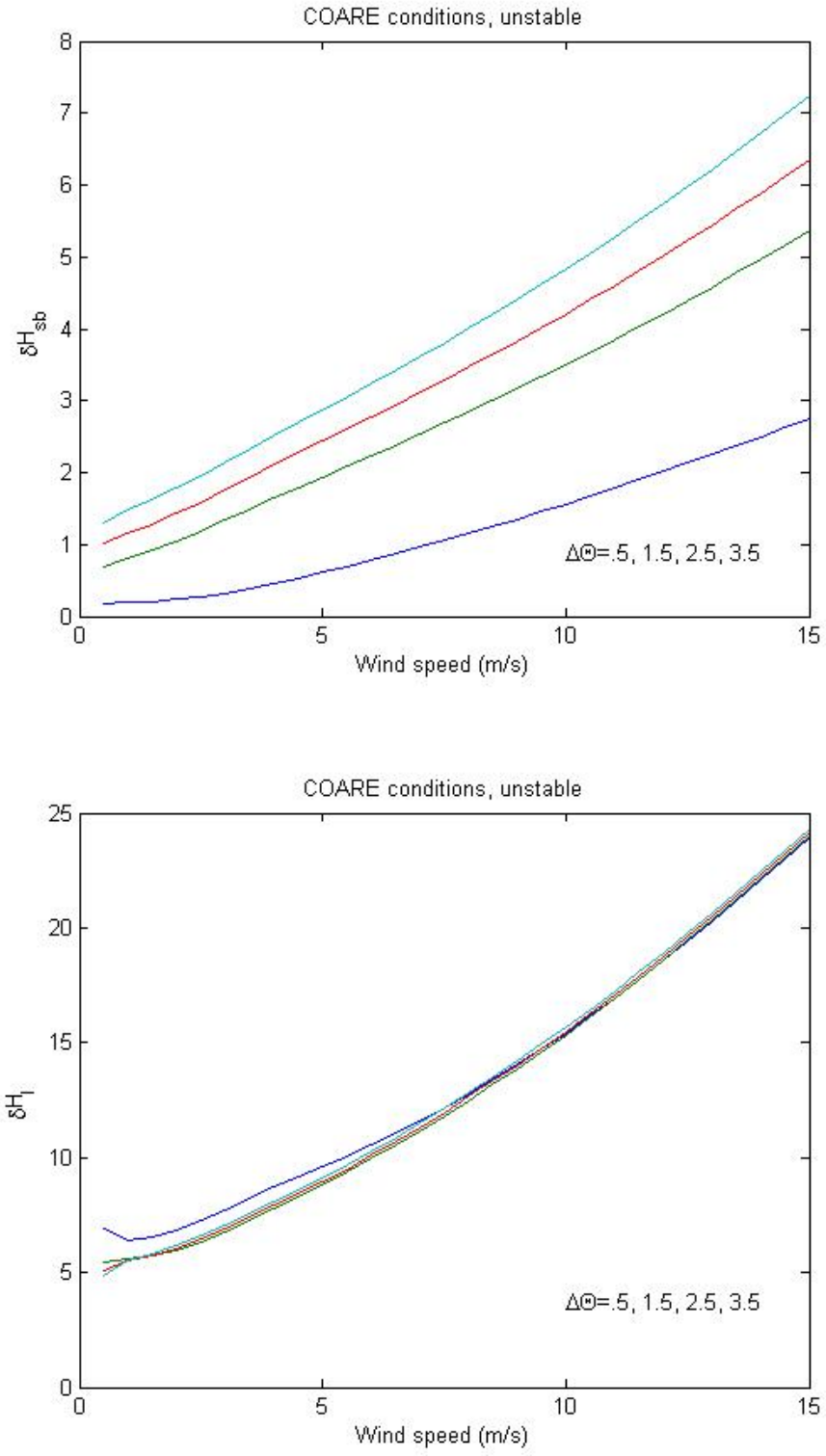

Figure B4. The uncertainty in the turbulent heat flux computed by expanding the basic bulk flux relationships with matlab program *err_driv.m* where the instrument uncertainties are specified as above. Different curves are for different values of the sea-air potential temperature difference, $\Delta\Theta$: upper panel, sensible heat flux error; lower panel, latent heat flux error.

Appendix C - IR Radiative Flux Errors Caused by Objects in the Field of View

Calculations of errors in standard PIR radiative flux radiometers (pyrgeometer) begins with the relationship of the radiance (radiant flux from a particular location in the sky), I, to the irradiance (total flux normal to a horizontal plane), R (W/m^2)

$$R = \iint I(\theta,\varphi)\cos(\theta)d\Omega\,,$$

where φ is the azimuth angle, θ is the zenith angle, and $d\Omega$=cos(θ)dθdφ is the incremental solid angle.

A pyrgeometer measures the downwelling IR radiation integrated over the hemisphere of the sky. If we assume the downwelling IR is isotropic (independent of φ and θ), the integral for a PIR with an unobstructed view of the sky becomes

$$R = I_0 \int_{-\pi}^{\pi} d\varphi \int_{0}^{\pi/2} \cos^2(\theta)d\theta = \pi^2 / 2I_0 = \sigma T_{sky}^4\,,$$

where σ is the Stefan-Boltzmann constant, and T_{sky} is an effective radiative temperature for the sky.

In fact, the IR radiation is somewhat anisotropic. At low elevation angles, the radiation temperature is close to the air temperature and at zenith it is lower than T_{sky}. The approximation used here will overestimate the effect of objects near the horizon and underestimate for objects near zenith.

We can also compute this integral for the energy received by the PIR from an object of intensity I_x in the field of view defined by some width w and some height h with its bottom some distance d away. In this case, the limits of the integral are from $\pm\delta\varphi$ and 0 to $\delta\theta$ where the angles depend on h:

$$\delta\varphi = atn(w/2/d)$$
$$\delta\theta = atn(h/d)$$

where δθ describes the elevation angle of the object above the horizon. This yields

$$R = I_1 \int_{-\varphi}^{+\varphi} d\varphi \int_{\pi/2-\delta\theta}^{\pi/2} \cos^2(\theta)d\theta = I_1\delta\varphi[\delta\theta + \cos(\delta\theta)\sin(\delta\theta)] = f\sigma T_x^4\,,$$

where T_x is the temperature of the object in question and

$$f = \frac{2}{\pi^2}\delta\varphi[\delta\theta + \cos(\delta\theta)\sin(\delta\theta)].$$

It now follows that the flux error (i.e., additional flux sensed by the PIR) is simply

$$\Delta R = f\sigma(T_x^4 - T_{sky}^4)\,.$$

We show two figures of examples of estimated errors for a 10-m tall pole of width 10 cm, a 10-m tall mast of width 30 cm, and a nearby ship bulkhead that is 6 m wide and 3 m high. The PIR (i.e., it is in the field of view). The results are given as a function of the distance of the object from the PIR.

In the case of the pole, the correction might be useful for a PIR mounted on the side of the pole or mounted on a forward rail where there are antennas or GPS receiver poles nearby. The mast example might be useful when mounting a PIR on the side of a mast. The bulkhead example describes the situation where a PIR is mounted on a lower deck some distance from higher parts of the ship (e.g., the bridge deck). Finally, note that the effects described here are functions of the angular size of the object (distance does not enter into it except as it relates to the angle). Thus, a 10-m-tall, 10-cm-wide pole 10 m away has the same effect as a 5-m-tall, 5-cm-wide pole 5 m away (because $\delta\varphi$ and $\delta\theta$ are the same). Also, the temperature effects scale almost linearly.

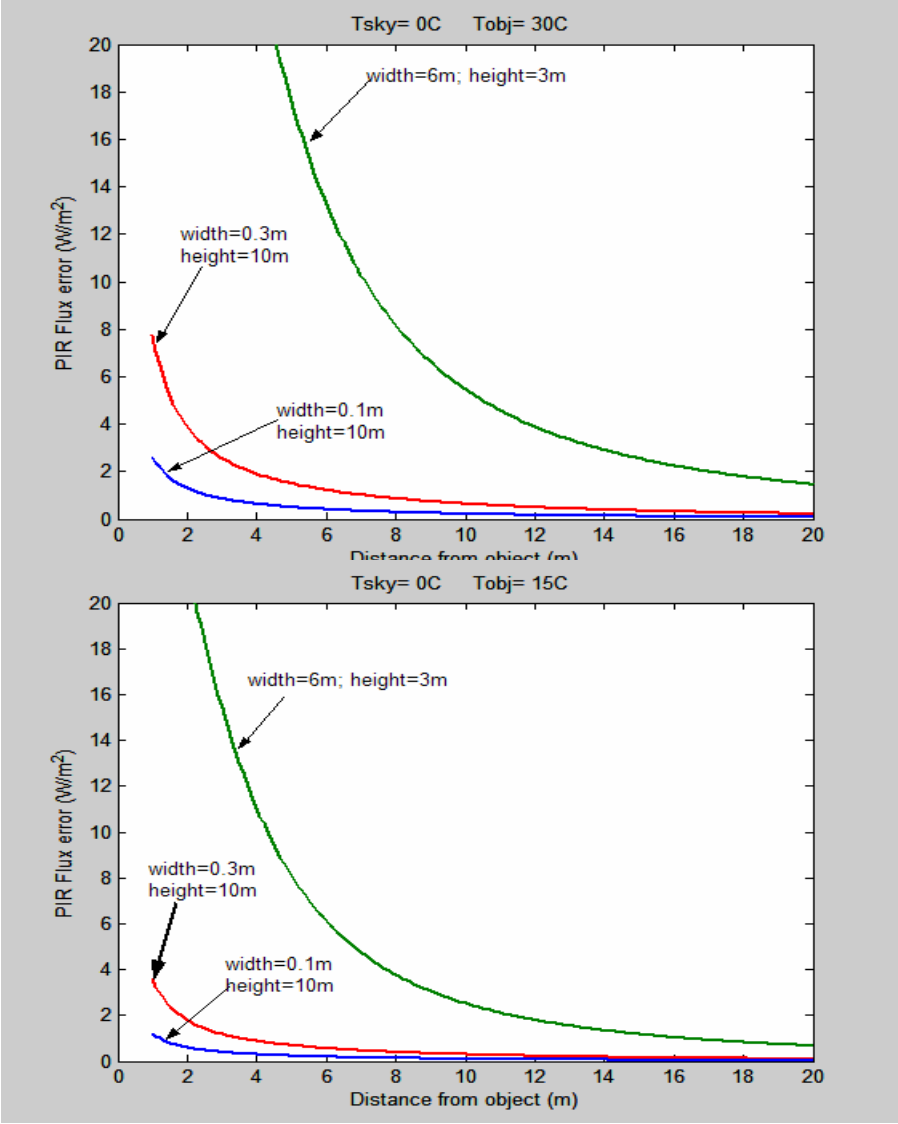

Figure C1. Longwave flux errors caused by shipboard objects in the field of view of a pyrgeometer; a tubular pole (blue), a mast (red), and a bulkhead (green). The assumed radiative sky temperature of 0ºC is typical of mid-latitude clear-sky conditions. The lower panel is for an object at roughly ambient temperature; the upper panel is for an object warmed considerably by strong sunlight.

Appendix D – Examples of Meteorological Observations and Fluxes

The magnitude and behaviour of the meteorological variables, and the resulting bulk air-sea fluxes are illustrated in the following figures. We give two contrasting cases in tropical waters, on consecutive days from EPIC2001, and one from a mid-latitude cruise (Stratus-5, 2005).

Figure D1 shows that conditions on day 258 were fairly steady with no sign of convective activity. There was no rain, although the solar trace R_s indicates broken cloud. The wind steadily increased from around 2 to 5 ms^{-1} during the course of the day. During the daylight hours, the wind was probably strong enough to prevent the formation of a warm layer, and the air-sea temperature difference was remarkably steady. Consequently, the sensible and latent heat fluxes increased modestly, without major fluctuations. The fairly high 420 Wm^{-2} of downward longwave radiation was mainly due to the high humidity typical of the atmospheric boundary layer over the tropical ocean; at a temperature of 30ºC the ocean surface emits about 465 Wm^{-2} of thermal energy so that R_{nl} is a loss of 45 Wm^{-2}. Thus, the net energy is a loss to the ocean at night, and a gain due to solar absorption during the day.

In contrast (Figure D2), day 259 was convectively active, with a series of rainstorms throughout the night. These were accompanied by increasing wind speed and humidity, while the air cooled through several degrees from the associated downdrafts. Over this period the sea surface temperature decreased only slightly (~1ºC) so the air-sea temperature difference varied considerably, reflected in variability of the turbulent heat fluxes. Note that the rain produced more ocean cooling than any other flux component at the time of the storm. The solar trace indicates considerable cloudiness, although the solar energy still peaked at over 1000 Wm^{-2}. However, the cloud caused much greater variability and larger values in downward longwave radiation than on the previous day.

The Stratus cruises study the climatology of the stratus cloud deck off the west coast of Ecuador, Peru and Chile. Day 287 of the 2005 cruise (Figure D3), contrasts markedly with the tropical examples; stronger winds (consistently around 9 ms^{-1}) sea temperature lower by about 10ºC, lower humidity, and the persistent stratus cloud cover. The air-sea temperature difference varied somewhat but, as with the tropical examples, H_s was very small. The drier air had two consequences for fluxes, tending to increase H_l and decrease R_l . However, because of the lower sea temperature, outgoing longwave radiation was only about 400 Wm^{-2} so **net** longwave radiation was small until breaks in the cloud cover late in the day. Despite the persistent cloud, shortwave radiation is substantial and the net heat input to the ocean is as in the other two examples; a small loss throughout the night and a gain during the day.

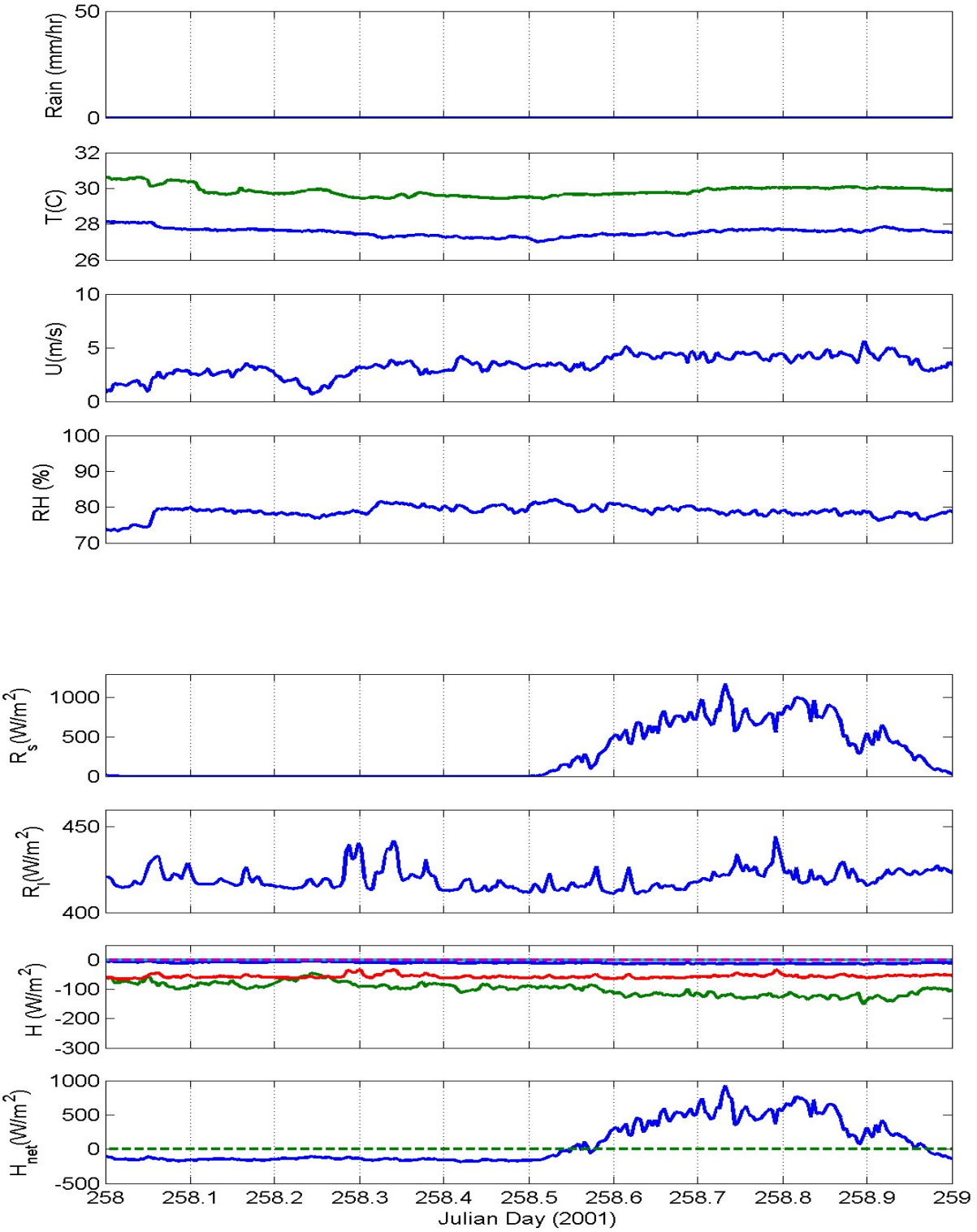

Figure D1. Bulk meteorology and flux variables from a typical relatively clear day in the tropics. Reading down from the upper panel, the variables are: rain rate; water (green line) and air temperature (blue line); wind speed; relative humidity; downward solar flux; downward IR flux; heat flux components [$-H_s$ (blue), $-H_l$,(green), R_{nl} (red), $-H_{rain}$ (cyan)]; and net heat flux.

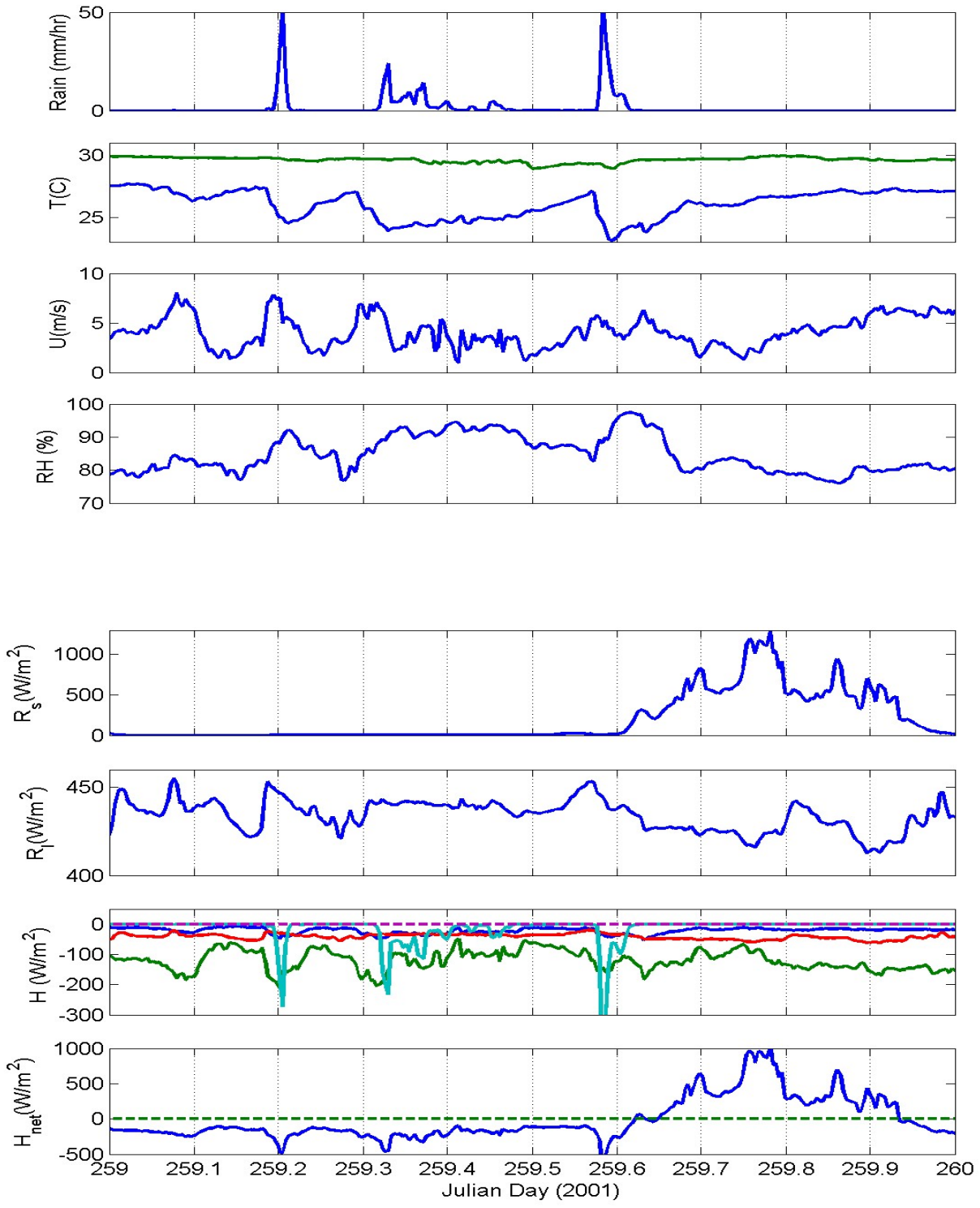

Figure D2. Bulk meteorology and flux variables for a convectively active day in the tropics. Reading down from the upper panel, the variables are: rain rate; water (green line) and air temperature (blue line); wind speed; relative humidity; downward solar flux; downward IR flux; heat flux components [$-H_s$ (blue), $-H_l$ (green), R_{nl} (red), $-H_{rain}$ (cyan)]; and net heat flux.

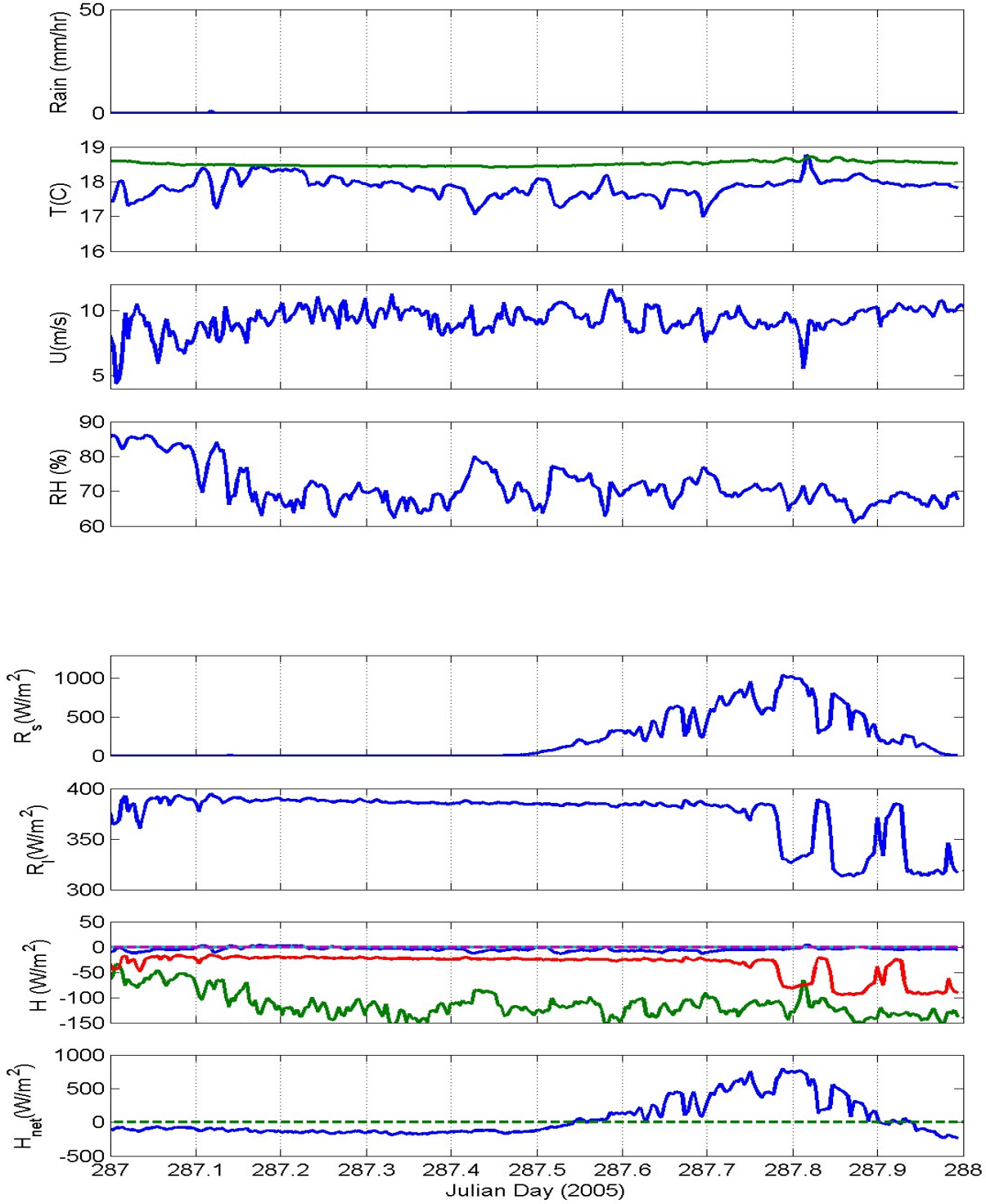

Figure D3. As for Figures D1 and D2, but for a region of ocean with quite different climatology; higher wind speeds, much lower sea and air temperatures, and lower humidity. Reading down from the upper panel, the variables are: rain rate; water (green line) and air temperature (blue line); wind speed; relative humidity; downward solar flux; downward IR flux; heat flux components [$-H_s$ (blue), $-H_l$ (green), R_{nl} (red), $-H_{rain}$ (cyan]; and net heat flux.

Appendix E: The Beaufort Wind Scale

In the early nineteenth century, Rear-Admiral Sir Francis Beaufort developed a 13-interval scale for wind force based on the behavior of a well-conditioned man-of-war sailing ship (Huler 2004). In 1838, the British Admiralty adopted this scale as a method for unifying the reporting of winds at sea. But not until the early twentieth century did that scale emerge as the descriptive list of wind effects on both land and seat that we now know as the Beaufort Scale (Huler 2004).

Reports of winds and sea state made using the Beaufort Scale still form an important part of the climate record.. Over time the Beaufort Scale has evolved to include descriptions of Beaufort Force depending on: conditions on land, in coastal waters an on sailing vessels (Simpson 1906); the open ocean sea state (Peterson 1927); and the conditions aboard a Canadian Ocean Weather Ship (Millar and McPhail 1951). Verploegh (1967) showed that all of these methods give similar estimates of the wind strength. There have been may studies which have attempted to define mean wind speeds and wind speed ranges for the intervals of the Beaufort Scale, known as Beaufort Equivalent Scales; one of the first was by Curtis (1897).

Recent research has refined the Beaufort Equivalents used in climate research and Kent and Taylor (1997) showed that the scale of Lindau (1995) produced the most consistent datasets of anemometer and Beaufort wind speeds. However the wind observations made at sea as part of the Voluntary Observing Ships (VOS) Program must be made using the Official International Codes for the Beaufort Scale (WMO 1995). Table E1 shows the Beaufort Scale and includes descriptions of conditions for a given Beaufort force over the sea.

References for Appendix E:

Curtis, R.H., 1897: An attempt to determine the velocity equivalents of wind forces estimated by Beaufort's scale. *Q. J. R. Meteorol. Soc.*, **23**, 24-61.

Huler, S., 2004: *Defining the wind*. Three Rivers Press, 290 pp.

Kent, E.C., and P.K. Taylor, 1997: Choice of a Beaufort Equivalent Scale. *J. Atmos. Oceanic Tech.*, **14**, 228-242.

Kinsman, B., 1965: *Wind Waves*. Prentice-Hall, 676 pp.

Lindau, R., 1995: A new Beaufort equivalent scale. Proc., *Internat. COADS Winds Workshop*, Kiel, Germany. H. F. Diaz and H.-J. Isemer (eds), 232-252.

Millar F.G., and H.W. McPhail, 1951: Beaufort Equivalents of the Apparent Wind on Shipboard. *The Marine Observer*, **21**(152), 126-130.

Petersen, P., 1927: Zur Bestimmung der Windstarke auf See. Annalen der Hydrographie 55, 69-72.

Simpson, C.G., 1906: The Beaufort Scale of Wind-Force. Report of the Director of the Meteorological Office, Official Report No 180, London.

Verploegh, G.,1967: Observation and Analysis of the Surface Wind over the Ocean, G, KNMI Report No. 89, 62 pp.

WMO, 1995: Manual on Codes. Vol. 1, Part A: Alphanumeric codes. WMO Report No. 306, loose leaf. See section E for Beaufort Scale definition. [Available from: http://www.wmo.int/web/www/WMOCodes/ManualCodes/WMO306vol-I-1PartA.pdf]

Table E1: Beaufort Force Intervals, Equivalent Speeds and Probable Wave Heights (Adapted from WMO 1995, *Manual on Codes*, volume 1, part A: Alphanumeric Codes, WMO Report No. 306, section E). $H_{1/3}$ is the significant wave height, the average height of the highest one-third of all waves occurring during a period (Kinsman 1965).

		Velocity equivalent at 10 m height				
Force	Descriptive Term	knots	ms^{-1}	m.p.h.	Sea specification	$H_{1/3}$ (m)
0	Calm	< 1	0.0-0.2	<1	Sea like a mirror.	-
1	Light air	1-3	0.3-1.5	1-3	Ripples with the appearance of scales are formed, but without foam crests.	0.1 (0.1)
2	Light breeze	4-6	1.6-3.3	4-7	Small wavelets, still short but more pronounced. Crests have a glassy appearance and do not break.	0.2 (0.3)
3	Gentle breeze	7-10	3.4-5.4	8-12	Large wavelets. Crests begin to break. Foam of glassy appearance. Perhaps scattered white horses.	0.6 (1)
4	Moderate breeze	11-16	5.5-7.9	13-18	Small waves, becoming longer, fairly frequent white horses.	1 (1.5)
5	Fresh breeze	17-21	8.0-10.7	19-24	Moderate waves, taking a more pronounced long form; many white horses are formed. Chance of some spray	2 (2.5)
6	Strong breeze	22-27	10.8-13.8	25-31	Large waves begin to form; the white foam crests are more extensive everywhere. Probably some spray.	3 (4)
7	Near gale	28-33	13.9-17.1	32-38	Sea heaps up and white foam from breaking waves begins to be blown in streaks along the direction of the wind.	4 (5.5)
8	Gale	34-40	17.2-20.7	39-46	Moderately high waves of greater length; edges of crests begin to break into spindrift. The foam is blown in well-marked streaks along the direction of the wind.	5.5 (7.5)
9	Strong gale	41-47	20.8-24.4	47-54	High waves. Dense streaks of foam along the direction of the wind. Crests of waves begin to topple, tumble and roll over. Spray may affect visibility.	7 (10)
10	Storm	48-55	24.5-28.4	55-63	Very high waves with long overhanging crests. The resulting foam, in great patches, is blown in dense white streaks along the direction of the wind. On the whole, the surface of the sea takes a white appearance. The 'tumbling' of the sea becomes heavy and shock-like. Visibility affected.	9 (12.5)
11	Violent Storm	56-63	28.5-32.6	64-72	Exceptionally high waves (small- and medium-sized ships might be lost to view for a time behind the waves). The sea is completely covered with long white patches of foam lying along the direction of the wind. Everywhere the edges of the wave crests are blown into froth. Visibility affected.	11.5 (16)
12	Hurricane	64 and over	32.7 and over	73 and over	The air is filled with foam and spray. Sea completely white with driving spray; visibility very seriously affected.	14 (-)

This table is only intended as a guide to show roughly what may be expected in the open sea, remote from land. It should never be used in the reverse way; i.e., for logging or reporting the state of the sea. In enclosed waters, or when near land, with an off-shore wind, wave heights will be smaller and the waves steeper. Figures in brackets indicate the probably maximum height of the waves.

Appendix F – Useful Websites

http://www.etl.noaa.gov/et6/wgsf/

http://www.gfdi.fsu.edu/SEAFLUX/

http://uop.whoi.edu/projects/projects.htm

http://woodshole.er.usgs.gov/operations/sea-mat/air_sea-html/index.html

http://oaflux.whoi.edu/

http://www.ncdc.noaa.gov/oa/climate/vosclim/vosclim.html

http://woodshole.er.usgs.gov/operations/sea-mat/

http://www.pmel.noaa.gov/home/data.shtml

http://www.ifremer.fr/ird/soopip/

http://www.meteo-technology.com/

http://seaboard.ndbc.noaa.gov/index.shtml

http://daac.gsfc.nasa.gov/CAMPAIGN_DOCS/hydrology/TRMM_analysis.html

http://www.researchvessels.org/

http://las.ngdc.noaa.gov/las/servlets/dataset?catitem=9

http://www.uea.ac.uk/env/solas/

http://en.wikipedia.org/wiki/Main_Page

http://www.noc.soton.ac.uk/JRD/MET/

http://amsglossary.allenpress.com/glossary

http://samos.coaps.fsu.edu/html/

http://www.coaps.fsu.edu/RVSMDC/

http://www.coaps.fsu.edu/RVSMDC/FSU/Fluxes/

Appendix G – Metadata Documentation: SAMOS Example

G1. Introduction

The importance of comprehensive metadata alongside the observations was stressed in section 9. Section 10 deals with the necessity of establishing a routine for transmitting both data and metadata to a secure archive, where it will be available for climate research far into the future. There are clearly many ways in which these measures can be achieved, and fresh ones surface under the title of Data Management during the planning of each new field programme.

This Appendix describes the procedures that are being put in place to ensure uniform metadata documentation and data format among ships participating in the Shipboard Automated Meteorological and Oceanographic System (SAMOS) Initiative. SAMOS is referred to briefly in the Background section, and described fully in COAPS (2004). The SAMOS Data Assembly Center (DAC) will collate the data and associated metadata, perform initial quality assurance and ensure archival and accessibility arrangements. The DAC has designed metadata forms (Figures G1 and G2) to be filled out when a vessel is recruited to the SAMOS data exchange. They are an indication of the wide range of metadata needed for quality-assurance purposes, to ensure long-term availability of the observations for climate research. Some notes on these forms are as follows:

G2. Vessel Metadata (Figure G1)

The vessel metadata are required to uniquely identify the vessel providing data to the SAMOS Initiative. They consist of the vessel identifiers, contact, layout and data file information.

Vessel Name - The registered name of the vessel (e.g., *Melville*).

Call Sign - Used to identify the vessel (e.g., WECB).

IMO Number - Issued by the International Maritime Organization (e.g., 8717283) to uniquely identify the vessel. This number stays with the vessel even if the name and call sign are changed.

Recruiting Country (if participating in the VOS program) - The International Organization for Standardization (ISO) 2-character code for the country whose Meteorological Service recruited the vessel (e.g., AU).

Vessel Type - A 2-letter code defining the type of vessel.

Operating Country - The country operating the research vessel or responsible for installing and maintaining the SAMOS on a merchant vessel.

Home Port (optional) - If no home port exists, then a commonly visited port.

Date of Recruitment - When a vessel agrees to participate in SAMOS (yyyymmdd).

Data Reporting Interval - Interval (seconds) between recorded values; ideally the same for each navigation, meteorological, and oceanographic parameter (SAMOS seeks a 60-sec interval).

Participation in other data exchanges (optional) - SAMOS would like to know if the vessel participates in VOS, VOSClim, SOOP, ASAP, SEAS, GOSUD, etc.).

The *contact* metadata are essential to maintain the open exchange of data, metadata, and data-quality information with the vessel and the vessel's home institution. Two-way communication is needed to provide data-quality feedback while the vessel is at sea.

Vessel Information

Vessel Name	Call Sign	IMO Number	Recruiting Country	Vessel Type

Operating Country	Home Port	Date of Recruitment	Data Reporting	Participation in other data exchanges

Contact Information

Home Institution		Aboard Vessel	
Name		Technician Name(s)	
Address		1	2
		Technician Email(s)	
		1	
Contact Person		2	
Name		Alternate Contact email(s)	
Email		1	
Phone	Fax	2	
Vessel Home Page			

Vessel Layout

Dimensions		Digital Imagery and Schematics	Date Submitted
Length	m	Photo – Vessel side view	
Breadth	m	Photo(s) – Instrument Mast(s) / Site(s)	
Freeboard	m	Schematic – Top View	
Draught	m	Schematic – Side View	
Cargo height*	m	Schematic – Bow / Stern View(s)	
*If applicable		Submit electronic imagery to: samos@coaps.fsu.edu	

Data File Specifications

File Format	Format Version	File Compression (zip, gzip, etc.)	Email Data Sent From
Submit Files as Email Attachments to: samos_data@coaps.fsu.edu			

Figure G1. Vessel metadata form used in SAMOS initiative.

Home Institution - Name and postal address of the institution that operates the vessel or, for merchant ships, the institution that installs and maintains the SAMOS.

Contact Person - Name, email, phone, and fax for the primary SAMOS data contact at the home institution. This person should have overall knowledge of the SAMOS installation and data-management procedures for the vessel.

Vessel Home Page URL (if available) - A link from the SAMOS data center web page will be made to each participating vessel's home page.

Technician Name(s) and Email(s) - of marine technician(s) responsible for meteorological data collection and SAMOS service while at sea, or "no tech onboard" if appropriate. Ability for the SAMOS data center to reach a technician will enable data quality feedback to the vessel while it is underway.

Alternate Contact(s) - for the purpose of real-time data quality feedback. Contact points should be decided by vessel operators and could include a generic email for the chief scientist or a contact at the vessel's home institution when no onboard technician is available.

The *dimensions and design* of the vessel are valuable information for data-quality evaluation. Knowing the position of the instruments relative to windward obstacles or to the vessel exhaust stack can help identify suspect data values. Dimensions should be expressed in meters to the nearest 0.1 m. These parameters are defined in WMO publication number 47, Annex V:

Length - The length overall (LOA) of the vessel (e.g., 94.9 m),

Breadth - The molded breadth (beam) of the vessel (e.g., 20.3 m),

Freeboard - The average freeboard of the vessel as measured from the maximum summer loadline (e.g., 2.6 m),

Draught - The average vertical distance between the vessel's keel and the maximum summer loadline (e.g., 7.9 m),

Cargo height - The average height of the cargo above the maximum summer load line on the particular route where observations are made (e.g., 6.5 m). If the cargo is below the main deck (e.g., a bulk tanker or in ballast), the height of the main deck itself.

Digital Photography and Vessel Schematics - Digital photos (.jpg format) and scanned schematics (.pdf format) of vessels and/or sensor locations provide a wide range of information for data quality assurance and applications.

Photos should include a side view of the entire vessel and the masts or sites that house the SAMOS instruments. The latter are most useful when taken at a distance sufficient to show the sensor's environment and possible obstacles to airflow around the sensor. The naming convention for the digital file(s) is in the following format:

xxxxxxxxxyyyymmddaaa...aaa.jpg, where

xxxxxxxxx	IMO number (a nine-digit number, include leading zeros if applicable)
yyyymmdd	year, month, day
aaa...aaa	short description of the photo or schematic

Example: 000851245200202 14anemometer_port_side.jpg

Schematics desired include a top, side, and bow or stern view of the vessel. Marking the location of the meteorological and oceanographic sensors on the schematics would be helpful.

Example 00085124520020214aft_view_schematic.pdf

Please send to samos@coaps.fsu.edu and provide the date submitted on the metadata form.

Examples of requested files can be viewed on the SAMOS web page under the "digital imagery" button on the metadata portal (http://samos.coaps.fsu.edu/html/meta.php).

SAMOS data exchange is designed around daily email attachments containing the observations collected over the previous day. The data file specification provides information needed by the DAC to uncompress and process each attached file. Although designed for SAMOS, the same principles would apply to any data exchange or archiving program.

File Format - Name of the format used for emailed data file attachments. The format must be self-describing (what variables are where in the file), have a known delimiter between values, and a known missing value (e.g., SAMOS data exchange format, see following section).

Format Version - Version number of the file format (e.g., 001 for SAMOS format).

File Compression - If files are compressed, please indicate the algorithm used (e.g., zip, gzip)

Email Data Sent From - The email address to verify that files originate from a known provider.

G3. Primary Instrument Metadata (Figure G2)

This form lists information related to the individual parameters typically observed by a SAMOS and suitable for the calculation of turbulent air-sea fluxes by bulk methods. It is critical for initial data quality evaluation and for the future scientific application of the data. Gray areas in Figure G2 indicate metadata that are not applicable to the particular parameter.

Logging System Name - Name or acronym to identify the combined instrument and data-logging system used on the vessel (e.g., NOAA SCS, WHOI IMET).

System Version - Version number of data-logging software.

Wind Direction Convention - Whether the direction given is toward or away from that from which the wind is blowing.

Anemometer Zero-line Reference - The installed orientation of the zero reference on the anemometer compass in degrees measured clockwise from the bow.

0˚ – reference pointed toward bow
90˚ – reference pointed toward starboard
180˚ – reference pointed toward stern
270˚ – reference pointed toward port

Pressure Adjusted to Sea Level – Yes or No.

Designator for SAMOS - For SAMOS, a short alphanumeric tag is used to identify the type of data value within each record (see section G4). For other data transmission systems, it might be the column heading for a fixed format tabular file.

Instrument Make - Manufacturer of the instrument (e.g., R.M. Young).

Instrument Model - Model or series number of instrument (e.g., 5103).

Units - Original units for each parameter (e.g., Deg. + East, knots, ˚C). SI units are preferred, but providing the original units are specified, the DAC can convert values to SI units.

Instrument Location – This is specified by measurements (to the nearest 0.1 m) that include:

From Bow - Distance from the foremost point of the vessel above the mean waterline back to the instrument on a line parallel to the vessel centerline (positive value);

From Center Line - Distance to port (P indicator or negative value) or starboard (S indicator or positive value) on a line perpendicular to the centerline;

Height/Depth - Height above (depth below) the mean waterline (positive above the water, negative for a depth measurement)

Measured vs. Calculated - Indicates whether the parameter was directly measured (M) or calculated (C) from other measured parameters (e.g., true winds must be derived from the vessel-relative winds, course, heading, and speed of the vessel). When possible, please provide (via email or an attached document) the formula used for each calculated value.

Data Averaging

Spot vs. Average Value – Indicates whether the parameter represents an instantaneous (spot) or a time-averaged value.

Value Time Center – When the value is time-averaged, indicate whether the time stamp associated with the value represents the beginning, center, or end of the averaging period.

Length – Of the averaging period (in seconds), if applicable.

Sampling Rate - The sampling rate from each individual instrument (Hertz).

Data Precision - The fractional value (decimal) to which the sensor can resolve changes in the measured parameter, as specified by the manufacturer.

Date In or Last Calibration - SAMOS will record the installation date or the last date of calibration for each sensor (yymmdd format).

Radiation Direction Convention - Indicates whether the sensor is measuring downwelling (dn) or upwelling (up) radiation.

Primary Instrument Metadata		Vessel Name		Use this form to provide primary sensor information for each available parameter.
Logging System Name		System Version		
Wind direction convention (to/from)		Anemometer zero-line reference (deg)		Pressure adjusted to sea level (yes/no)	

Parameter	Instrument			Distance (nearest 0.1 m)				Data Averaging					
	Make	Model	Units	From bow	P/S from center line	Height /depth	Measured/ Calculated	Spot vs. Average Value	Value Time Center	Length (sec)	Sampl-ing rate (Hz)	Data precision (decimal)	Date in/last calibration (YYMMDD)
Latitude													
Longitude													
Heading													
Course over ground													
Speed over ground													
Speed over water													
Vessel-relative wind direction													
Vessel-relative wind speed													
Earth-relative wind direction													
Earth-relative wind speed													
Atm. pressure													
Air temperature													
Wet-bulb temperature													
Dewpoint temperature													
Relative humidity													
Specific humidity													
Precipitation													
Shortwave radiation (up/dn)													
Longwave radiation (up/dn)													
Visibility													
Ceiling height													
Sea temperature													
Salinity													
Conductivity													

Figure G2. Instrument metadata form used in SAMOS initiative.

G4. SAMOS Data Format

There are two ways of providing unique identifiers for each data element within a data storage format; as a header line at the top of a fixed format tabular file or imbedded within the individual data records. In the former, missing values must be replaced with a dummy, or the file may be impossible to interpret. Although the latter results in longer data lines, pairs (identifier:value) can drop out when the value is missing. This is the scheme adopted for SAMOS.

The SAMOS exchange format uses two separators, "," between tagged pairs and ":" between the designator and the data value ":". Each tagged pair consists of an alphanumeric designator and the associated data value. Therefore an example record at date (YMD) and time (HMS) will read:

$SAMOS:001,CS:KAOU,YMD:20030907,HMS:000011,AT:17.40,BP:1010.27,…,

WSP:5.6,WDP:354.4,TWP:5.4,TIP:278.3,WSS:6.7,WDS:350.5,TWS:6.6,TIS:274.4,...,

LA:44.66956,LO:-130.35859,COG:149.5,SOG:0.9,GY:284.7,CS8:23,

where air temperature (AT) is 17.40ºC, relative wind speed (WSP) is 5.6 m/s, etc., and the units and other value identifiers, etc., are known by reference to the metadata form (Figure G2).

1. Observation times must be in the Universal Time Coordinate (UTC).

2. $SAMOS:001 represents the first version of the SAMOS data format, and is followed with the ship call sign pair (CS:call_sign). Beyond these first two tagged pairs, the order of the data is immaterial since the designators uniquely identify each tagged pair and their data values.

3. Each institute can decide whether or not to include an 8-bit checksum for each line in the file (at the end of each line). If you do plan to have a CS8, please provide us with details on how the number is calculated so we can decode the value.

REFERENCES

Andreas, E.L., 2005: *Handbook of physical constants and functions for use in atmospheric boundary layer studies*. ERDC/CRREL M-05-1, Cold Regions Research and Engineering Laboratory, U.S Army Res. and Dev. Center, 75 Lyme Road, Hanover NH 03755, 43 pp.

Beljaars, A.C.M., and A.A.M. Holtslag, 1991: Flux parameterization over land surfaces for atmospheric models. *J. Appl. Meteor.*, **30**, 327-341.

Bohren, C.F., and B.A. Albrecht, 1998: *Atmospheric Thermodynamics*. Oxford University Press, 402 pp.

Bowditch, N., 1977: *American Practical Navigator.* Vol. 1, Publication No. 9, Defense Mapping Agency Hydrographic Center, Washington, DC, 1386 pp.

Bradley, E.F., P.A. Coppin, and J.S. Godfrey, 1991: Measurements of sensible and latent heat flux in the western tropical Pacific Ocean. *J. Geophys. Res.*, **96**, 3375-3389.

Brunt, D., 1932: Notes on radiation in the atmosphere. *Q. J. Roy. Meteor. Soc.*, **58**, 389-420.

Buck, A.L., 1981: New equations for computing vapor pressure and enhancement factor. *J. Appl. Meteor.*, **20**, 1527–1532.

Businger, J.A., J.C. Wyngaard, Y. Izumi, and E.F. Bradley, 1971: Flux profile relationships in the atmospheric surface layer. *J. Atmos. Sci.* **28**, 181-189.

Caldwell, D.R., and W.P. Elliott, 1971: Surface stresses produced by rainfall. *J. Phys. Oceanog.*, **1**, 145-148

Charnock, H., 1955: Wind stress on a water surface. *Q. J. Roy. Meteor. Soc.,* **81,** 639–640.

Charnock, H., 1958: A note on empirical wind-wave formulae. *Q. J. Roy. Meteor. Soc.,* **84,** 443–447.

COAPS, 2003: Report 03-01; *Report and recommendations from the Workshop on High Resolution Marine Meteorology, 3-5 March 2003.* Shawn R. Smith (Ed.), Centre for Ocean-Atmosphere Prediction Studies, Florida State University, Tallahassee, FL, 32306, USA.

COAPS, 2004: Report 04-01; *Report from the 2nd Workshop on High Resolution Marine Meteorology, 14-15 April 2004, Silver Spring, MD, USA.* Shawn R. Smith (Ed.), Centre for Ocean-Atmosphere Prediction Studies, Florida State University, Tallahassee, FL, 32306, USA.

Deardorff, J.W, 1970: Convective velocity and temperature scale for the unstable planetary boundary layer and for Rayleigh convection. *J. Atmos. Sci.* **27**, 1211.

DeCosmo, J., K.B. Katsaros, S.D. Smith, R.J. Anderson, W.A. Oost, K. Bumke, and H. Chadwick, 1996: Air-sea exchange of water vapor and sensible heat: The Humidity Exchange Over the Sea (HEXOS) results. *J. Geophys. Res.*, **101**, 12,001-12,016.

Drennan , W.M., P.K. Taylor, and M.J. Yelland, 2005: Parameterizing the sea surface roughness. *J. Phys. Oceanog.*, **35,** 835-848.

Fairall, C.W., E.F. Bradley, J.S. Godfrey, G.A. Wick, J.B. Edson, and G.S. Young, 1996a: The cool skin and the warm layer in bulk flux calculations. *J. Geophys. Res*., **101**, 1295-1308.

Fairall, C.W., E.F. Bradley, D.P. Rogers, J.B. Edson, G.S. Young, 1996b: Bulk parameterization of air-sea fluxes for TOGA COARE. *J. Geophys. Res.,* **101**, 3747-3764.

Fairall, C.W., A.B. White, J.B. Edson, and J.E. Hare, 1997: Integrated shipboard measurements of the marine boundary layer. *J. Atmos. Oceanic Tech.,* **14**, 338-359.

Fairall, C.W., P.O.G. Persson, E.F. Bradley, R.E. Payne, and S. Anderson, 1998: A new look at calibration and use of Eppley Precision Infrared radiometers: Part I - Theory and application. *J. Atmos. Oceanic Tech*., **15**, 1230-1243.

Fairall, C.W., J.E. Hare, A.A. Grachev, E.F. Bradley, and J.B. Edson, 2001: Preliminary results from the ETL open ocean air-sea flux database. *Proc., 11th Conf. on Interaction of the Sea and Air,* AMS, San Diego, CA, 14-18 May, 5-8.

Fairall, C.W., E.F. Bradley, J.E. Hare, A.A. Grachev, and J.B. Edson, 2003: Bulk parameterization of air-sea fluxes: Updates and verification for the COARE Algorithm. *J. Climate*, **16**, 571-591.

Garratt, J.R., 1992: *The Atmospheric Boundary Layer.* Cambridge University Press, Cambridge, Mass., 316 pp.

Godfrey, J.S., and A.C.M. Beljaars, 1991: On the turbulent fluxes of buoyancy, heat, and moisture at the air-sea interface at low wind speeds. *J. Geophys. Res.*, **96**, 22,043-22,048.

Gosnell, R., C.W. Fairall, and P.J. Webster, 1995: The sensible heat of rainfall in the tropical ocean. *J. Geophys. Res.*, **100**, 18,437-18,442.

Grachev, A.A., and C.W. Fairall, 1997: Dependence of the Monin-Obukhov stability parameter on the bulk Richardson number over the ocean. *J. Appl. Meteor.*, **36**, 406-414.

Grachev, A.A., C.W. Fairall, and E.F. Bradley, 2000: Convective profile constants revisited. *Bound.-Layer Meteorol*., **94**, 495-515.

Hankin, S., and the DMAC Steering Committee, 2005: Data Management and Communications Plan for Research and Operational Integrated Ocean Observing Systems: I. Interoperable Data Discovery, Access, and Archive, Ocean.US, Arlington, VA, 304 pp. http://dmac.ocean.us/dacsc/imp_plan.jsp.

Hare, J.E., P.O.G. Persson, C.W. Fairall, and J.B. Edson, 1999: Behavior of Charnock's relationship for high wind conditions. *Proc., 13th Symposium of Boundary Layers and Turbulence.* AMS. Dallas, TX, Jan. 15-20, paper 5B.8.

Hare, J.E., C. Fairall, T. Uttal, D. Hazen, M.F. Cronin, N. Bond, and D. Veron, 2005: Cloud, radiation, and surface forcing in the equatorial eastern Pacific. *NOAA Technical Memorandum OAR PSD-307*, U.S. Dept. of Commerce, 59 pp.

Hasse, L., M. Grossklaus, K. Uhlg, and P. Timm, 1998: A ship rain gage for use in high winds. *J. Atmos. Oceanic. Tech.*, **15**, 380-386.

Huler, S., 2004: *Defining the Wind.* Three Rivers Press, 290 pp.

Kinsman, B., 1965: *Wind Waves.* Prentice-Hall, 676 pp.

Kraus, E.B., and J.A. Businger, 1994: *Atmosphere-Ocean Interaction*. Oxford University Press, New York, NY, 352 pp.

Large, W.G., and S. Pond, 1982: Sensible and latent heat flux measurements over the ocean. *J. Phys. Oceanog.*, **12**, 464-482.

List, R.J., 1984: *Smithsonian Meteorological Tables*. Sixth ed., Smithsonian Institution Press, 527 pp.

Liu, W.T., K.B. Katsaros, and J.A. Businger, 1979: Bulk parameterization of the air-sea exchange of heat and water vapor including the molecular constraints at the interface. *J. Atmos. Sci*., **36**, 2052-2062.

Minnett, P.J., K.A. Maillet, J.A. Hanafin, and B. J. Osborne, 2005: Infrared Interferometric Measurements of the near-nurface air temperature over the oceans. *J. Atmos. Oceanic Tech.*, **22**, 1019–1032.

Oost, W.A., G.J. Komen, C.M.J. Jacobs, and C. van Oort, 2002: New evidence for a relation between wind stress and wave age from measurements during ASGAMAGE. *Bound.-Layer Meteorol.*, **103**, 409-438.

Persson, O.G.P., C.W. Fairall, E.L Andreas, P.S. Guest, and D.K. Perovich, 2002: Measurements near the atmospheric surface flux group tower at SHEBA: Near-surface conditions and surface energy budget. *J. Geophys. Res.,* **107**, 8045.

Price, J.F., R.A. Weller, and R. Pinkel, 1986: Diurnal cycling: Observations and models of the upper ocean response to diurnal heating, cooling and wind mixing. *J. Geophys. Res*., **91**, 8411-8427.

Smith, S.D., 1980: Wind stress and heat flux over the ocean in gale force winds. *J. Phys. Oceanogr*., **10**, 709-726.

Smith, S.D., 1988: Coefficients for sea surface wind stress, heat flux, and wind profiles as a function of wind speed and temperature. *J. Geophys. Res.*, **93**, 15,467-15,472.

Smith, S.D., 1989: Water vapor flux at the sea surface. *Bound.-Layer Meteorol.*, **47**, 277-293.

Smith, S.R, M.A. Bourassa, and R.J. Sharpe, 1999: Establishing more truth in true winds. *J. Atmos. Oceanic Tech.*, **16**, 939-952.

Strangeways, I., 2001: Back to Basics: The 'Met Enclosure:' Part 6–Wind. *Weather*, **56**, 154–161.

Taylor, P.K., and M.A. Yelland, 2001: The dependence of sea surface roughness on the height and steepness of the waves. *J. Phys. Oceanogr*., **31**, 572-590.

WCRP, 1985: Scientific Plan for the Tropical Ocean and Global Atmosphere Programme. WCRP Publications Series, No. 3, WMO Tech. Doc. 64, Geneva, 146 pp.

WCRP, 1989: WOCE Surface Flux Determinations – A strategy for *in situ* measurements. Working Group on *in situ* measurements for Fluxes WCRP-23 (WMO/TD No.304), WMO, Geneva.

WCRP, 2000: World Climate Research Programme, Final report of the Joint WCRP/SCOR Working Group on Air-Sea Fluxes (SCOR Working Group 110): Intercomparison and Validation of Ocean-Atmosphere Energy Flux Fields. WCRP-112, WMO/TD-No. 1036, Case Postale No. 2300, CH-1211 Geneva 2, Switzerland. 303 pp.

WCRP, 2001: World Climate Research Programme, Proceedings of the Workshop on Intercomparison and Validation of Ocean-Atmosphere Flux Fields. Potomac, MD, USA, 21-24 May 2001. WCRP-115, WMO/TD-No. 1083, Case Postale No. 2300, CH-1211 Geneva 2, Switzerland. 362 pp.

Webb, E.K., G.I. Pearman, and R. Leuning, 1980: Correction of flux measurements for density effects due to heat and water vapour transfer. *Q. J. Roy. Met. Soc.*, **106**, 85-100.

Webster, P.J., and R. Lukas, 1992: TOGA-COARE: The Coupled Ocean-Atmosphere Response Experiment. *Bull. Amer. Meteor. Soc.*, **73**, 1377-1416.

Weller, R.A., E.F. Bradley, and R. Lukas, 2004: The interface or air-sea flux component of the TOGA Coupled Ocean-Atmosphere Response Experiment and its impact on subsequent air-sea interaction studies. *J. Atmos. Oceanic Tech.*, **21**, 223-257.

Wick, Gary A., J. Carter Ohlmann, Christopher W. Fairall, and Andrew T. Jessup, 2005: Improved oceanic cool-skin corrections using a refined solar penetration model. *J. Phys. Oceanogr.*, **35**, 1986-1996.

Yelland, M.J., B.I. Moat, P.K. Taylor, R.W. Pascal, J. Hutchings, and V. C. Cornell, 1998: Wind stress measurements from the open ocean corrected for air flow distortion by the ship. *J. Phys. Oceanogr.*, **28**, 1511-1526.

BIBLIOGRAPHY

Atmospheric Boundary Layer and Structure

Businger, J.A., J.C. Wyngaard, Y. Izumi, and E.F. Bradley, 1971: Flux profile relationships in the atmospheric surface layer. *J. Atmos. Sci.*, **28**, 181-189.

Deardorff, J.W., 1970: Convective velocity and temperature scales for the unstable planetary boundary layer and for Rayleigh convection. *J. Atmos. Sci.*, **27**, 1211-1213

Garratt, J.R., 1992: *The Atmospheric Boundary Layer.* Cambridge University Press, Cambridge, Mass., 316 pp.

Grachev, A.A., and C.W. Fairall, 1997: Dependence of the Monin-Obukhov stability parameter on the bulk Richardson number over the ocean. *J. Appl. Meteor.*, **36**, 406-414.

Grachev, A.A., C.W. Fairall, and E.F. Bradley, 2000: Convective profile constants revisited. *Bound.-Layer Meteorol*., **94**, 495-515.

Haugen, D.A., Ed., 1973: *Workshop on Micrometeorology*. American Meteorological Society, Boston, 392 pp.

Lumley, J.L., and H.A. Panofsky, 1964: *The Structure of Atmospheric Turbulence*. Wiley-Interscience, New York, NY, 239 pp.

Kraus, E.B., and J.A. Businger, 1994: *Atmosphere-Ocean Interaction*. Oxford University Press, New York, NY, 352 pp.

Panofsky, H. A., and J. A. Dutton, 1984: *Atmospheric Turbulence*: *Models and Methods for Engineering Applications*. Wiley-Interscience, New York, NY, 397 pp.

Paulson, C.A., 1970: The mathematical representation of wind speed and temperature profiles in the unstable atmospheric surface layer. *J. Appl. Meteorol.*, **9**, 857-861.

Sorbjan, Z., 1989: *Structure of the Atmospheric Boundary Layer*. Prentice-Hall, Englewood Cliffs, NJ, 317 pp.

Stull, R.B., 1988: *An Introduction to Boundary Layer Meteorology*. Kluwer, Dordrecht, 666 pp.

Webb, E.K., G.I. Pearman, and R. Leuning, 1980: Correction of flux measurements for density effects due to heat and water vapour transfer. *Q. J. Roy. Meteor. Soc.*, **106**, 85-100.

Bulk Algorithms and Parameterizations

Andreas, E.L, 2004: A bulk air-sea flux algorithm for high-wind spray conditions. Version 2.0. Preprints, *13th Conf. on Interactions of the Sea and Atmosphere*, Portland, ME, 9–13 August 2004, American Meteorological Society, CD-ROM P1.5, 8 pp.

Andreas, E.L, and J. DeCosmo, 2002: The signature of sea spray in the HEXOS turbulent heat flux data. *Bound.-Layer Meteor.*, **103**, 303–333.

Beljaars, A.C.M., and A.A.M. Holtslag, 1991: On flux parameterization over land surfaces for atmospheric models. *J. Appl. Meteor.*, **30**, 327-341

Beljaars, A.C.M., 1994: The parameterization of surface fluxes in large-scale models under free convection. *Q. J. Roy. Meteor. Soc.*, **121**, 255-270.

Blanc, T.V., 1985: Variation of bulk-derived surface flux, stability, and roughness results due to the use of different transfer coefficient schemes. *J. Phys. Oceanogr.*, **15**, 650-669.

Bourassa, M.A., D.G. Vincent, and W.L.Wood, 1999: A flux parameterization including the effects of capillary waves and sea state. *J. Atmos. Sci.*, **56**, 1123-1139.

Brunke, M.A., C.W. Fairall, and X. Zeng, 2003: Which bulk aerodynamic algorithms are least problematic in computing ocean surface turbulent fluxes? *J. Climate*, **16**, 619-635.

Brutsaert, W.A., 1975: A theory for local evaporation (or heat transfer) from rough and smooth surfaces at ground level. *Water Resour. Res.,* **11**, 543-550.

DeCosmo, J., K.B. Katsaros, S.D. Smith, R.J. Anderson, W.A. Oost, K. Bumke, and H. Chadwick, 1996: Air-sea exchange of water vapor and sensible heat: The Humidity Exchange over the Sea (HEXOS) results. *J. Geophys. Res.*, **101**, 12,001–12,016.

Fairall, C.W., E.F. Bradley, D.P. Rogers, J.B. Edson, G.S. Young, 1996: Bulk parameterization of air-sea fluxes for TOGA COARE. *J. Geophys. Res.*, **101**, 3747-3764.

Fairall, C.W., E.F. Bradley, J.E. Hare, A.A. Grachev, and J.B. Edson, 2003: Bulk parameterization of air-sea fluxes: Updates and verification for the COARE algorithm. *J. Climate*, **16**, 571-591.

Geernaert, G.L., 1990: Bulk parameterizations for the wind stress and heat fluxes. In S*urface Waves and Fluxes*, Vol. 1, G.L. Geernaert and W.J. Plant (eds.), pp. 91-172, Kluwer, Dordrecht.

Jabouille, P., J.L. Redelsperger, and J.P. Lafore, 1995: Modification of surface fluxes by atmospheric convection in the TOGA COARE region. *Mon. Wea. Rev*., **124**, 816-837.

Large, W.G. and S. Pond, 1982: Sensible and latent heat flux measurements over the ocean. *J. Phys. Oceanogr.*, **12**, 464-482.

Lindau, R., 1995: A new Beaufort equivalent scale. *Proc., Internat. COADS Winds Workshop*, Kiel, Germany. H.F. Diaz and H.-J. Isemer (eds), 232-252.

Liu, W.T., K.B. Katsaros, and J.A. Businger, 1979: Bulk parameterization of the air-sea exchange of heat and water vapor including the molecular constraints at the interface. *J. Atmos. Sci*., **36**, 2052-2062.

Redelsperger, J.L., F. Guichard, and S. Mondon, 2000: A parameterization of mesoscale enhancement of surface fluxes for large scale models. *J. Climate*, **13**, 402-421.

Zeng, X., M. Zhao, and R.E. Dickinson, 1998: Intercomparison of bulk aerodynamic algorithms for the computation of sea surface fluxes using TOGA-COARE and TAO data. *J. Climate*, **11**, 2628-2644

Corrections to Ship Observations, and Quality Control

Anderson, S.P., and M.F. Baumgartner, 1998: Radiative heating errors in naturally ventilated air temperature measurements made from buoys. *J. Atmos. Oceanic Tech.*, **15**, 157-173.

Berry, D.I., and E.C. Kent, 2005: The effect of instrument exposure on marine air temperatures: An assessment using VOSClim data. *Int. J. Climatol.,* **25**, 1007-1022, DOI: 10.1002/joc.1178.

Berry, D.I., E.C. Kent, and P.K. Taylor, 2004: An analytical model of heating errors in marine air temperatures from ships. *J. Atmos. Oceanic Tech.*, **21**, 1198-1215.

Blanc, T.V., 1986: The effect of inaccuracies in weather-ship data on bulk-derived estimates of flux, stability and sea-surface roughness. *J. Atmos. Oceanic Tech.*, **3**, 12–26.

Bourassa, M.A., D.M. Legler, J.J. O'Brien, and S.R. Smith, 2003: SeaWinds validation with research vessels. *J. Geophys. Res.*, **108**, DOI 10.1029/2001JC001081.

Bush, C.B., F.P.J. Valero, and A.S. Simpson, 2000: Characterization of thermal effects in pyranometers: A data correction algorithm for improved measurement of surface insolation. *J. Atmos. Oceanic Tech.*, **17**, 165-175.

Ching, J.K.S., 1976: Ship's influence on wind measurements determined from BOMEX mast and boom data. *J. Appl. Meteor.*, **15**, 102–106.

Dobson, F.W., 1981: *Review of Reference Height for and Averaging Time of Surface Wind Measurements at Sea.* Marine Meteorology and Related Oceanographic Activities Report No. 25, WMO, Geneva, 64 pp.

Goerss, J.S., and C.E. Duchon, 1980: Effect of ship heating on dry-bulb temperature measurements in GATE. *J. Phys. Oceanogr.*, **10**, 478–479.

Hinton, B.B., and D.P. Wylie, 1985: A correction for the errors in ship reports of light winds. *J. Atmos. Oceanic Tech.*, **2**, 353–356.

Kahma, K.K., and M. Leppäranta, 1981: On errors in wind speed observations on R/V *Aranda*. *Geophysica*, **17**, 155–165.

Kent, E.C., and A. Kaplan, 2006: Towards estimating climatic trends in SST data. Part 3: Systematic errors. *J. Atmos. Oceanic Tech.*, **23**, 487-500.

Kent, E.C., and P.G. Challenor, 2006: Towards estimating climatic trends in SST data. Part 2: Random errors. *J. Atmos. Oceanic Tech.*, **23**, 476-486.

Kent, E.C., and P.K. Taylor, 2006: Towards estimating climatic trends in SST data. Part 1: Methods of measurement. *J. Atmos. Oceanic Tech*., **23**, 464-475.

Kent, E.C., and D.I. Berry, 2005: Quantifying random measurement errors in Voluntary Observing Ships meteorological observations. *Int. J. Climatol.*, **25**, 843-856.

Kent, E.C., P.K. Taylor, B.S. Truscott, and J.S. Hopkins, 1993a: The accuracy of voluntary observing ship's meteorological observations - Results of the VSOP-NA. *J. Atmos. Oceanic Tech.*, **10**, 591-608.

Kent, E.C., S.D. Woodruff, and D.I. Berry, 2006: WMO Publication No. 47. Metadata and an Assessment of Voluntary Observing Ships Observation Heights in ICOADS. Submitted to *J. Atmos. Oceanic Tech.*.

MacWhorter, M.A., and R.A. Weller, 1991: Error in measurements of incoming shortwave radiation made from ships and buoys. *J. Atmos. Oceanic Tech.*, **8**, 108-117.

Met Office, 1995: *Marine Observers Handbook.* UK Meteorological Office 1016, Eleventh Edition, HMSO, 227 pp.

Mollo-Christensen, E., 1979: Upwind distortion due to probe support in boundary-layer observation. *J. Appl. Meteor.*, **18**, 367–370.

Pierson, W.J., Jr., 1990: Examples of, reasons for, and consequences of the poor quality of wind data from ships for the marine boundary layer: Implications for remote sensing. *J. Geophys. Res.*, **95**, 13,313–13,340.

Rahmstorf, S., 1989: Improving the accuracy of wind speed observations from ships. *Deep-Sea Res.*, **36**, 1267–1276.

Reynolds, R.M., 1982: Comparison of surface meteorological observations from ship and toroid buoy in the North Pacific during STREX. *J. Appl. Meteor.*, **21**, 1032–1037.

Romanov, Yu. A., I.B. Fedorova, M.S. Chervyakov, and G.I. Shapiro, 1983: An improvement in the accuracy of shipboard measurements of wind speed and direction based on aerodynamic tests of a ship model. *Oceanology*, **23**, 267–270.

Seguin, W.R., and M. Garstang, 1971: A comparison of meteorological sensors used on the USCGSS *Discoverer* during the 1968 Barbados Experiment. *Bull. Amer. Meteor. Soc.*, **52**, 1071–1076.

Smith, S.R., M.A. Bourassa, and R. J. Sharp, 1999: Establishing more truth in true winds. *J. Atmos. Oceanic Tech.,* **16**, 939–952.

Smith, S.R., C. Harvey, and D.M. Legler, 1996: *Handbook of Quality Control Procedures and Methods for Surface Meteorology Data*. **COAPS Report No. 96-1**, WOCE Data Assembly Center for Surface Meteorology, Center for Ocean Atmospheric Prediction Studies, Florida State University, Tallahassee, Florida, 49pp. [Available on line: http://www.coaps.fsu.edu/woce/docs/qchbook/qchbook.htm]

Stevenson, R.E., 1964: The influence of a ship on the surrounding air and water temperatures. *J. Appl. Meteor.*, **3**, 115–118.

Wylie, D.P., and C.F. Ropelewski, 1980: The GATE Boundary Layer Instrumentation System (BLIS). *Bull. Amer. Meteor. Soc.*, **61**, 1002–1011.

Field Campaigns

Curry, J.A., and 18 coauthors, 2004: SEAFLUX. *Bull. Amer. Meteor. Soc.,* **85**, 409-424.

DeCosmo, J., K.B. Katsaros, S.D. Smith, R.J. Anderson, W.A. Oost, K. Bumke, and H. Chadwick, 1996: Air-sea exchange of water vapor and sensible heat: The Humidity Exchange Over the Sea (HEXOS) results. *J. Geophys. Res.*, **101**, 12,001-12,016.

Eymard, L., S. Planton, P. Durand, and coauthors, 1996: Study of the air-sea interactions at the mesoscale: The SEMAPHORE experiment. *Ann. Geophysicae*, **14**, 986-1015.

Joly, A., and 19 others, 1997: The Fronts and Atlantic Storm-Track Experiment (FASTEX): Scientific objectives and experimental design. *Bull. Amer. Meteor. Soc.*, **79**, 1917–1940.

Katsaros, K.B., J. DeCosmo, R.J. Lind, R.J. Anderson, S.D. Smith, R. Kraan, W. Oost, K. Uhlig, P.G. Mestayer, S.E. Larsen, M.H. Smith, and G. De Leeuw, 1994: Measurements of humidity and temperature in the marine environment during the HEXOS Main Experiment. *J. Atmos. Oceanic Tech.*, **11**, 964–981.

Katsaros, K.B., S.D. Smith, and W.A. Oost, 1987: HEXOS—Humidity Exchange over the Sea, a program for research on water-vapor and droplet fluxes from sea to air at moderate to high wind speeds. *Bull. Amer. Meteor. Soc.*, **68**, 466–476.

Persson, P.O.G., J.E. Hare, C.W. Fairall, W.D. Otto, 2005: Air-sea interaction processes in warm and cold sectors of extratropical cyclonic storms observed during FASTEX. *Q. J. Roy. Meteor. Soc.*, **131**, 877-912.

Post, M.J., and coauthors, 1998: The Combined Sensor Program: An air-sea science mission in the central and western Pacific Ocean. *Bull. Amer. Meteor. Soc.,* **78**, 2797-2815.

Smith, S.D., C.W. Fairall, G.L. Geernaert, and L. Hasse, 1996: Air-sea fluxes: 25 years of progress. *Bound.-Layer Meteor.*, **78**, 247–290.

Smith, S.D., K.B. Katsaros, W.A. Oost, and P.G. Mestayer, 1990: Two major experiments in the Humidity Exchange over the Sea (HEXOS) program. *Bull. Amer. Meteor. Soc.*, **71**, 161–172.

Smith, S.D., K.B. Katsaros, W.A. Oost, and P.G. Mestayer, 1996: The impact of the HEXOS programme. *Bound.-Layer Meteor.*, **78**, 121–141.

Smith, S.D., and coauthors, 1992: Sea surface wind stress and drag coefficients: The HEXOS results. *Bound.-Layer Meteor.*, **60**, 109-142.

Webster, P.J., and R. Lukas, 1992: TOGA-COARE: The Coupled Ocean-Atmosphere Response Experiment. *Bull. Amer. Meteor. Soc.*, **73**, 1377-1416.

Webster, P.J., E.F. Bradley, C.W. Fairall, J.S. Godfrey, P. Hacker, R.A. Houze Jr., R. Lukas, Y. Serra, J.M. Hummon, T.D.M. Lawrence, C.A. Russell, M.N. Ryan, K. Sahami, and P. Zuidema, 2002: The JASMINE pilot study. *Bull. Amer. Meteor. Soc.*, **83**, 1603-1630.

Weller, R.A., E.F. Bradley, and R. Lukas, 2004: The interface or air-sea flux component of the TOGA Coupled Ocean-Atmosphere Response Experiment and its impact on subsequent air-sea interaction studies. *J. Atmos. Oceanic Tech.*, **21**, 223-257.

Yu, L., R.A. Weller, and B. Sun, 2004: Mean and variability of the WHOI daily latent and sensible heat fluxes at *in situ* flux measurement sites in the Atlantic Ocean. *J. Climate*, **17**, 2096-2118.

Flow Distortion

Moat, B.I., M.J. Yelland, R.W. Pascal, and A.F. Molland, 2005: An overview of the airflow distortion at anemometer sites on ships. *Int. J. Climatol. (CLIMAR-II Special Issue)*, **25**, 997-1006, DOI: 10.1002/joc.1177.

Moat, B.I., M.J. Yelland, R.W. Pascal, and A.F. Molland, 2006: Quantifying the airflow distortion over merchant ships. Part I: Validation of a CFD model. *J. Atmos. Oceanic. Tech.*, **23**, 341-350.

Moat, B.I., M.J. Yelland, and A.F. Molland, 2006: Quantifying the airflow distortion over merchant ships. Part II: Application of model results. *J. Atmos. Oceanic Tech.*, **23**, 351-360.

Popinet, S., M. Smith, and C. Stevens, 2004: Experimental and numerical study of the turbulence characteristics of airflow around a research vessel. *J. Atmos. Oceanic Tech.*, **21**, 1575-1589. [Code freely available from: http://gfs.sourceforge.net/]

Yelland, M.J., B.I. Moat, P.K. Taylor, R.W. Pascal, J. Hutchings, and V.C. Cornell, 1998: Wind stress measurements from the open ocean corrected for air flow distortion by the ship. *J. Phys. Oceanogr.*, **28**, 1511-1526.

Yelland, M.J., B.I. Moat, R.W. Pascal, and D.I. Berry, 2002: CFD model estimates of the airflow over research ships and the impact on momentum flux measurements. *J. Atmos. Oceanic Tech.*, **19**, 1477-1499.

Flux Measurement and Exchange Coefficients

Andreas, E.L., 1992: Sea spray and the turbulent air-sea heat fluxes. *J. Geophys. Res.*, **97**, 11,429-11,441.

Andreas, E.L., J.B. Edson, E.C. Monohan, M.P. Rouault, and S.D. Smith, 1995: The spray contribution to net evaporation from the sea: A review of recent progress. *Boundary-Layer Meteorol.*, **72**, 3-52.

Bradley, E.F., P.A. Coppin, and J.S. Godfrey, 1991: Measurements of sensible and latent heat fluxes in the western equatorial Pacific Ocean. *J. Geophys. Res.*, **96**, Suppl. 3375-3389.

Brutsaert, W.A., 1982: *Evaporation into the Atmosphere*. Reidel, Dordrecht, 299 pp.

Dobson, F., L. Hasse, and R. Davis, Eds., 1980: *Air-Sea Interaction*: *Instruments and Methods*. Plenum Press, New York, NY, 801 pp.

Edson, J.B., C.W. Fairall, P.G. Mestayer, and S.E. Larsen, 1991: A study of the inertial-dissipation method for computing air-sea fluxes. *J. Geophys. Res.*, **96**, 10,689-10,711.

Edson, J.B., A.A. Hinton, K.E. Prada, J.E. Hare, and C.W. Fairall, 1998: Direct covariance flux estimates from moving platforms at sea. *J. Atmos. Oceanic Tech.*, **15,** 547-562.

Fairall, C.W., and S.E. Larsen, 1986: Inertial dissipation methods and turbulent fluxes at the air ocean interface. *Bound.-Layer Meteor.*, **34**, 287-301.

Fairall, C.W., J.B. Edson, S.E. Larsen, and P.G. Mestayer, 1990: Inertial-dissipation air-sea flux measurements: A prototype system using real-time computations. *J. Atmos. Oceanic Tech.,* **7**, 425-453.

Finkelstein, P.L., and P.F. Sims, 2001: Sampling error in eddy correlation flux measurements. *J. Geophys. Res.*, **106**, 3503-3509.

Godfrey, J.S., M. Nunez, E.F. Bradley, P.A. Coppin, and E.J. Lindstrom, 1991: On the net surface heat flux into the western equatorial Pacific. *J. Geophys. Res.,* **96**, suppl., 3391-3400.

Godfrey, J.S., and A.C.M. Beljaars, 1991: On the turbulent fluxes of buoyancy, heat, and moisture at the air-sea interface at low wind speeds. *J. Geophys. Res.*, **96**, 22,043-22,048.

Gosnell, R., P.J. Webster, and C.W. Fairall, 1995: The sensible heat flux due to rain in TOGA COARE. *J. Geophys. Res.*, **100**, 18,437-18,442.

Grachev, A.A., C.W. Fairall, and S.E. Larsen, 1998: On the determination of the neutral drag coefficient in the convective boundary layer. *Bound.-Layer Meteor*., **86**, 257-278.

Large, W.G., and S. Pond, 1982: Sensible and latent heat flux measurements over the ocean. *J. Phys. Oceanog.*, **12**, 464-482.

Liu, W.T., K.B. Katsaros, and J.A. Businger, 1979: Bulk parameterization of the air-sea exchange of heat and water vapor including the molecular constraints at the interface. *J. Atmos. Sci*., **36**, 2052-2062.

Oost, W.A., G.J. Komen, C.M.J. Jacobs, and C. van Oort, 2002: New evidence for a relation between wind stress and wave age from measurements during ASGAMAGE. *Bound.-Layer Meteor.*, **103**, 409-438.

Persson, O.G.P., C.W. Fairall, E.L Andreas, P.S. Guest, and D.K. Perovich, 2002: Measurements near the atmospheric surface flux group tower at SHEBA: Near-surface conditions and surface energy budget. *J. Geophys. Res.,* **107**, 8045.

Smith, S.D., 1980: Wind stress and heat flux over the ocean in gale force winds. *J. Phys. Oceanogr*., **10**, 709-726.

Smith, S.D., 1988: Coefficients for sea surface wind stress, heat flux, and wind profiles as a function of wind speed and temperature. *J. Geophys. Res.*, **93**, 15,467-15,472.

Smith, S.D., and coauthors, 1992: Sea surface wind stress and drag coefficients: The HEXOS results. *Bound.-Layer Meteor.*, **60**, 109-142.

Smith, S.D., 1989: Water vapor flux at the sea surface. *Bound.-Layer Meteor.*, **47**, 277-293.

Smith, S.D., C.W. Fairall, G.L. Geernaert, and L. Hasse, 1996: Air-sea fluxes: 25 years of progress. *Bound.-Layer Meteor.*, **78**, 247-290.

Taylor, P.K., and M.A. Yelland, 2001: The dependence of sea surface roughness on the height and steepness of the waves. *J. Phys. Oceanogr*., **31**, 572-590.

Vickers, D., and L. Mahrt, 2006: Evaluation of the air-sea bulk formula and sea-surface temperature variability from observations. *J. Geophys. Res.,* **111**, No. C5, C05002. 10.1029/2005JC003323.

Yelland, M., and P.K. Taylor, 1996: Wind stress measurements from the open ocean. *J. Phys. Oceanogr.*, **26**, 541-558.

Yelland, M., B.I. Moat, P.K. Taylor, R.W. Pascal, J. Hutchings, and V.C. Cornell, 1998: Measurements of the open ocean drag coefficient corrected for air flow disturbance by the ship. *J. Phys. Oceanogr.*, **28**, 1511-1526.

Instrument and Data Comparisons

Barton, I.J., P.J. Minnett, K.A. Maillet, C.J. Donlon, S.J. Hook, A.T. Jessup, and T.J. Nightingale, 2004: The Miami2001 infrared radiometer calibration and intercomparison. Part II: Shipboard results. *J. Atmos. Oceanic Tech.*, **21**, 268-283.

Bourassa, M.A., D.M. Legler, J.J. O'Brien, and S.R. Smith, 2003: SeaWinds Validation with Research Vessels. *J. Geophys. Res.*, **108**, DOI 10.1029/2001JC001081.

Burns, Sean P., and 13 coauthors, 1999: Comparisons of aircraft, ship, and buoy meteorological measurements from TOGA COARE. *J. Geophys. Res.*, **104**, 30,853-30,884.

Burns, Sean P., and 14 coauthors, 2000: Comparisons of aircraft, ship, and buoy radiation and SST measurements from TOGA COARE. *J. Geophys. Res.*, **105**, 15,627-15,652.

Colbo, K., and R.A. Weller, 2006: The accuracy of the IMET sensor package. Submitted to. *J. Atmos. Oceanic Tech.*

Cronin, M., C.W. Fairall, and M.J. McPhaden, 2006: Accuracy of buoy-derived and NWP surface heat fluxes in the Tropical Pacific. *J. Geophys. Res.*, accepted.

Ebert, E.E., and M.J. Manton, 1998: Performance of satellite rainfall estimation algorithms during TOGA-COARE. *J. Atmos. Sci.*, **55**, 1537-1557.

Gulev, S.K., D. Cotton, and A. Sterl, 1998: Intercomparison of the North Atlantic wave climatology from voluntary observing ships, satellite data, and modelling. *Phys. Chem. Earth*, **23**, 587-592.

Johnson, R.H., and P.E. Ciesielski, 2000: Rainfall and radiative heating rates from TOGA COARE atmospheric budgets. *J. Atmos. Sci.*, **57**, 1497-1514.

Kent, E.C., P.K. Taylor, and P.G. Challenor, 1998: A comparison of ship and scatterometer-derived wind speed data in open ocean and coastal areas. *Int. J. Remote Sensing*, **19**, 3361-3381.

Kristensen, L., J. Mann, S.P. Oncley, and J.C. Wyngaard, 1997: How close is close enough when measuring scalar fluxes with displaced sensors. *J. Atmos. Oceanic Tech.*, **14**, 814-821.

Renfrew, I.A., G.W.K. Moore, P.S. Guest, and K. Bumke, 2002: A comparison of surface-layer and surface turbulent flux observations over the Labrador Sea with ECMWF analyses and NCEP reanalyses. *J. Phys. Oceanogr.,* **32** (2), 383-400.

Smith, S.R., D.M. Legler, K.V. Verzone, 2001: Quantifying uncertainties in NCEP reanalyses using high-quality research vessel observations. *J. Climate,* **14** (20), 4062-4072.

Sun, B., L. Yu, and R.A. Weller, 2003: Comparisons of surface meteorology and turbulent heat fluxes over the Atlantic: NWP model analyses versus moored buoy observations. *J. Climate*, **16**, 679-695.

Weller, R.A., E.F. Bradley, and R. Lukas, 2004: The interface or air-sea flux component of the TOGA Coupled Ocean-Atmosphere Response Experiment and its impact on subsequent air-sea interaction studies. *J. Atmos. Oceanic Tech.*, **21**, 223-257.

Radiometry

Albrecht, B.A., M. Poellot and S.K. Cox, 1974: Pyrgeometer measurements from aircraft. *Rev. Sci. Instrum.*, **45**, 33-38.

Curry, J.A., W.B. Rossow, D. Randall and J.L. Schramm, 1996: Overview of Arctic cloud and radiation characteristics. *J. Climate,* **9**, 1731-1764.

Dutton, E.G, 1993: An extended comparison between LOWTRAN7 computed and observed broadband thermal irradiances: Global extreme and intermediate surface conditions. *J. Atmos. Oceanic Tech.*, **10**, 326-336.

Fairall, C.W., O.P.G. Persson, R.E. Payne, and E.F. Bradley, 1998: A new look at calibration and use of Eppley precision infrared radiometers. *J. Atmos. Oceanic Tech.*, **15**, 1230-1243.

Guest, P.S., 1998: Surface longwave radiation conditions in the eastern Weddell sea during winter. *J. Geophys. Res.,* **103**, 30,761-30,771.

Paltridge, G.W., and C.M.R Platt, 1976: *Radiative Processes in Meteorology and Climatology*, Elsevier, New York, NY, 318 pp.

Payne, R.E., 1972: Albedo of the sea surface. *J. Atmos. Sci.*, **29**, 959-970.

Philipona, R., C. Frohlich, and C. Betz, 1995: Characterization of pyrgeometers and the accuracy of atmospheric long-wave radiation measurements. *Appl. Opt.*, **34**, 1598-1605.

Sea Surface Temperature, Waves and Ocean Mixing

Bourassa, M.A**.**, 2006: Satellite-based observations of surface turbulent stress during severe weather, Atmosphere - Ocean Interactions. Vol. 2., ed., W. Perrie, Wessex Institute of Technology Press, 35-52.

Coppin, P.A., E.F. Bradley, I.J. Barton and J.S. Godfrey, 1991: Simultaneous observations of sea surface temperature in the western equatorial Pacific Ocean by bulk, radiative, and satellite methods. *J. Geophys. Res.,* **96**, supplement, 3401-3409.

Donelan, M.A., F.W. Dobson, S.D. Smith and R.J. Anderson, 1993: On the dependence of sea surface roughness on wave development. *J. Phys. Oceanogr.*, **23**, 2143-2149.

Donelan, M.A., W.M. Drennan, and K.B. Katsaros, 1997: The air-sea momentum flux in conditions of wind sea and swell. *J. Phys. Oceanogr.*, **27**, 2087-2099.

Donlon, C.J., S.J. Keogh, D.J. Baldwin, I.S. Robinson, I. Ridley, T. Sheasby, I.J. Barton, E.F. Bradley, T.J. Nightingale, and W. Emery, 1998: Solid-state radiometer measurements of sea surface skin temperature. *J. Atmos. Oceanic Tech.*, **15**, 775-787.

Donlon, C.J., P. Minnett, C. Gentemann, T.J. Nightingale, I..J. Barton, B. Ward, and J. Murray, 2002: Towards improved validation of satellite sea surface skin temperature measurements for climate research. *J. Climate*, **15**, 353-369.

Fairall, C.W., E.F. Bradley, J.S. Godfrey, G.A. Wick, J.B. Edson, and G.S. Young, 1996a: The cool skin and the warm layer in bulk flux calculations. *J. Geophys. Res*., **101**, 1295-1308.

Feng, Ming, P. Hacker, and R. Lukas, 1998: Upper ocean heat and salt balances in response to a westerly wind burst in the western equatorial Pacific during TOGA COARE. *J. Geophys. Res.,* **103**, 10,289-10,311.

Feng, M., P. Hacker, R. Lukas, R. Weller, and S.P. Anderson, 2000: Upper ocean heat and salt balances in the western equatorial Pacific in response to the intraseasonal oscillation during TOGA COARE. *J. Climate*, **13**, 2409-2427.

Godfrey, J.S., E.F. Bradley, P.A. Coppin, L. Pender, T.J. McDougall, E.W. Schulz, and I. Helmond, 1999: Measurements of upper ocean heat and freshwater budgets near a drifting buoy in the equatorial Indian Ocean. *J. Geophys. Res.*, **104**, 13,269-13,302.

Kudryavtsev, V.N., and A.V. Soloviev, 1990: Slippery near-surface layer of the ocean arising due to daytime solar heating. *J. Phys. Oceanogr.*, **20**, 617-628.

Paulson, C.A., and J.J. Simpson, 1981: The temperature difference across the cool skin of the ocean. *J. Geophys. Res.*, **86**, 11,044-11,054.

Price, J.F., R.A. Weller and R. Pinkel, 1986: Diurnal cycling: observations and models of the upper ocean response to diurnal heating, cooling and wind mixing. *J. Geophys. Res*., **91**, 8411-8427.

Saunders, P.M., 1967: The temperature at the ocean-air interface. *J. Atmos. Sci.*, **24**, 269-273.

Smith, W.L., and coauthors, 1996: Observations of the infrared radiative properties of the ocean: implications for the measurement of sea surface temperature via satellite remote sensing. *Bull. Amer. Meteor. Soc*., **77**, 41-51.

Soloviev, AV., and P. Schluessel, 1994: Parameterization of the cool skin of the ocean and of the air-ocean gas transfer on the basis of modelling surface renewal. *J. Phys. Oceanogr.*, **24**, 1339-1346.

Soloviev, A.V., and P. Schluessel, 1996: Evolution of cool skin and direct air-gas transfer coefficient during daytime. *Bound.-Layer Meteor.*, **77**, 45-68.

Soloviev, A.V., and R. Lukas, 2006: *The Near-Surface Layer of the Ocean.* Structure Dynamics and Applications. Springer, P.O. Box 17, 3300 A.A. Dordrecht, The Netherlands, 572 pp.

Webster, P.J., C.A. Clayson, and J.A. Curry, 1996: Clouds, radiation and the diurnal cycle of sea surface temperature in the tropical Western Pacific. *J. Climate*, **9**, 1712-1730.

Wick, G.A., J.C. Ohlmann, C.W. Fairall, and A.T. Jessup, 2005: Improved oceanic cool-skin corrections using a refined solar penetration model. *J. Phys. Oceanogr.*, **35**, 1986-1996.

Technology

Carter, D.A., K.S. Gage, W.L. Ecklund, W.M. Angevine, P.E. Johnston, A.C. Riddle, J. Wilson, and C.R. Williams, 1995: Developments in lower tropospheric wind profiling at the NOAA Aeronomy Laboratory. *Radio Sci.*, **30**, 977-1001.

Fairall, C.W., A.B. White, J.B. Edson, and J.E. Hare, 1997: Integrated shipboard measurements of the marine boundary layer. *J. Atmos. Oceanic Tech.,* **14**, 338-359.

Folland, C.K., 1988: Numerical models of the rain gage exposure problem, field experiments and an improved collector design. *Q. J. Roy. Meteor. Soc.*, **114**, 1485-1516.

Grossklaus, M., K. Uhlig, and L. Hasse, 1998: An optical disdrometer for use in high wind speeds. *J. Atmos. Oceanic Tech*., **15**, 1051-1059.

Hasse, L., M. Grossklaus, K. Uhlig, and P. Timm, 1998: A ship rain gauge for use in high winds. *J. Atmos. Oceanic Tech*., **15**, 380-386.

Hosom, D.S., R.A. Weller, R.E. Payne, and K.E. Prada, 1995: The IMET (Improved Meteorology) ship and buoy systems. *J. Atmos. Oceanic Technol.*, **12**, 527-540.

Hubbard, K.G., X. Lin, and E.A. Walter-Shea, 2001: The effectiveness of the ASOS, MMTS, Gill and CRS air temperature radiation shields. *J. Atmos. Oceanic Tech.*, **18**, 851-864.

Kaimal, J.C., and J.J. Finnigan, 1994: *Atmospheric Boundary Layer Flows: Their Structure and Measurement*. Oxford University Press, Oxford, UK, 289 pp.

Kent, E.C., and P.K. Taylor, 1997: Choice of a Beaufort Equivalent Scale. *J. Atmos. Oceanic Tech.*, **14**(2), 228-242.

Nystuen, J.A., M.J. McPhaden, and H.P. Freitag, 2000: Surface measurements of precipitation from an ocean mooring: The underwater acoustic log from the South China Sea. *J. Appl. Meteor.*, **39**, 2182-2197.

Payne, R.E., 2002: Recognising problems in shipboard logging meteorology systems. Woods Hole Oceanog. Inst. Tech. Rept. WHOI-2002-05, Woods Hole, MA 02543, USA.

Tanner, C.B., and G.W. Thurtell, 1969: Anemoclinometer measurements of Reynolds stress and heat transport in the atmospheric surface layer. University of Wisconsin Technical Report ECOM-66-G22-F, 82 pp. [Available from US Army Electronic Command, Atmospheric Sciences Laboratory, Ft. Huachuca, AZ 85613.]

Wang, T., K.B.Earnshaw, and R.S.Lawrence, 1978: Simplified optical path-average rain gauge. *Appl. Opt.*, **17**, 385-390.

Wang, T., K.B.Earnshaw, and R.S.Lawrence, 1979: Path-averaged measurements of rain rate and raindrop size distribution using a fast-response optical sensor. *J. Appl. Meteor.*, **18**, 654-660.

Wyngaard, J.C., 1981: The effects of probe-induced flow distortion on atmospheric turbulence measurements. *J. Appl. Meteor.*, **20**, 784–794.

Wyngaard, J.C., 1988: Flow-distortion effects on scalar flux measurements in the surface layer: Implications for sensor design. *Bound.-Layer Meteor.*, **42**, 19–26.

Wyngaard, J.C., 1988: The effects of probe-induced flow distortion on atmospheric turbulence measurements: Extension to scalars. *J. Atmos. Sci.*, **45**, 3400–3412.